

**PL-TR-97-2135**

**MFD-TR-97-15887**

## **Improved Methods for Regionalized Surface Wave Analysis**

**J. L. Stevens  
K. L. McLaughlin**

**Maxwell Technologies – Federal Division  
8888 Balboa Ave  
San Diego, CA 92123-1506**

**September 1997**

**Final Report  
31 July 1995 – 30 July 1997**

**DTIC QUALITY INSPECTED 4**

**APPROVED FOR PUBLIC RELEASE; DISTRIBUTION UNLIMITED**



**PHILLIPS LABORATORY  
Directorate of Geophysics  
AIR FORCE MATERIEL COMMAND  
HANSCOM AFB, MA 01731-3010**

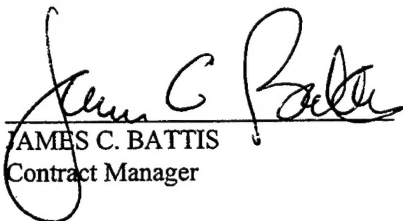
**19980217 490**

SPONSORED BY  
Air Force Technical Applications Center  
Directorate of Nuclear Treaty Monitoring  
Project Authorization T/5101


MONITORED BY  
Phillips Laboratory  
CONTRACT No. F19628-95-C-0110

The views and conclusions contained in this document are those of the authors and should not be interpreted as representing the official policies, either express or implied, of the Air Force or U.S. Government.

This technical report has been reviewed and is approved for publication.



JAMES C. BATTIS  
Contract Manager



CHARLES P. PIKE, Director  
Business Management Division

This report has been reviewed by the ESD Public Affairs Office (PA) and is releasable to the National Technical Information Service (NTIS).

Qualified requestors may obtain copies from the Defense Technical Information Center. All others should apply to the National Technical Information Service.

If your address has changed, or you wish to be removed from the mailing list, or if the addressee is no longer employed by your organization, please notify PL/IM, 29 Randolph Road, Hanscom AFB, MA 01731-3010. This will assist us in maintaining a current mailing list.

Do not return copies of the report unless contractual obligations or notices on a specific document requires that it be returned.

REPORT DOCUMENTATION PAGE			Form Approved OMB No. 0704-0188	
Public reporting burden for this collection of information is estimated to average 1 hour per response, including the time for reviewing instructions, searching existing data sources, gathering and maintaining the data needed, and completing and reviewing the collection of information. Send comments regarding this burden estimate or any other aspect of this collection of information, including suggestions for reducing this burden, to Washington Headquarters Services, Directorate for Information Operations and Reports, 1215 Jefferson Davis Highway, Suite 1204, Arlington VA 22202-4302, and to the Office of Management and Budget, Paperwork Reduction Project (0704-0188), Washington, DC 20503.				
1. AGENCY USE ONLY (Leave blank)		2. REPORT DATE September 1997		3. REPORT TYPE AND DATES COVERED Final Report (31 Jul 1995-30 Jul 1997)
4. TITLE AND SUBTITLE  Improved Methods for Regionalized Surface Wave Analysis			5. FUNDING NUMBERS  Contract No. F19628-95-C-0110  PE 35999F PR 5101 TAGM WU AE	
6. AUTHOR(S)  J. L. Stevens                      K.L. McLaughlin				
7. PERFORMING ORGANIZATION NAME(S) AND ADDRESS(ES)  Maxwell Technologies, Inc. 8888 Balboa Avenue San Diego, CA 92123-1506			8. PERFORMING ORGANIZATION REPORT NUMBER  MFD-TR-97-15870	
9. SPONSORING/MONITORING AGENCY NAME(S) AND ADDRESS(ES)  Phillips Laboratory 29 Randolph Road Hanscom AFB, MA 01731-3010  Contract Manager: James Battis/GPS			10. SPONSORING/MONITORING AGENCY REPORT NUMBER  PL-TR-97-2135	
11. SUPPLEMENTARY NOTES				
12a. DISTRIBUTION/AVAILABILITY STATEMENT  Approved for public release; distribution unlimited.			12b. DISTRIBUTION CODE	
13. ABSTRACT (Maximum 200 words)  We develop optimized methods for measuring surface waves for event screening under a CTBT. The optimization techniques are: a regionalized earth model, phase-matched filtering, path corrected surface wave spectral magnitude; maximum likelihood magnitudes and upper bounds. A regionalized earth model is developed by tomographic inversion of surface wave data starting with the Crust 5.1 earth models, and using dispersion measurements from PIDC data, historic explosion data, and data sets from the University of Colorado, Harvard, and St. Louis University. Dispersion curves derived from the final earth models are sufficient to predict dispersion and to generate phase-matched filters for most regions of the world. (Continued on pg II)				
14. SUBJECT TERMS  Surface Wave, Rayleigh Wave, Earthquake/Explosion Discrimination, M <sub>S</sub> , Maximum Likelihood, Moment, CTBT			15. NUMBER OF PAGES  68	
			16. PRICE CODE	
17. SECURITY CLASSIFICATION OF REPORT  Unclassified	18. SECURITY CLASSIFICATION OF THIS PAGE  Unclassified	19. SECURITY CLASSIFICATION OF ABSTRACT  Unclassified	20. LIMITATION OF ABSTRACT  SAR	

**UNCLASSIFIED**

SECURITY CLASSIFICATION OF THIS PAGE

CLASSIFIED BY:

DECLASSIFIED ON:

13. ABSTRACT (Continued)

The detection threshold of the automatic surface wave processor at the PIDC is found to be one magnitude unit lower than NEIC bulletins. Maximum likelihood magnitudes are calculated for a data set of 700 events using 10,000 PIDC and historical explosion seismograms. Maximum likelihood magnitudes combined with maximum likelihood upper bounds allow discrimination to about  $m_b$  4.0. The  $M_S:m_b$  discrimination line between earthquakes and explosions has a slope of 1.4.

We recommend redefining  $M_S$  as  $M_S = \log A/T + k \log \Delta + 1/2 \log(\sin \Delta) + \gamma \Delta \log e + D$  using the parameters found by Rezapour and Pearce (1997), and recommend using path corrected spectral magnitudes as an alternative to  $M_S$ .



## Table of Contents

Summary .....	1
1.0 Introduction .....	2
2.0 Surface Wave Propagation in a Regionalized Structure – Theory .....	3
2.1 Scalar Moment and Broadband Path Corrected Spectral Magnitude .....	3
3.0 Development Of Regionalized Earth Models .....	5
3.1 Previous Earth Structure and Dispersion Models .....	5
3.2 Tomographic Inversion to Improve Crust 5.1 Models .....	5
3.3 Dispersion, Attenuation, and Amplitude Factors Calculated from Earth Models .....	8
4.0 Automatic Surface Wave Identification and Measurement at the PIDC .....	15
4.1 Optimum Parameters for Surface Wave Processing .....	16
4.2 Comparison of PIDC $M_s$ with USGS $M_s$ .....	17
5.0 Maximum Likelihood Moment and $M_s$ .....	19
6.0 Earthquake/Explosion Discrimination Using the $M_s:m_b$ and $M_0:m_b$ Methods .....	23
7.0 Optimum Distance Corrections for Moment and $M_s$ .....	25
8.0 Conclusions and Recommendations .....	30
9.0 References .....	32
10.0 Acknowledgements .....	33
Appendix A. Surface Wave Excitation by Arbitrary Sources and Explosions .....	34
Appendix B. Surface Wave Transmission Through Laterally Heterogeneous Media .....	35
Appendix C. Modified Crust 5.1 Models and Group Velocity Contour Plots .....	37
Appendix D. Maximum Likelihood Station Corrections for $M_s$ .....	41
Appendix E. Maximum Likelihood Station Corrections for $\log M_0$ .....	42
Appendix F. Maximum Likelihood $M_s$ and $\log M_0$ for Explosions .....	43
Appendix G. Maximum Likelihood $M_s$ and $\log M_0$ for Earthquakes .....	48

## List of Figures

<b><u>Figure</u></b>	<b><u>Page</u></b>
1 Scalar moment for an explosion and earthquake (Eq (2.2)) calculated for several earthquake depths .....	4
2 Group velocity contours of the inversion model at 50 seconds period .....	7
3 Continental phase velocities .....	9
4 Oceanic phase velocities.....	9
5 Continental group velocities .....	10
6 Oceanic group velocities .....	10
7 Continental attenuation coefficients $\gamma$ ( $10^{-4}/\text{km}$ ) .....	11
8 Oceanic attenuation coefficients $\gamma$ ( $10^{-4}/\text{km}$ ) .....	11
9 Continental amplitude factor $S_1$ at 1 km depth .....	12
10 Continental amplitude factor $S_1$ at zero depth .....	12
11 Oceanic amplitude factor $S_1$ at depth 1 km below the ocean bottom .....	13
12 Oceanic source amplitude factor $S_1$ at zero depth (at the ocean bottom).....	13
13 Continental receiver amplitude factor $S_2$ .....	14
14 Oceanic receiver amplitude factor $S_2$ .....	14
15 Cumulative distribution of PIDC and NEIC amplitudes .....	18
16 PIDC vs. NEIS $M_s$ shows a bias that increases with decreasing magnitude .....	19
17 Histograms of maximum likelihood station corrections for $M_s$ (left) and $\log M_0$ (right) .....	20
18 Maximum likelihood GLM $M_s$ with and without censoring correction.....	21
19 Maximum likelihood GLM $\log M_0$ with and without censoring correction .....	21
20 Maximum likelihood log moment plotted vs. maximum likelihood $M_s$ .....	22
21 Maximum likelihood GLM station corrected $\log M_0$ and $\log M_0$ upper bounds plotted vs. $m_b$ for PIDC earthquakes and historical explosion data .....	24
22 Maximum likelihood GLM station corrected $M_s$ and $M_s$ upper bounds plotted vs. $m_b$ for PIDC earthquakes and historical explosion data .....	25
23 Moment residuals vs. distance derived using regionalized earth models.....	26
24 $M_s$ residuals vs. distance calculated using the IASPEI $M_s$ formula.....	28

25	Comparison of distance corrections from the best fit $\gamma=0.012$ Eq (7.3), the Rezapour and Pearce (1997) Eq (7.4), Marshall and Basham (1972), and the IASPEI formula .....	29
26	Regionalized inversion models derived from Crust 5.1 .....	37
27	Group velocity contours at 0.02 Hz .....	38
28	Group Velocity contours at 0.03 Hz.....	38
29	Group velocity contours at 0.04 Hz .....	39
30	Group velocity contours at 0.05 Hz .....	39
31	Group velocity contours at 0.06 Hz .....	40

### List of Tables

Table	Page
1 40 Second group velocity % average residuals (standard deviations) .....	7
2 20 Second group velocity % average residuals (standard deviations) .....	7
3 Effect of revised distance corrections on network $M_s$ .....	30

## Summary

Surface waves are of primary importance for CTBT monitoring because the  $M_s:m_b$  discriminant and its regional variants are among the most reliable means of determining whether an event is an earthquake or an explosion. In this project, we have developed improved methods for measuring surface wave amplitudes in order to reduce the threshold for which surface waves can be reliably measured, and to develop a consistent way of measuring surface waves that is valid at regional and teleseismic distances. The basic elements of the procedure are: development of a regionalized earth model for determining surface wave phase velocity, amplitude, dispersion, and attenuation; phase-matched filtering to improve signal/noise ratio with phase-matched filters derived from the regionalized earth model; a regionalized surface wave spectral magnitude, the scalar moment; and maximum likelihood magnitudes which correct for censoring and allow an upper bound on the magnitude to be determined for events with no measurable surface waves.

A regionalized earth model was developed by starting with the Crust 5.1 earth models developed by Mooney *et al.* (1997) with some additional regionalization of the oceans and then varying the shear velocities in each model to obtain a better fit to observed dispersion curves. Dispersion information from the University of Colorado, Harvard University, and St. Louis University were combined with dispersion curves from historic explosion data and PIDC data to perform a tomographic inversion of about 90,000 data points to determine the shear velocity structure of 149 earth models on a 5 degree grid. Dispersion curves derived from the final earth models are sufficient to predict dispersion and to generate phase-matched filters for most regions of the world.

The detection threshold of the automatic surface wave processor at the PIDC is about one magnitude unit lower than NEIC bulletins, and there is a bias between the two bulletins of  $M_s(\text{NEIS})-M_s(\text{PIDC}) \approx 0.1$  magnitude units. Maximum likelihood scalar moments and  $M_s$  were calculated for a data set of 700 events using 10,000 PIDC seismograms and historical explosion seismograms. The reliability of maximum likelihood magnitudes has been greatly improved through improved methods for automatic identification of surface waves, although problems can still occur due to low amplitude noise measurements from malfunctioning stations. Maximum likelihood magnitudes combined with maximum likelihood upper bounds allow reliable discrimination down to at least  $m_b$  4.0. The  $M_s:m_b$  discrimination line between earthquakes and explosions has a slope of 1.4, rather than the expected 1.0 at low magnitudes.

The distance correction for  $M_s$  is reevaluated. The standard  $M_s$  formula with a distance correction of  $1.66 \log \Delta$  is inconsistent with the theoretical formula for surface wave attenuation, and cannot be adjusted to match surface wave attenuation at both near and far distances. We recommend replacing the  $M_s$  formula with  $M_s = \log A/T + k \log \Delta + \frac{1}{2} \log(\sin \Delta) + \gamma \Delta \log e + D$  and recommend using the parameters found by Rezapour and Pearce (1997):  $k=1/3$ ,  $\gamma=0.0105/\text{degree}$ ,  $D=2.484$  where  $A$  is the zero to peak amplitude in nanometers. We also recommend the use of the logarithm of the scalar moment,  $\log M_0$ , as an alternative to  $M_s$ .  $\log M_0$  has the advantages of being inherently regionalizeable, more stable than  $M_s$  at regional distances, unaffected by dispersion, and having a consistent value over different frequency bands and distance ranges.

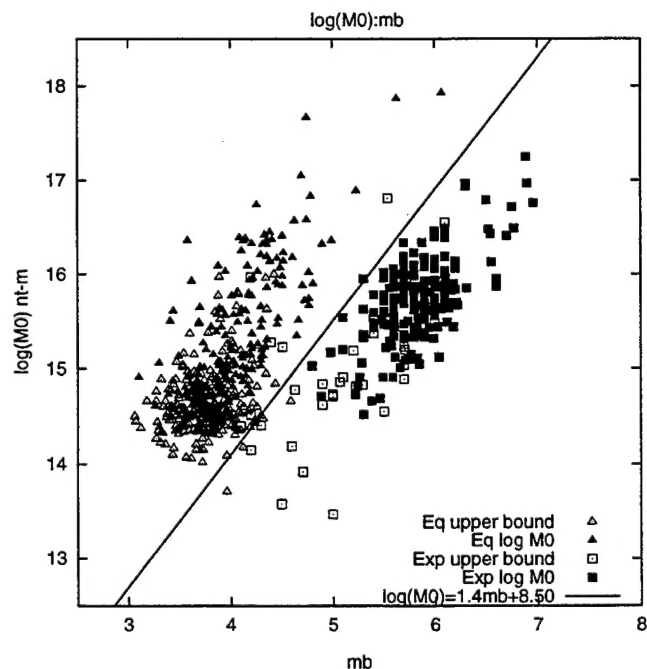
## 1.0 Introduction

Surface waves are of primary importance for CTBT monitoring because the  $M_s:m_b$  discriminant and its regional variants are among the most reliable means of determining whether an event is an earthquake or an explosion. With the International Data Center identifying approximately 20,000 events per year, it is particularly important to be able to unambiguously identify as many of these events as possible. The primary objective of this research program is to develop improved methods for measuring surface waves in order to reduce the magnitude threshold for which surface waves can be reliably measured, minimize the number of events that require more detailed analysis, decrease the number of unidentified events, avoid unnecessary on-site inspections, and allow identification of underground nuclear tests.

Under this project, we have developed a framework for optimum measurement of surface waves, and implemented and tested this framework using data from the prototype International Data Center (PIDC) and historic nuclear explosion data. The elements of the framework are:

1. a regionalized earth model for determining surface wave phase, amplitude, dispersion, and attenuation.
2. phase-matched filtering to improve signal/noise ratio, with phase matched filters regionalized worldwide.
3. a unified surface wave magnitude, the scalar moment, which has a consistent value over different frequency bands and distance ranges.
4. maximum likelihood magnitudes, which correct for censoring and allow an upper bound on the magnitude to be determined for events with no measurable surface waves.

The end result of this processing is shown in the figure to the right reproduced from Section 6 of this report, showing log moment plotted vs.  $m_b$  for a data set of PIDC data and historical nuclear explosions. Earthquakes and explosions separate very well, even for many events that have no observable surface wave data. Continuing analysis, including the development of improved earth models for predicting surface wave amplitudes and dispersion, will result in further improvement of discrimination capability and reduction of the explosion identification threshold.



## 2.0 Surface Wave Propagation in a Regionalized Structure – Theory

The theory for surface waves from an explosion or other source, and surface wave transmission through a regionalized earth model are summarized in Appendix A and Appendix B. The notation used in this section follows the notation of these appendices.

### 2.1 Scalar Moment and Broadband Path Corrected Spectral Magnitude

The key to developing a surface wave magnitude that is regionalizeable, and gives consistent values at regional and teleseismic distances and in different frequency bands, is to use the equation for surface waves in a plane-layered structure to correct the spectrum. This equation can be factored into functions that depend on the source and receiver earth structure and the phase velocity and attenuation integrated over the path. The displacement spectrum for a Rayleigh wave at distance  $r$  from an *explosion* is given by (from Eq (B.8)-(B.10)):

$$U(\omega, r) = M_0 \frac{S_1^x(\omega, h_x) S_2(\omega) \exp[-\gamma_p(\omega)r + i(\phi_0 - \omega r / c_p(\omega))]}{\sqrt{a_e \sin(r / a_e)}} \quad (2.1)$$

$S_1^x$  depends on the source region elastic structure and the explosion source depth.  $S_2$  depends on the receiver region elastic structure,  $\gamma_p$  is the attenuation coefficient that depends on the attenuation integrated over the path between the source and receiver.  $c_p$  is the phase velocity integrated over the source to receiver path.  $\phi_0$  is the initial phase of the source.  $a_e$  is the radius of the earth.  $M_0 = \frac{3\beta^2}{\alpha^2} M_0$  where  $M_0$  is the explosion isotropic moment. This definition is introduced so that the function  $S_1^x$  does not depend explicitly on the material properties at the source depth.

We can use Eq (2.1) to define a spectral magnitude corrected for distance and spectral shape. We define, for any event, earthquake or explosion, the estimated scalar moment:

$$M_0 = \left| U(\omega, r, \theta) \frac{S_1^x(\omega, h_x) S_2(\omega) \exp[-\gamma_p(\omega)r + i(\phi_0 - \omega r / c_p(\omega))]}{\sqrt{a_e \sin(r / a_e)}} \right| \quad (2.2)$$

$\log M_0$  is then a spectral magnitude that can be evaluated over any desired frequency band. This is similar to the approach taken by Okal and Talandier (1987) in defining a mantle magnitude  $M_m$ , except that they used an averaged earthquake source spectrum that they referred to as the Rayleigh Wave "Excitability" instead of the explosion excitation function  $S_1^x$  at the reference depth  $h_x$ . Although the imaginary part of the exponential is removed by the absolute value, it is shown here explicitly because in practice the phase is used to generate a phase-matched filter to compress the signal and improve signal/noise ratio prior to taking the spectrum. The spectrum is then averaged over a frequency band to smooth the spectrum and obtain a stable measurement.

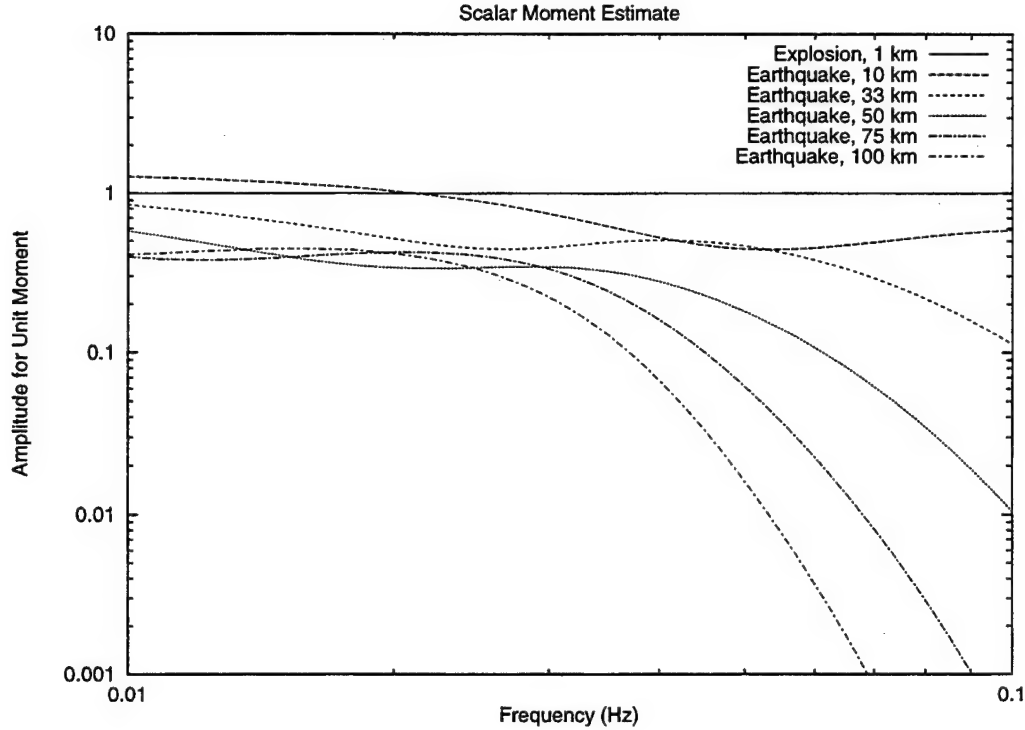


Figure 1. Scalar moment for an explosion and earthquake (Eq (2.2)) calculated for several earthquake depths. The spectral amplitude decays more rapidly with increasing frequency for deeper sources.

For an isotropic explosion source at depth  $h_x$ ,  $M_0$  is independent of frequency. Equation (2.2) therefore corrects completely for all frequency dependent and distance dependent factors in the observed spectrum. In general,  $M_0$  for an earthquake is not completely frequency independent, but it is partially corrected for frequency dependence by removal of the path attenuation and receiver structure and similarities in the explosion and earthquake excitation functions in the same source region. The remaining differences mean that the earthquake magnitude will vary somewhat when measured over different frequency bands while the explosion will not. In particular, the spectra of deeper earthquakes will decline more rapidly with increasing frequency, while the path corrected spectra of shallow earthquakes is approximately flat over the frequency band of about 0.01-0.08 Hz. Figure 1 shows the scalar moment calculated with Eq (2.2) of an explosion and a typical earthquake with strike 0, dip 80, rake 15, observed at an azimuth of 45 degrees for several depths in a Eurasian earth structure. The explosion has unit scalar moment, and the earthquake has unit double couple moment.

By defining the scalar moment with Eq (2.2), we obtain a measure of surface wave magnitude that is independent of range, nearly independent of frequency, and regionalizeable. The functions  $S_1^x$  and  $S_2$  depend only on the source and receiver points and can be stored in a simple lookup table. The functions  $\gamma_p$  and  $c_p$  depend on the source to receiver path and can be found by integrating along a great circle path between the source and receiver in a regionalized earth model.



### 3.0 Development of Regionalized Earth Models

With a set of regionalized earth models that maps any point on the earth into the earth structure at that point, we can calculate all of the quantities in Eq (2.2) for any source and receiver point and calculate the scalar moment from any observed seismogram. In addition, we can use the phase velocity for the path to construct phase matched filters, and use the predicted group velocity arrival times as part of an existence test for surface waves in automatic processing (see Section 4).

Observed surface waves provide strong constraints on earth structure, so development of regionalized earth models can be a self-correcting process. That is, surface wave dispersion and amplitudes can be used to infer earth structure, and earth structure can be used to calculate surface wave dispersion and amplitudes. So with a data center such as the IDC which collects surface wave data on a continuous basis, it should be possible to implement a program of continuous improvements in regionalization and surface wave processing using this extensive data set.

#### 3.1 Previous Earth Structure and Dispersion Models

Many studies have been performed to analyze surface wave dispersion and infer earth structure in specific regions, but few studies have attempted to regionalize the entire world, particularly at shorter periods. Mooney *et al.* (1997) developed the Crust 5.1 earth model which consists of 139 distinct earth models regionalized on a  $5^\circ$  by  $5^\circ$  grid, each using a seven layer crustal model over a single layer mantle model. Each model is characterized by compressional velocity, shear velocity, and density for each layer. Stevens and McLaughlin (1996) developed a set of regionalized group velocity models on a  $10^\circ$  by  $10^\circ$  grid. These models are currently used in automatic surface wave processing at the PIDC to predict group velocity arrival times. Ekstrom *et al.* (1996) developed a global phase velocity model valid a periods greater than 35 seconds expressed as a spherical harmonic expansion. These and similar global studies, as well as many other regional studies, may present results in terms of phase velocity, group velocity, or earth structure, and the optimum regionalized earth model would be consistent with the most robust properties of each of these models.

#### 3.2 Tomographic Inversion to Improve Crust 5.1 Models

The Crust 5.1 model provides an excellent starting point for development of regionalized surface wave parameters. Comparisons with surface wave dispersion data showed that although group velocities predicted by Crust 5.1 were quite good on continental paths at periods close to 20 seconds, they were not as good as models currently in use at the PIDC for oceanic paths, particularly at periods  $< 25$  seconds, or for continental paths at periods  $> 30$  seconds. In order to make the models more useful for surface wave analysis, we improved the models using the following procedure.

We assume that the 139 models in Crust 5.1 are an adequate classification of the earth's structure in continental regions, but that the constraints on the shear velocity in each model are weak and that a first order improvement can be made by varying the shear velocity in each model. In oceanic regions, we created some additional models corresponding to different ocean ages, using the Crust 5.1 model as a starting model, but then allowing the new models in these distinct regions to vary independently. We also removed 5 models with very thick low velocity sediments that led to unrealistic dispersion curves. The final model has 149 distinct earth structures.



The following data sets were used in the inversion:

1. Global surface wave group velocities from earthquakes derived using PIDC data (Stevens and McLaughlin, 1996), *augmented* with more recent measurements derived from PIDC data, for a total of 1500 paths at 6 frequencies from 0.02-0.06 Hz.
2. Surface wave phase and group velocity dispersion curves from underground nuclear test sites (Stevens, 1986; Stevens and McLaughlin, 1988), calculated from earth models for 270 paths at 10 frequencies between 0.015 and 0.06 Hz.
3. Phase and group velocity measurements for western Asia and Saudi Arabia from Mitchell *et al.* (1996) for 12 paths at 17 frequencies between 0.012 and 0.14 Hz.
4. Global phase velocity model of Ekstrom *et al.* (1996) for 9 periods between 35 and 150 seconds calculated for each 5° grid block from a spherical harmonic expansion of order  $l=40$ .
5. Group velocity measurements for Eurasia from Ritzwoller *et al.* (1996) and Levshin *et al.* (1996) for 20 frequencies between 0.004 and 0.1 Hz with 500 to 5000 paths per frequency.

The complete data set of approximately 90,000 data points was used to invert for shear velocity structure in each model. This was accomplished using a tomographic inversion of the entire data set for all models at the same time. That is, we solve the equation  $\mathbf{A}\mathbf{m}=\mathbf{d}$  where  $\mathbf{m}$  is the change in the shear slowness of each model layer with dimension equal to the total number of layers being varied in the 149 models,  $\mathbf{d}$  is the difference between the observed and predicted slowness of each data point with dimension equal to the number of data points, and  $\mathbf{A}$  is a matrix constructed from the partial derivatives of phase or group velocity with respect to shear velocity in each layer, and the fraction of each model crossed by each data point. The inversion was limited to depths of 3-200 km, with fixed water layers, and with Crust 5.1 extended to greater depths using PREM (Dziewonski and Anderson, 1981). A smoothness condition that minimizes the change in adjacent layer velocities was also applied. The calculations were performed on a DEC Alpha 2100 dual-processor computer using the LSQR algorithm as described by Nolet (1987). The group velocities calculated from the models at 50 seconds are contoured in Figure 2. Additional description of the models and group velocity contours at other frequencies are in Appendix C.

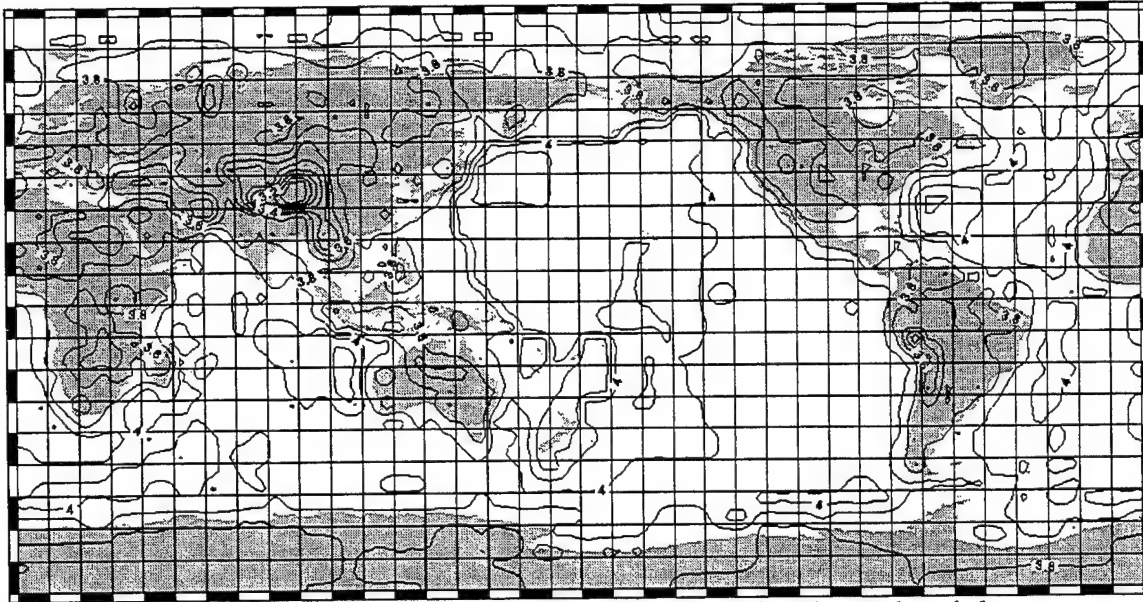


Figure 2. Group velocity contours of the inversion model at 50 seconds period.

The results show some significant improvements over both the model currently being used at the PIDC and the Crust 5.1 model. The following tables show group velocity residuals (and standard deviations) in percent for the three models for data from nuclear test sites and for the global travel times derived from PIDC data. The three group velocity models below are the model currently used at the PIDC (Stevens and McLaughlin, 1996), as modified by Harkrider (personal communication) to a 5-degree grid; the original Crust 5.1 model, and the inversion results described above.

Table 1. 40 Second Group Velocity % Average Residuals (Standard Deviations)

Source	PIDC	Crust 5.1	Inversion
NTS (59)	0.93 (1.80)	2.08 (2.46)	0.15 (1.40)
East Kazakh (40)	1.20 (3.53)	5.00 (3.47)	0.80 (2.21)
Mururoa (13)	-0.80 (1.74)	-2.45 (1.73)	-0.78 (1.43)
Novaya Zemlya (99)	2.01 (2.39)	2.00 (2.28)	-0.06 (2.06)
Amchitka (55)	1.68 (1.58)	0.51 (2.54)	0.25 (1.39)
Earthquakes (1572)	1.44 (4.98)	1.68 (5.32)	0.46 (3.48)

Table 2. 20 Second Group Velocity % Average Residuals (Standard Deviations)

Source	PIDC	Crust 5.1	Inversion
NTS (58)	-1.83 (4.85)	-1.17 (2.48)	-0.47 (2.25)
East Kazakh (40)	-2.61 (3.23)	-0.31 (2.46)	-0.75 (1.96)
Mururoa (11)	-1.43 (2.30)	-1.47 (1.84)	0.41 (1.43)
Novaya Zemlya (99)	2.44 (6.15)	0.35 (4.68)	-0.26 (3.61)
Amchitka (54)	-1.23 (4.43)	1.42 (4.33)	0.83 (3.76)
Earthquakes (1673)	0.31 (5.82)	2.17 (6.31)	2.00 (5.46)

The average shear velocity change was -0.16 (2.57) %, with extreme values of -11% and 15%. Additional improvements could be made in these models, particularly in the western Pacific, where many rays follow grazing paths along continental boundaries, and in areas such as the south Pacific where coverage is limited. There is more variation and more error at periods less than 25 seconds than at longer periods. Nevertheless, the models work quite well for predicting group velocity dispersion and generating phase-matched filters over a frequency band of .01-.06 Hz.

Although surface wave attenuation was not explicitly modeled in this study, the earth models include a Q structure based on PREM in the mantle and on "Swanger's law"  $Q=\beta/10$  where  $\beta$  is the shear velocity in m/sec in each crustal layer. Attenuation coefficients were calculated from these Q structures and used for moment estimation as discussed in the following sections.

The final models and calculated dispersion curves and other calculated quantities discussed in the next section are available for download from the World Wide Web at [http://www.maxwell.com/products/geop/DSWA97\\_Surf/LP\\_export.html](http://www.maxwell.com/products/geop/DSWA97_Surf/LP_export.html).

### *3.3 Dispersion, Attenuation, and Amplitude Factors Calculated from Earth Models*

In order to calculate regionalized surface wave moments using Eq (2.2), we need to calculate the phase and group velocities, attenuation coefficients and amplitude factors  $S_1$  and  $S_2$  for all of the models. In this section, we show these calculated quantities, separated into continental and oceanic structures, for each of the models. Figures 3-14 show the phase velocity, group velocity, attenuation coefficients, and amplitude factors  $S_1$  and  $S_2$ , respectively, as a function of frequency. The source region amplitude factor  $S_1$  depends on source depth, and any fixed depth could be selected for the purpose of normalizing the moments. In the analysis done in this study, we used a fixed source depth of one kilometer. Figures 9 through 12 show  $S_1$  for depths of zero and one kilometers. For continental structures,  $S_1$  depends only weakly on source depth in the upper few kilometers. For oceanic paths, the effect is stronger, and the effect of low velocity sediments at the source depth may not be negligible.

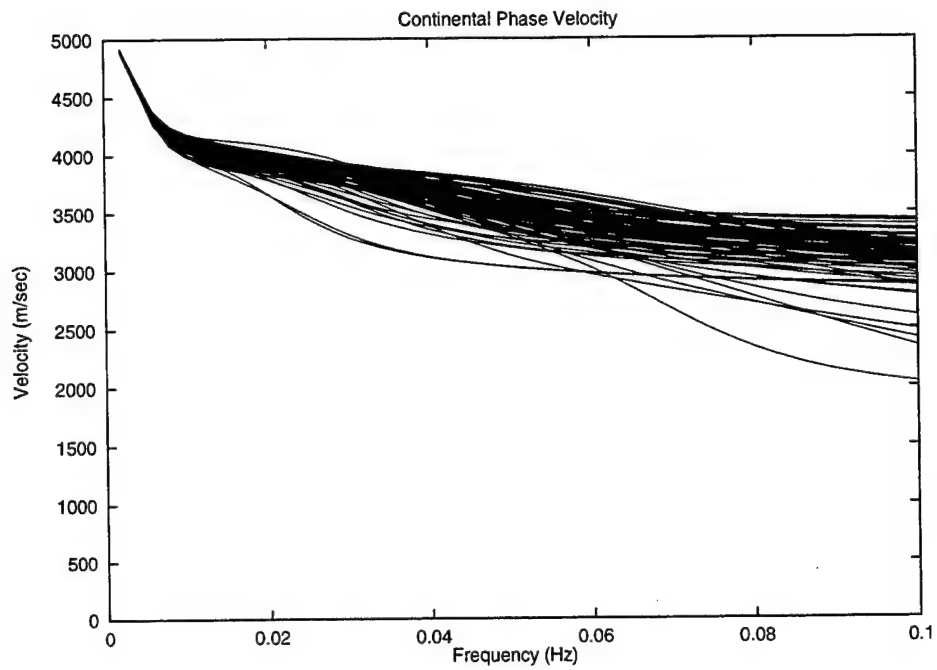


Figure 3. Continental phase velocities.

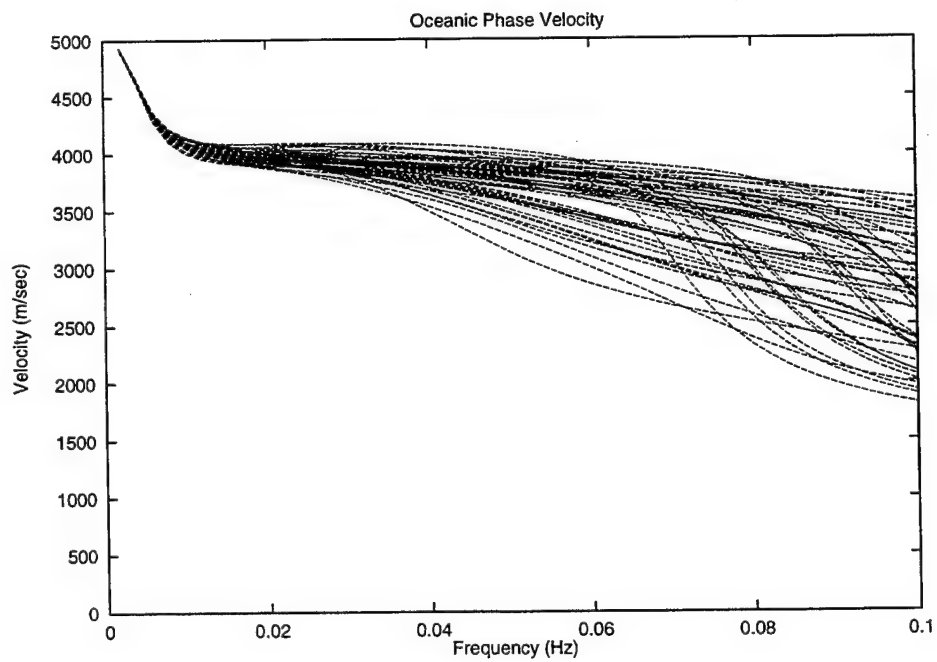


Figure 4. Oceanic phase velocities.

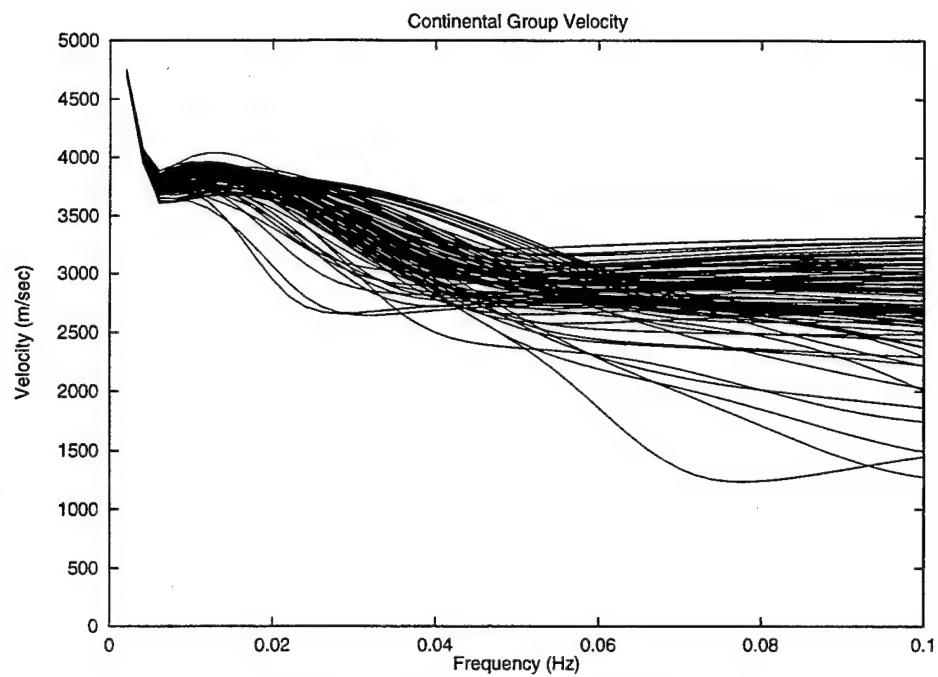


Figure 5. Continental group velocities.

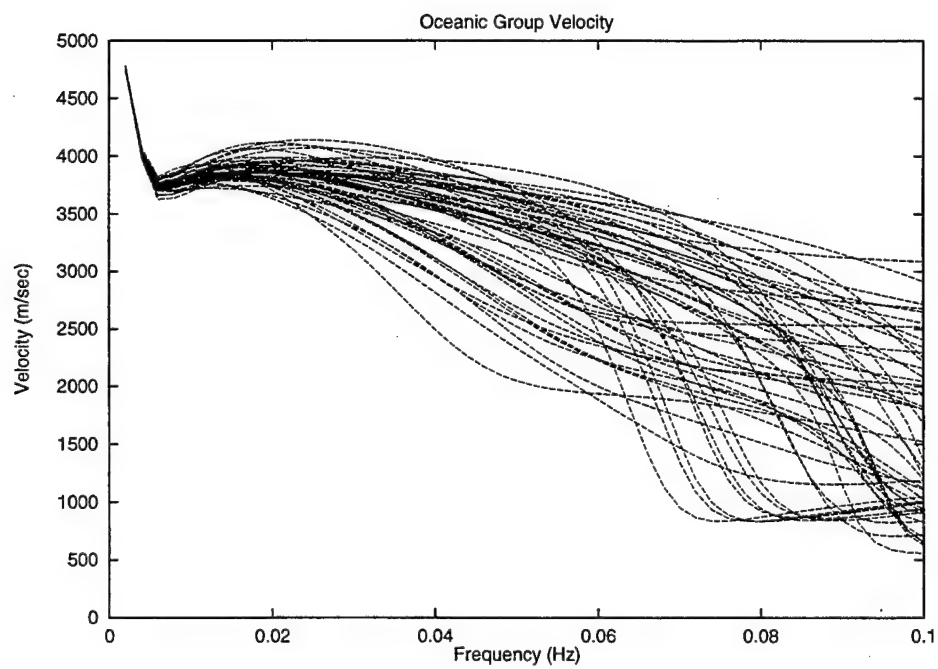


Figure 6. Oceanic group velocities.

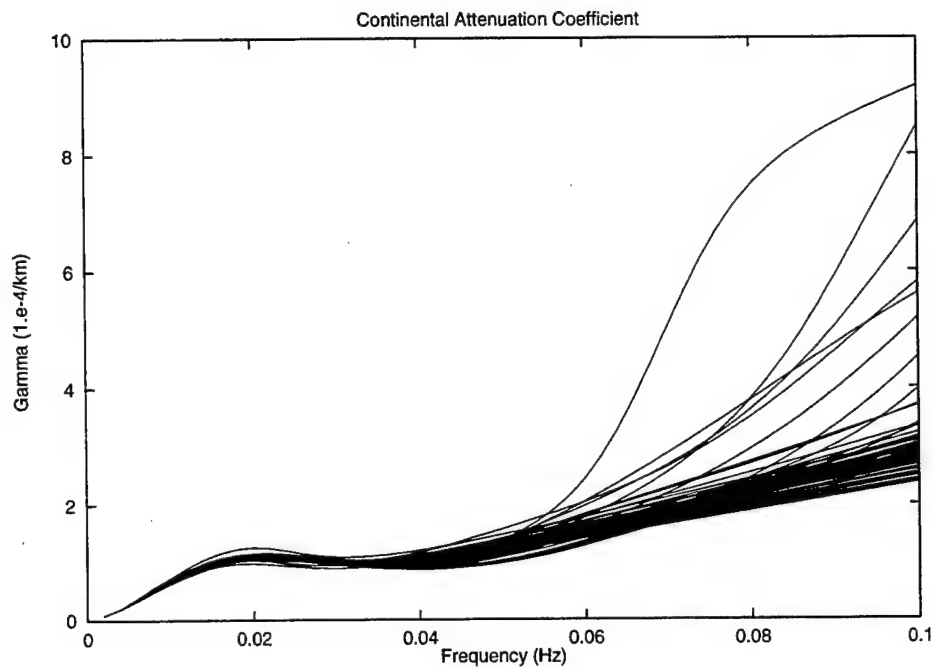


Figure 7. Continental attenuation coefficients  $\gamma$  ( $10^{-4}/\text{km}$ ).

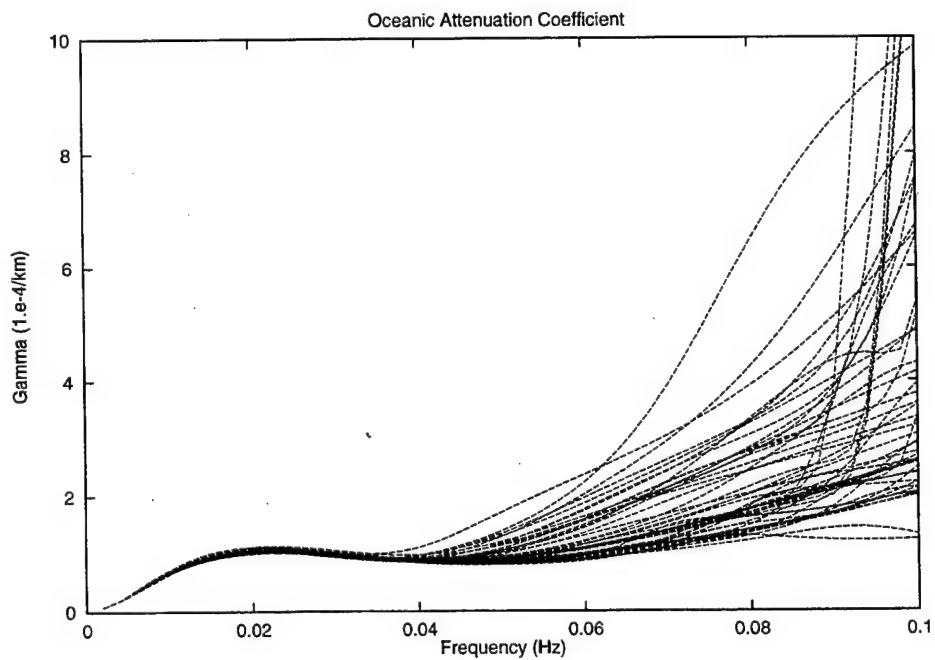


Figure 8. Oceanic attenuation coefficients  $\gamma$  ( $10^{-4}/\text{km}$ ).

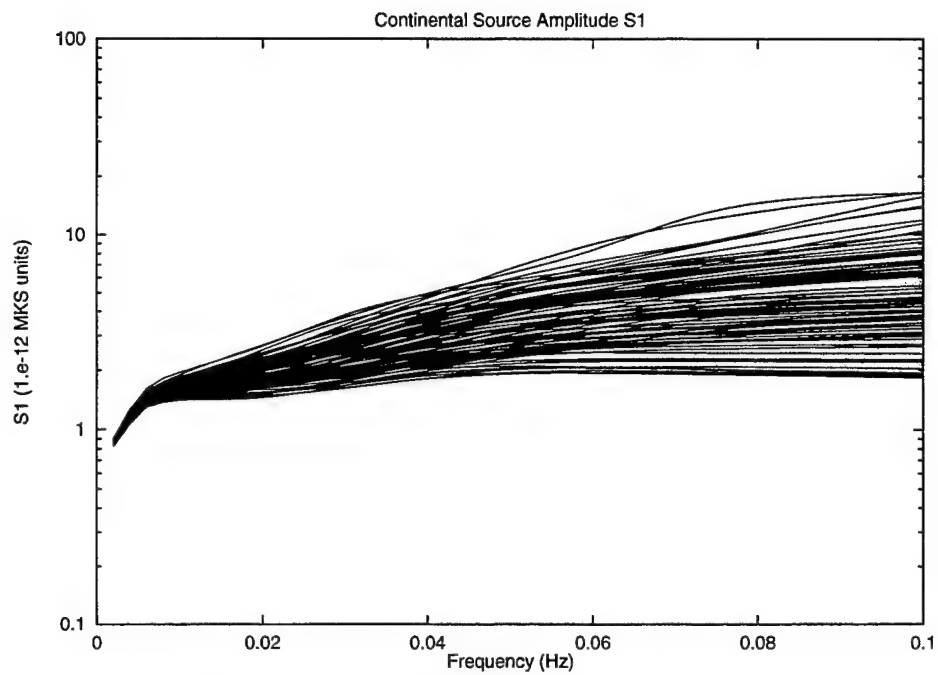


Figure 9. Continental amplitude factor  $S_1$  at 1 km depth.

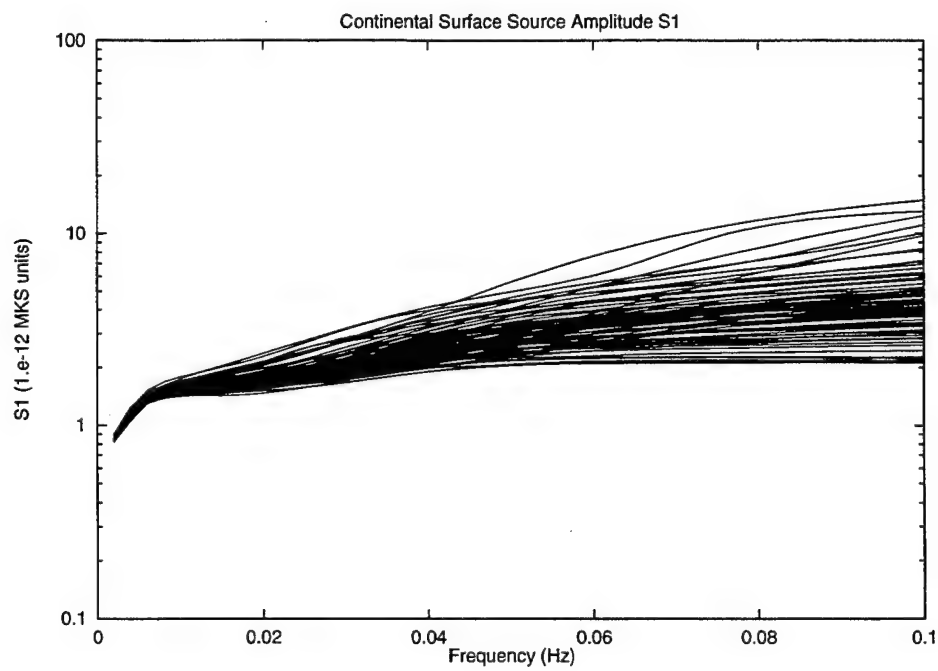


Figure 10. Continental amplitude factor  $S_1$  at zero depth.

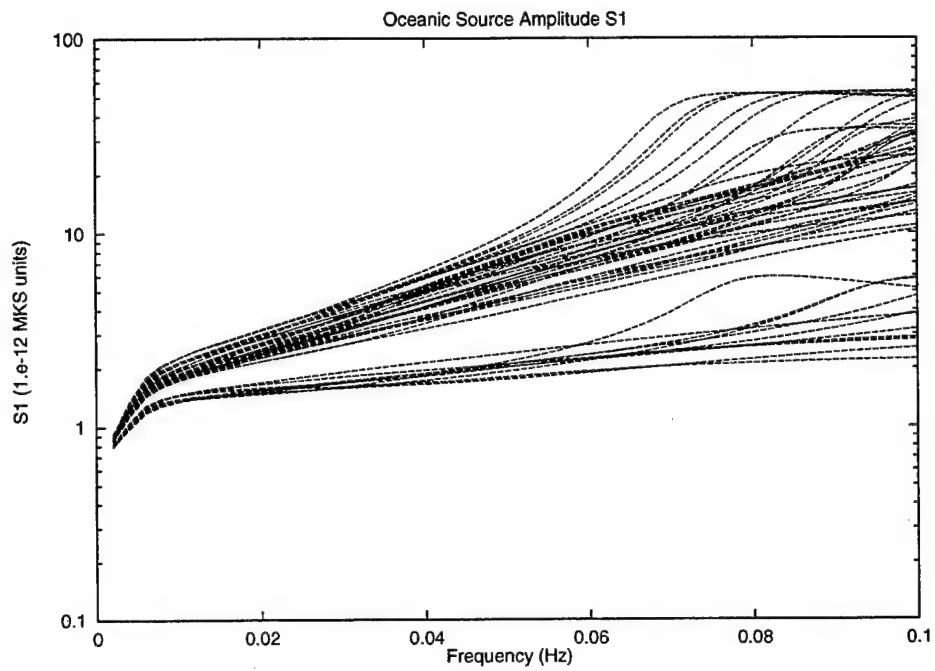


Figure 11. Oceanic amplitude factor  $S_1$  at depth 1 km below the ocean bottom.

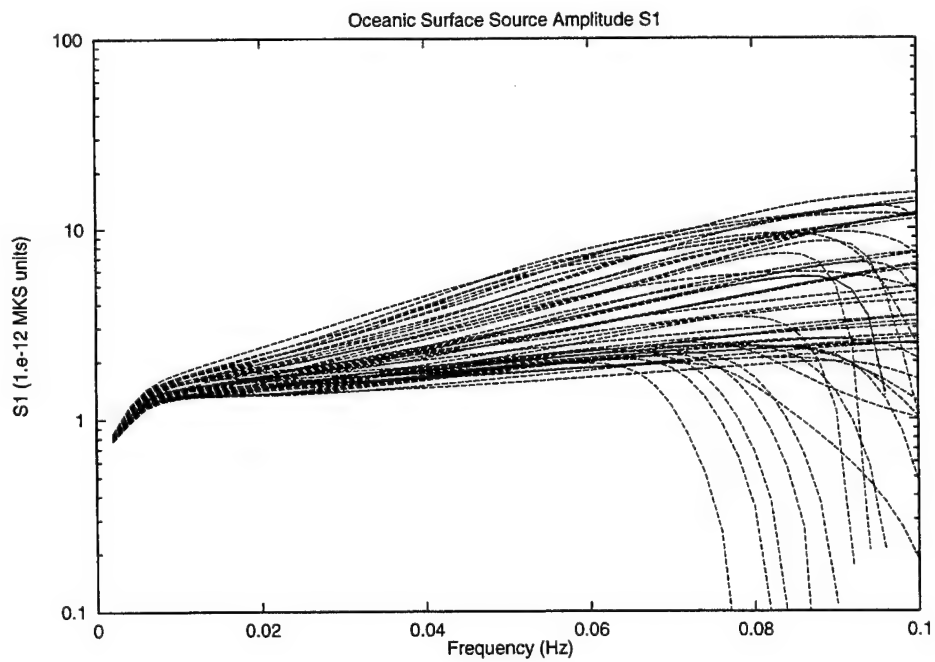


Figure 12. Oceanic source amplitude factor  $S_1$  at zero depth (at the ocean bottom).



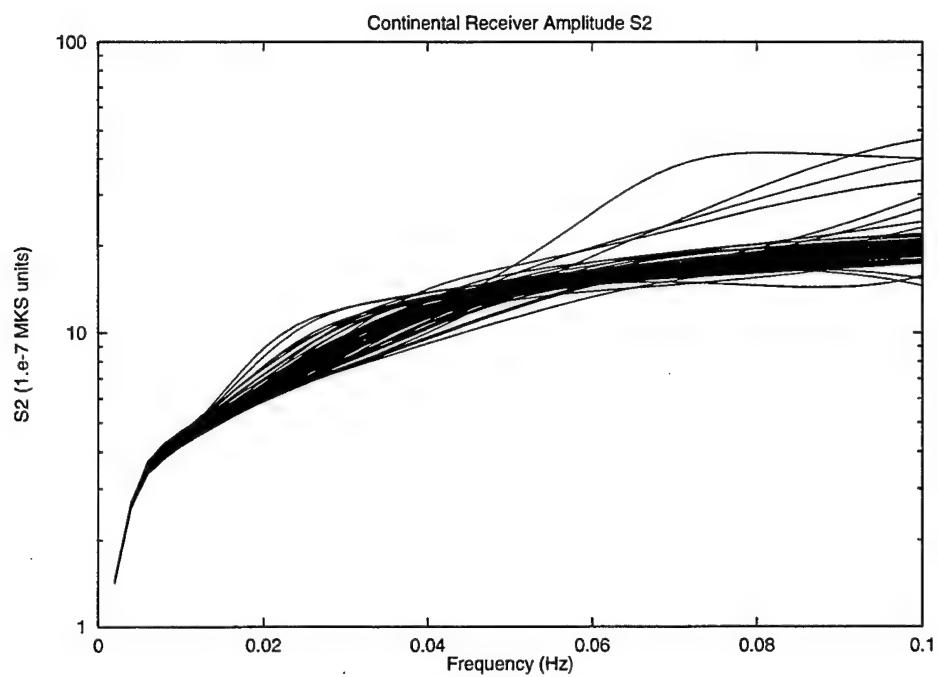


Figure 13. Continental receiver amplitude factor  $S_2$ .

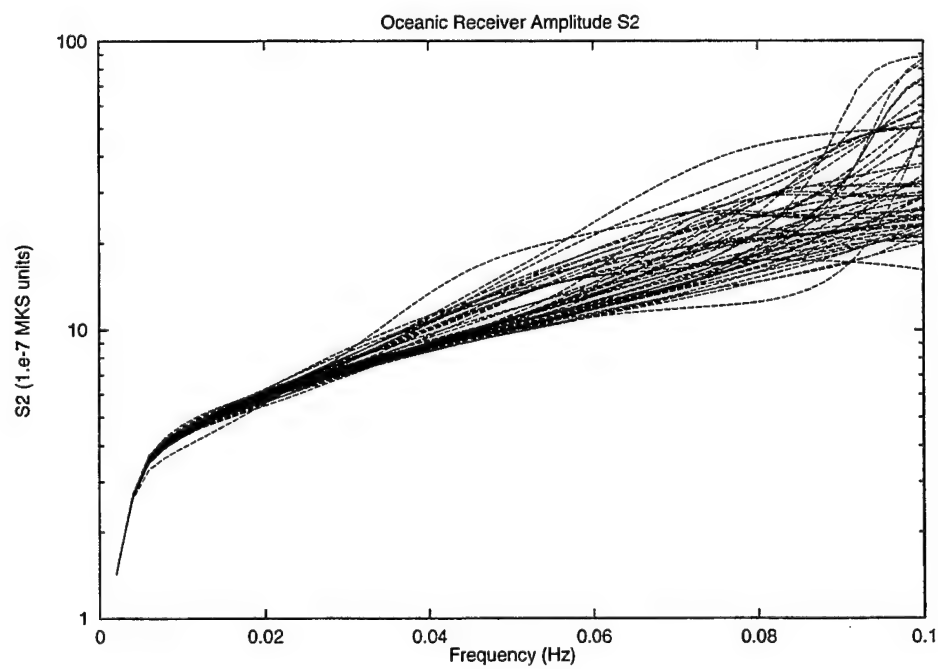


Figure 14. Oceanic receiver amplitude factor  $S_2$ .

#### 4.0 Automatic Surface Wave Identification and Measurement at the PIDC

All of the surface wave magnitudes currently being measured at the PIDC are identified and measured automatically with no operator intervention using the program Maxsurf, which has been developed and maintained by Maxwell Technologies. Surface waves are only measured using primary stations; for economic reasons, the PIDC does not request auxiliary station data in the surface wave arrival time window. Surface waves are identified in the following way: a set of narrow band filters are applied to the data over a set of 8 frequencies from 0.02 to 0.06 Hz. The arrival times at each frequency are then compared with predicted arrival times generated from the regionalized group velocity model described earlier. Until recently, the PIDC also applied a test based on azimuth estimated by 3-component polarization filtering; however, this test proved to be unreliable because of high noise levels on the horizontal components, frequent polarity errors and other problems. Consequently, this test was discontinued, although the azimuth is still estimated and stored in the database. At long period arrays, azimuths are estimated by beamforming, which is much more reliable than 3-component polarization filtering.

A few spurious or misassociated arrivals pass the dispersion test, and these are removed with a set of queries designed to identify them. Such misassociated arrivals may occur for several reasons. First, two events closely spaced in time may have surface waves in the same arrival time window. A common occurrence, for example, is an aftershock immediately following a large earthquake, or two aftershocks closely spaced in time and location. Second, two earthquakes in different locations may generate surface waves in the arrival time window at a small subset of stations. Third, a local event or random noise may just by chance pass the dispersion test. Until recently, the PIDC assigned multiple associations to the event with the larger magnitude. This is a dangerous assumption in a CTBT context, however, where an explosion hidden in an earthquake coda is a serious concern. A better assumption is to assign the arrival to the event with more arrivals at other stations.

A set of four queries are used to remove spurious and misassociated arrivals. First, a query is performed to identify all events with four or more arrivals and an initial assessment is made that these arrivals are properly associated. Second, association of any of these arrivals with other events are assumed to be incorrect and the redundant arrivals are removed. Third, isolated arrivals, which are defined as events with fewer than three arrivals all at distances greater than 60 degrees, are removed. Fourth, arrivals associated with more than one well-recorded event are removed. A side effect of this is that two large events closely spaced in time and location may have no surface wave arrivals in the REB because it is not possible to determine which event generated the surface waves; however, this is the correct approach for a CTBT monitoring system.

Surface waves are measured by first transforming the seismogram to a common (KS36000 long period) instrument. The largest amplitude in the 18-22 second period range within the predicted arrival time window is then identified and measured. Currently, the standard IASPEI formula  $M_s = \log A / T + 1.66 \log \Delta + 0.3$  is used to calculate  $M_s$  from the measured amplitude.

Spectral magnitudes can also be measured automatically, and the program Maxpmf was designed for this purpose. It performs all of the functions of Maxsurf, and adds a phase-matched filtering and path correction module which integrates a regionalized phase velocity model to generate a phase-matched filter and applies amplitude corrections to generate a path-corrected

spectral magnitude (scalar moment). Maxpmf works in essentially the same manner as Maxsurf, with the exception that Maxsurf will reject a seismogram if it can't find a 20 second (time domain) arrival within the predicted arrival time window. This often occurs at regional distances and there is no reason for such a restriction for spectral magnitudes. Consequently, moments will be measured for regional seismograms in many cases where standard  $M_s$  measurements cannot be made.

#### *4.1 Optimum Parameters for Surface Wave Processing*

In addition to the regionalized models, there are a few processing parameters that must be defined in order to perform automatic processing of surface wave arrivals. Following are a list of these parameters and their optimum values as determined by processing a large body of PIDC data and reviewing the results. These parameters are:

1. The phase-matched filtering time window. Phase-matched filtering (e.g. Herrin and Goforth, 1977) compresses the waveform into a narrow time window centered near zero time, allowing noise to be windowed out by taking the spectrum of this narrow window rather than the full seismogram time window. However, the amount of compression depends on how well the phase-matched filter matches the actual phase of the seismogram. With accurate phase-matched filters and event origin time and locations, it is possible to use a time window as small as  $\pm 50$  seconds. However, if the time window selected is too small, part of the signal will be windowed out, resulting in inaccurate, low amplitude estimates. Our review of the compressed spectra showed that while compression along most paths is very good, complex paths such as paths grazing the Pacific rim, and certain other paths not well constrained by data in the inversion, such as paths near and across Antarctica, either do not compress as well, or compress to an arrival time different from zero. We found that a time window of  $\pm 150$  seconds is sufficient to capture the complete surface wave arrival for nearly all paths while still providing significant noise reduction.
2. The frequency band used to average the spectrum to estimate the moment. For our test cases we used a frequency band of 0.02-0.05 Hz for all data, and found that this worked quite well, giving a nearly flat spectrum over this frequency band for most data. As discussed in Section 2, in principle any frequency band could be used, and a higher frequency band may be required for very short paths. For oceanic paths, however, the surface wave spectra and dispersion curves become quite variable above frequencies of about 0.06-0.08 Hz. In our tests, we found that oceanic spectra were flat up to about this range and then dropped precipitously at higher frequencies. We therefore recommend using frequencies below 0.06-0.08 Hz for oceanic paths, while higher frequencies should be usable for continental paths, particularly if the earth structure and dispersion are well defined.
3. The frequencies used for narrow band filtering to compare with predicted group velocity arrival times. For all of our test cases we used the following 8 frequencies: 0.02, 0.025, 0.03, 0.035, 0.04, 0.045, 0.05, 0.06 Hz. Again, for short continental paths, a higher set of frequencies could be used.
4. The allowable error in the group velocity arrivals, and the fraction of group velocities that are required to match the predicted arrival times. We require that a minimum of 70% of the group

velocity points, 6 out of 8 in this case, fall within the predicted arrival time window. This is sufficient to remove most "accidental" arrivals where the arrival peaks of noise just happen to fall into the arrival window. Frequently, one or two arrival times will be out of range because of low signal/noise, interference, or other factors, and this requirement allows such arrivals to be identified. The group arrival time  $t$  is required to be within the time window given by

$$\frac{r}{v_p + v_0} - p_0 T - t_0 < t < \frac{r}{v_p - v_0} + p_0 T + t_0 \quad (4.1)$$

where  $r$  is the source to receiver distance,  $v_p$  is the predicted group arrival time,  $T$  is the period, and  $v_0$ ,  $p_0$ , and  $t_0$  are user definable constants. For our test cases we used  $v_0=0.2$ ,  $p_0=1.0$ , and  $t_0=0$ . This has the effect of changing the allowed group velocity window from about 0.2 km/s at large distances to about 0.3 km/s at regional distances. This is necessary because a fixed group velocity window corresponds to a very large time window at large distances, increasing the chance for spurious arrivals.

5. The narrow band filter  $Q$ . The narrow band filter  $F(f)$  is defined by  $F(f) = \exp(-\alpha(f - f_c)^2)$

where  $\alpha = \frac{\ln 2}{2} \left( \frac{Q}{f_c} \right)^2$ ,  $f_c$  is the center frequency, and  $Q$  is the filter  $Q$ . In general,  $Q$  should be smaller for closer distances and larger for large distances, with a reasonable range being from about 8 to 20. A lower  $Q$  value gives better time resolution, while a higher  $Q$  smoothes the time series for more distant seismograms have traveled on complex paths. A narrow band filter  $Q$  of 15 is a good average value to use over a wide distance range.

#### 4.2 Comparison of PIDC $M_s$ with USGS $M_s$

The U. S. Geological Survey (USGS) publishes reports of surface wave arrivals in the Earthquake Data Reports (EDR). It is instructive to compare the arrivals in the EDR's with the arrivals in the Reviewed Event Bulletin (REB) produced by the PIDC. There are some significant differences in the way the events are processed. All PIDC arrivals are generated automatically as described above, while USGS  $M_s$  values are measured manually. The network reporting to the USGS is much larger than the International Monitoring System (IMS) network used at the PIDC. The average number of stations reporting surface wave arrivals in the EDR's is 24, compared with 5 in the REB. The networks are almost completely disjoint. There are only 9 stations in common to the two networks. All surface waves seismograms measured by the PIDC are first transformed to a KS36000 instrument response, while data reported to NEIC is recorded on a wide variety of long period and broadband systems. The PIDC processes surface wave arrivals only in the distance range 20-100° while the EDR's include more distant stations. Comparison of the two bulletins therefore can be used to test the consistency of surface wave measurements made almost completely independently.

Surface wave analysis procedures at the PIDC were changed significantly on February 15, 1997. Prior to that time the measurement algorithm picked a peak close to 20 seconds using a weighting scheme based on the difference between the measured peak and 20 seconds. The revised procedures are identical to those used by the USGS, where the largest peak in the 18-22 second period range is used. Also, prior to this time the surface wave identification test was overly

conservative, causing many valid surface wave arrivals to be rejected. The change in procedures resulted in an increase in LR detection rate of about a factor of 3. The following analysis uses data from the EDR and REB for the time period February 15, 1997 through July 29, 1997. We exclude the time period from April 3, 1997 through June 23, 1997. During this time period an error in the database caused errors in the amplitudes at 9 of the IMS stations and caused no arrivals to be reported from 10 other stations with long period or broadband data. For the remaining time period there were 187 events with  $M_s$  reported in both bulletins. There were 234 arrivals measured by stations that are common to both networks. During this time period, there were a total of 6600 surface wave arrivals from 269 events reported in the EDR and 5414 arrivals from 1221 events reported in the REB, so although there were 20% more arrivals reported in the EDR, surface waves were reported from 4.5 times as many events in the REB.

Figure 15 shows a cumulative distribution (fraction of arrivals reported greater than a given amplitude) of arrival amplitudes in the EDR and REB for the time period studied, with the REB bulletin also separated into arrivals reported by 3 component stations and the four long period arrays. The 90% detection thresholds calculated from this data are 55 nm, 95 nm, and 645 nm for IDC arrays, IDC 3-component stations, and the EDR bulletin, respectively, so the detection threshold for the REB is about an order of magnitude lower than for the EDR.

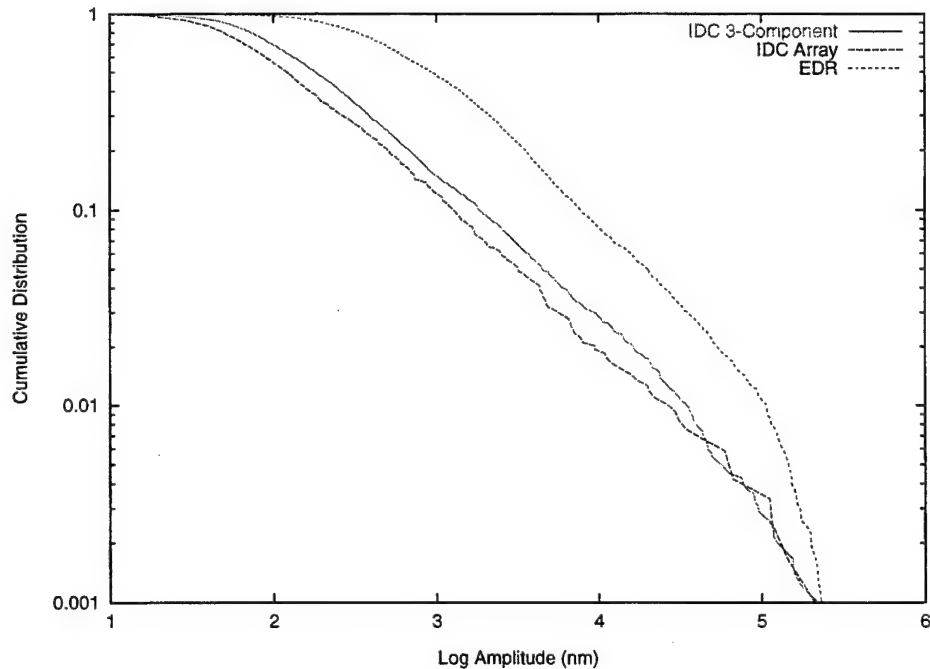


Figure 15. Cumulative distribution of PIDC and NEIC amplitudes.

There is also a small bias between the REB and the EDR. The average difference in  $M_s$  between the two bulletins is  $M_s(\text{EDR}) - M_s(\text{REB}) = 0.12 \pm 0.23$ . However, closer examination of the station data showed that station ILAR is consistently low and probably contains a calibration error. Removing this station reduces the bias to  $M_s(\text{EDR}) - M_s(\text{REB}) = 0.08 \pm 0.23$ . Figure 16 shows  $M_s(\text{REB})$  plotted as a function of  $M_s(\text{EDR})$  with ILAR removed from the REB.

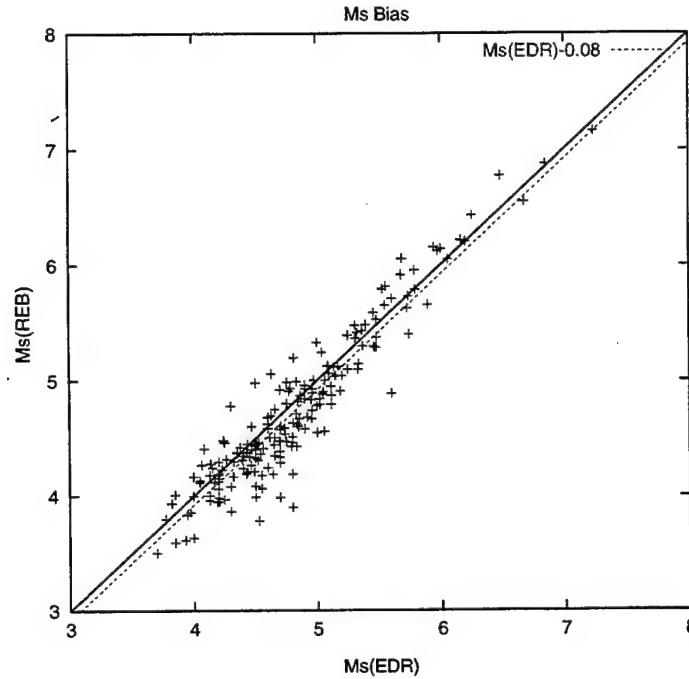


Figure 16. PIDC vs. NEIS  $M_s$  shows a bias that increases with decreasing magnitude.

We investigated several possible causes for the bias. First, we looked at measurements at the stations that are common to the two networks. For these arrivals, the bias is  $M_s(\text{EDR}) - M_s(\text{REB}) = -0.02 \pm 0.10$ , so the station bias is very small and in the opposite direction from the network bias. The effects of the difference in measurement methods therefore do not appear to be significant. Another contributing factor is the distance range. The average reporting distance for the REB is  $63^\circ$  compared with  $79^\circ$  in the EDR. As discussed later in this report (Section 7), the  $1.66 \log \Delta$  distance correction used in the  $M_s$  formula overcorrects the amplitude causing  $M_s$  to increase with distance. This causes a bias of about 0.03 magnitude units between the two networks. The main remaining difference appears to be censoring in the EDR data, the loss of low amplitude signals near the detection threshold. This can be seen by looking at the bias for different magnitude ranges. For events with  $M_s > 5$  in both bulletins, the bias is  $M_s(\text{EDR}) - M_s(\text{REB}) = -0.03 \pm 0.016$  (48 events), while for events with  $M_s < 5$  the bias is  $M_s(\text{EDR}) - M_s(\text{REB}) = 0.11 \pm 0.023$  (124 events). So the bias increases by 0.14 magnitude units over this magnitude range. Censoring also occurs in the REB data; however, because the detection threshold is lower, it occurs at a lower magnitude.

## 5.0 Maximum Likelihood Moment and $M_s$

Maximum likelihood magnitudes were originally developed to correct for censoring. As discussed in the last section, for small events it is common for larger arrivals to be measurable while smaller arrivals are lost in noise, causing the average magnitude of the observed arrivals to be biased high. Similarly, for very large events, the largest arrivals may be clipped and therefore discarded, causing the average magnitude of the remaining arrivals to be biased low. Maximum likelihood magnitudes correct for censoring by including the measured noise level as an upper

bound on the observed amplitude at a station. This correction, together with station corrections that are derived as part of the processing, lead to more consistent and reliable network magnitudes.

To evaluate the effect of using maximum likelihood time domain and spectral magnitudes, we ran the automatic surface wave processing program Maxpmf on a data set of 10 days of continuous PIDC data from June, 1997, with data from 517 earthquakes, together with a data set of historical explosion seismograms from 253 underground nuclear tests from several test sites. All data was processed and measurements from seismograms for which a signal was not found were used as noise measurements in the maximum likelihood processing. Maximum likelihood magnitudes and moments were calculated using the method of McLaughlin (1988). Network magnitudes for all events and station corrections for all stations were calculated simultaneously using a maximum likelihood general linear model (GLM). One complication is that the networks used for recording nuclear explosions and the current IMS network have no stations in common, which causes nonuniqueness in the GLM calculation. The nonuniqueness exists despite the standard constraint that the sum of all station corrections is zero. To address this problem we added a fictitious station with a magnitude equal to the average magnitude of each event to all of the events. This has the effect of linking the old and new data and stabilizing the inversion. The expectation maximization algorithm used in the GLM minimizes the offset for the fictitious "station" and therefore we find the solution "closest" to the network average. Tables of station corrections derived from the calculation are given in Appendices D and E, and tables of maximum likelihood magnitudes and moments are given in Appendices F and G. Histograms of station corrections for  $M_s$  and moment are shown in Figure 17. 90% of station corrections are within  $\pm 0.35$  magnitude units. Some of the larger station corrections may indicate calibration errors at those stations.

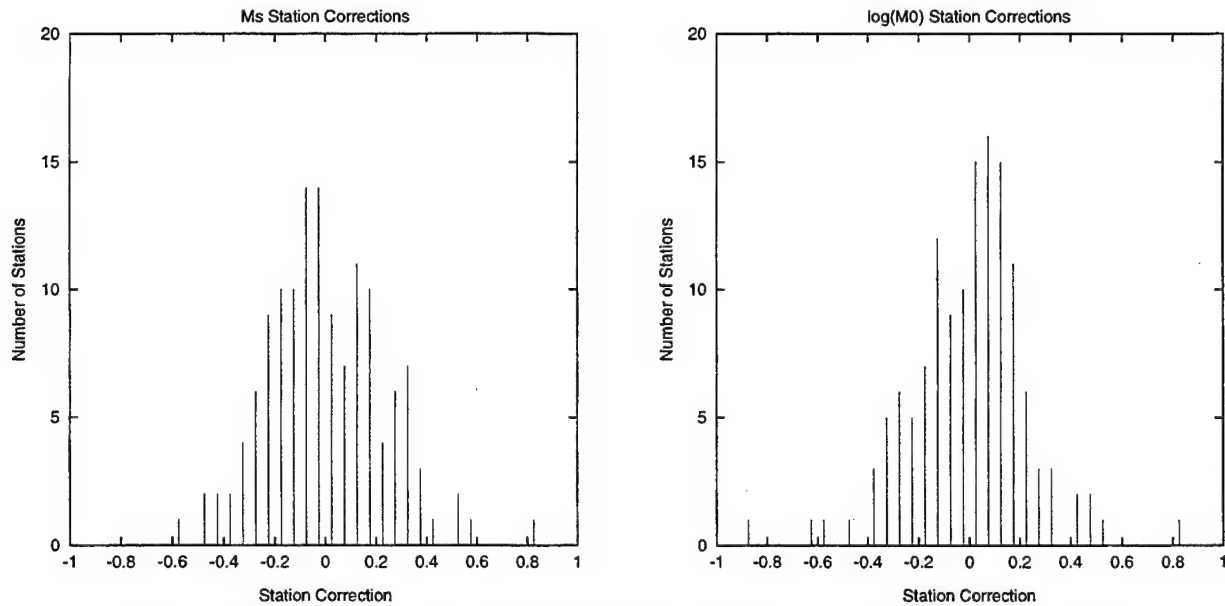


Figure 17. Histograms of maximum likelihood station corrections for  $M_s$  (left) and  $\log M_0$  (right).

Figure 18 and Figure 19 show the effect of the censoring correction on  $M_s$  and  $\log M_0$  for this data set. Note the resemblance between Figure 17,  $M_s$  with and without the censoring correction, and Figure 16 showing REB  $M_s$  plotted vs. EDR  $M_s$ .

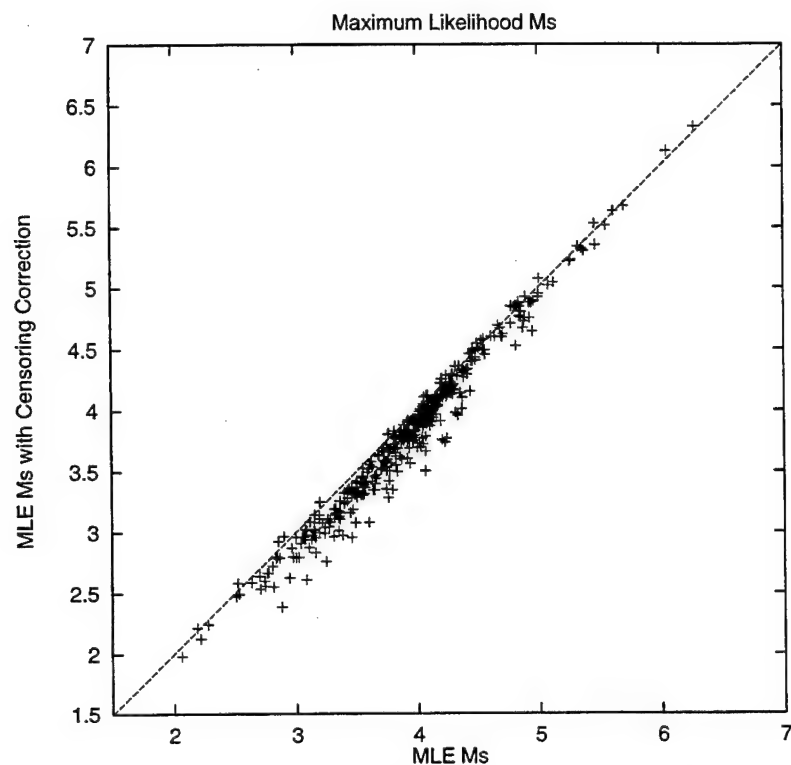


Figure 18. Maximum likelihood GLM  $M_s$  with and without censoring correction.

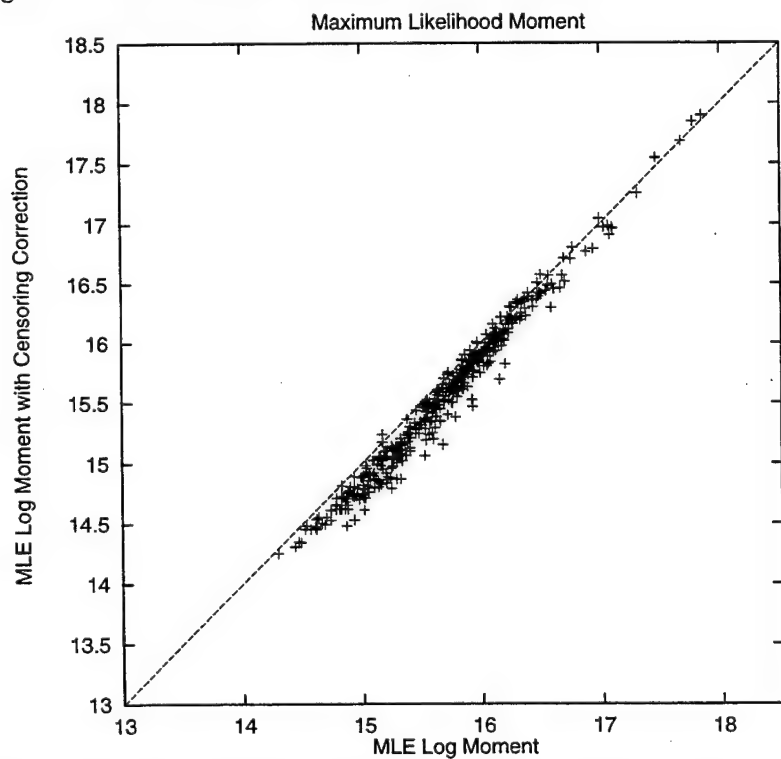


Figure 19. Maximum likelihood GLM  $\log M_0$  with and without censoring correction.



In a CTBT context, the most important consequence of using maximum likelihood magnitudes is the ability to determine an upper bound on a magnitude when there is no measurable data. Because  $m_b - M_s$  may be as large as 2 magnitude units for an underground nuclear test, surface waves will rarely be observable for explosions with  $m_b$  less than 4, and may be difficult to observe up to  $m_b$  5. A large earthquake may obscure surface waves from even larger explosions. However, it is possible to determine an upper bound on  $M_s$  for these events and in many cases this will be sufficient to identify the event as an explosion. The definition of "upper bound" used here is the magnitude that has a 50% probability of having no detections at the stations recording noise in the arrival time window. This definition was selected because it is consistent with the definition of maximum likelihood magnitudes. The "upper bound" magnitude of an event with only noise measurements is approximately the same as the magnitude of an event with the same noise measurements except for a single signal with the amplitude of the smallest noise measurement. Both magnitudes and upper bounds are calculated using the maximum likelihood station corrections described above. For the events studied here, we found upper bounds on  $M_s$  and  $\log M_0$  for 298 earthquakes and 46 explosions. Figure 20 shows maximum likelihood  $M_s$  plotted vs. maximum likelihood moment, including both values and upper bounds. Maximum likelihood  $M_s$  and  $\log M_0$  are related by  $\log M_0 = M_s + 11.74 \pm 0.21$ .

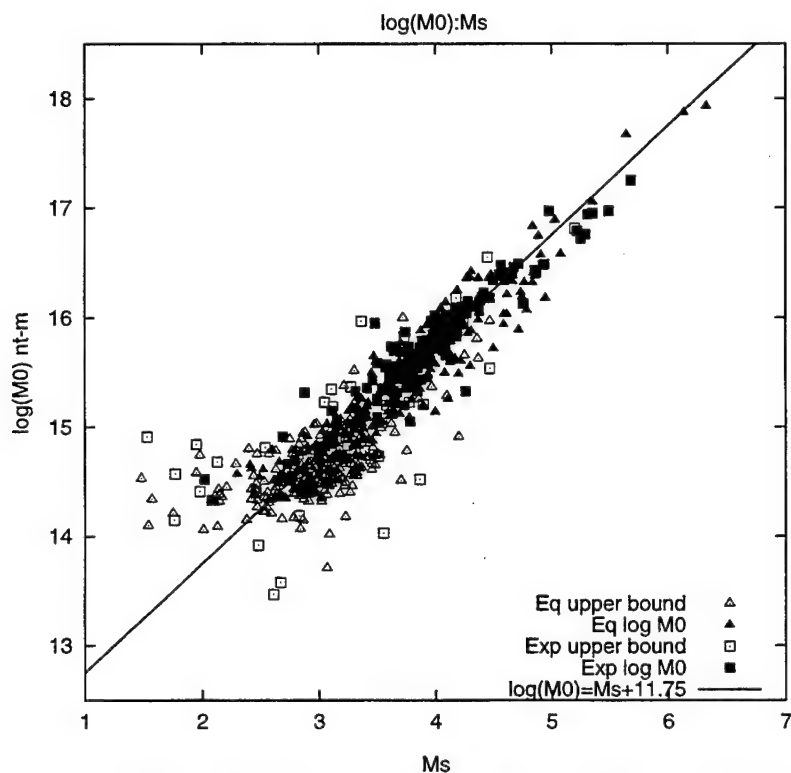


Figure 20. Maximum likelihood log moment plotted vs. maximum likelihood  $M_s$ .

Following are some factors that need to be kept in mind when using maximum likelihood magnitudes.

1. Noise measurements need to be made as accurately as signal measurements. In particular, it is extremely important to avoid including bad data from a malfunctioning instrument. In a

maximum likelihood calculation a low but meaningless value will strongly bias the results causing an unrealistically low magnitude. This is true both for maximum likelihood magnitudes and maximum likelihood upper bounds.

2. Signal identified as noise will cause the magnitudes to be biased slightly low. This may or may not be significant depending on how frequently it occurs. Stevens and McLaughlin (1996) identified this as a problem with PIDC  $M_s$  values because the overly conservative identification criteria missed a large fraction of the signals. With the new procedures in place since February 1997, however, this no longer appears to be a problem.
3. For time domain magnitudes, it may not be possible to obtain a reliable noise measurement in the 18-22 second period range, particularly when broadband instruments are used. Replacing the instrument with a standard long period instrument helps significantly, but will not completely eliminate the problem. Spectral magnitudes including  $\log M_0$  are not affected by this problem.
4. Very small events may still be biased by censoring. This occurs, for example, when a small event is recorded only at one close station and all noise measurements are significantly higher than the signal. In that case, the maximum likelihood magnitude will be equal to the signal measured magnitude.
5. Maximum likelihood procedures and upper bounds reduce but do not eliminate the problem of masking by coda of large events. As can be seen in the figures in the following section, it is sometimes possible to identify an event as an explosion if surface waves from the explosion are hidden in earthquake coda; however, if the coda is large enough the explosion will still be obscured. An earthquake cannot be identified by the upper bound alone. The use of regional data and auxiliary stations would help to alleviate this problem.

## 6.0 Earthquake/Explosion Discrimination Using the $M_s:m_b$ and $M_0:m_b$ Methods.

Figures 21 and 22 show maximum likelihood GLM  $\log M_0$  and  $M_s$  plotted vs.  $m_b$  for the data set of PIDC data and historical explosion data described above.  $M_b$  values for earthquakes are from the PIDC database, and for explosions are a mixture of values from AWRE, NEIS and ISC. Open symbols indicate upper bounds on moment and  $M_s$ , while solid symbols indicate events with at least one measured surface wave.

Also shown in Figures 21 and 22 is an approximate discrimination line between the earthquake and explosion populations. Note that most of the explosions with no observations clearly fall into the explosion population based on the upper bound of either moment or  $M_s$  for the event. The best separation line has a slope of 1.4, which differs from the 1.0 slope that is expected at low magnitudes (e.g. Stevens and Day, 1985). There are several possible reasons for this. First, although only events with depths less than 75 km are plotted here, many small earthquakes have constrained or inaccurate depths. Small earthquakes with large  $m_b$ - $M_s$  may therefore be deep in many cases. Second, the  $m_b$  values are not maximum likelihood values, and therefore are subject to censoring, causing  $m_b$  to be biased high for small events. Consequently, we can expect that discrimination will be improved, and the slope of the discrimination line reduced, if maximum likelihood  $m_b$ 's are used, and deep earthquakes are removed. The explosion  $m_b$  values should also

be systematically reevaluated since the PIDC measurements are biased low relative to current NEIS  $m_b$  values (Murphy and Barker, 1996) due to differences in the way instrument response corrections are implemented, and the bias compared to historical  $m_b$  values has not been assessed.

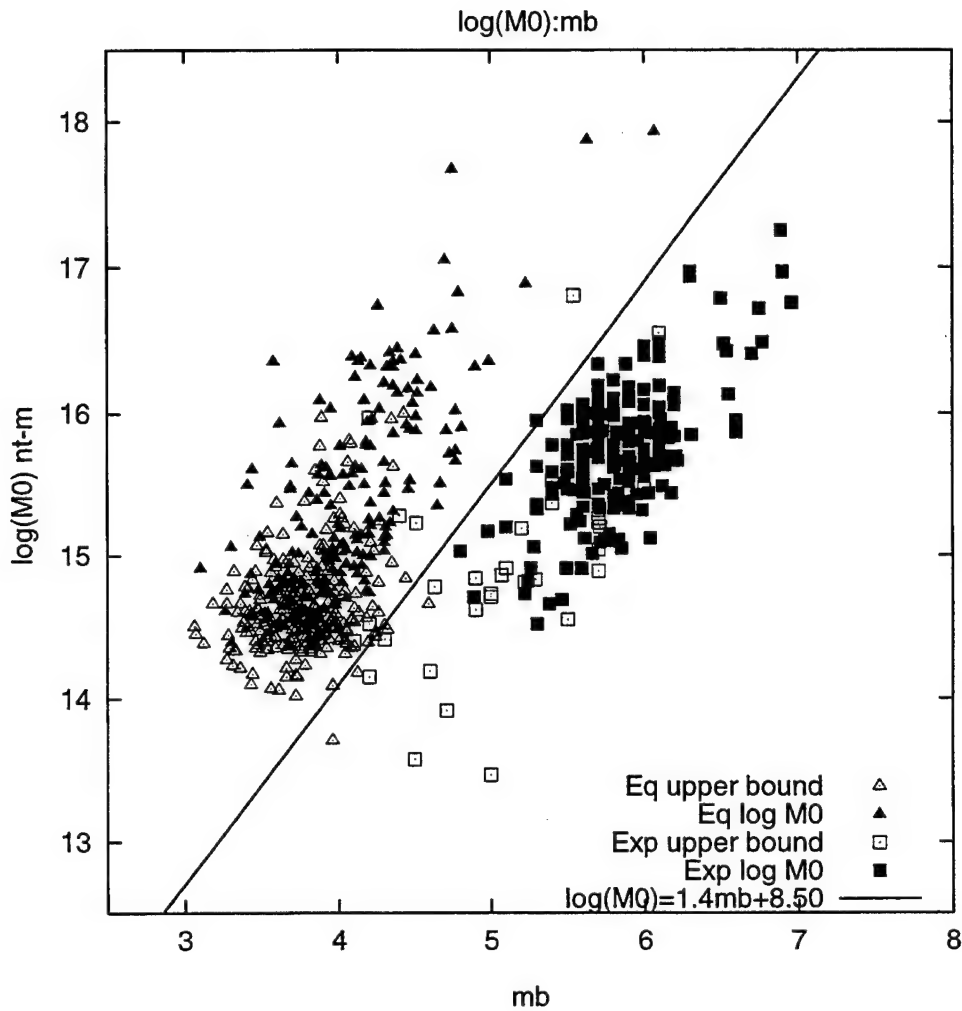


Figure 21. Maximum likelihood GLM station corrected  $\log M_0$  and  $\log M_0$  upper bounds plotted vs.  $m_b$  for PIDC earthquakes and historical explosion data.

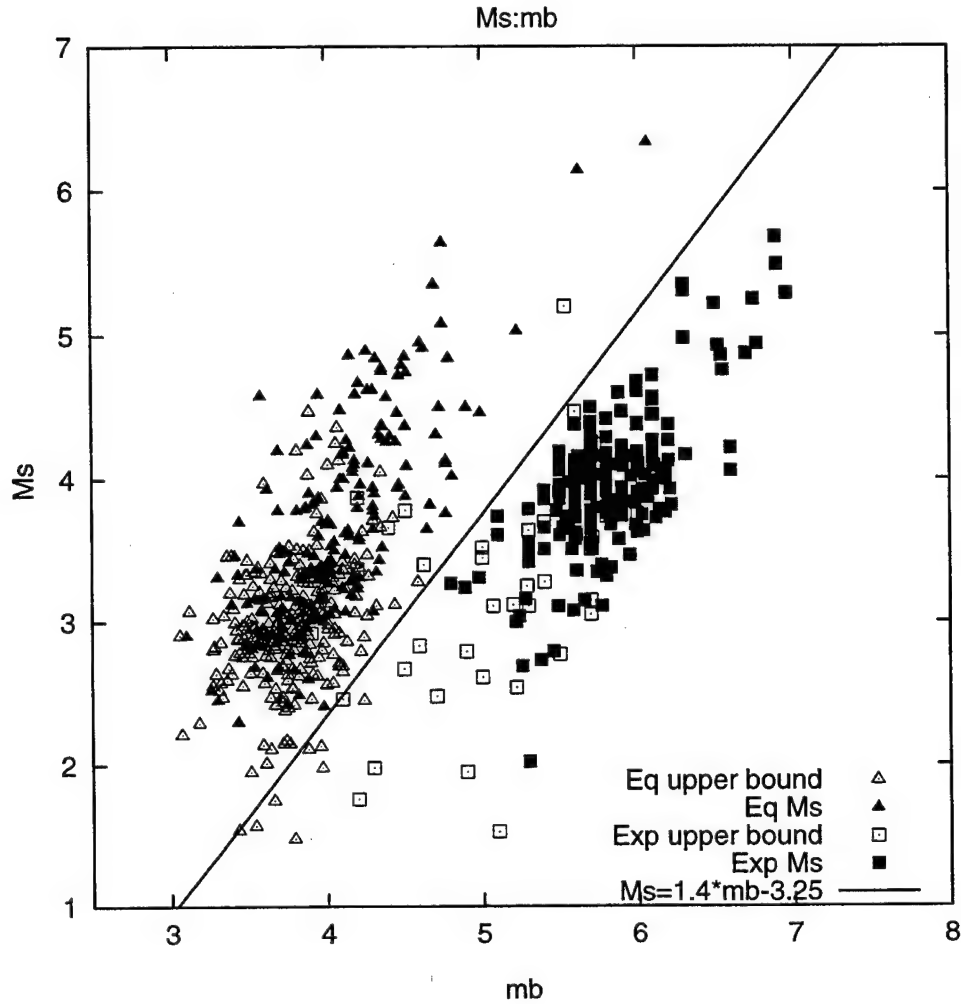


Figure 22. Maximum likelihood GLM station corrected  $M_s$  and  $M_s$  upper bounds plotted vs.  $m_b$  for PIDC earthquakes and historical explosion data.

### 7.0 Optimum Distance Corrections for Moment and $M_s$

A serious problem when using  $M_s$  for discrimination purposes is the variation in  $M_s$  with distance. In particular,  $M_s$  based on the IASPEI formula becomes anomalously small at distances less than about  $25^\circ$ , where the surface wave signal to noise ratio is best, because the standard  $M_s$  distance correction is incorrect. Consequently, a different distance correction is required if surface waves are to be used for discrimination at close range.

Similarly, spectral magnitudes also require an accurate distance correction. For the scalar moment,  $\log M_0$ , described previously, distance correction depends on the accuracy of the attenuation coefficients (Eq (2.2)) derived from a regionalized earth model. Unlike  $M_s$ , however, errors in  $\log M_0$  become smaller with decreasing distance as the attenuation term  $-\gamma_p(\omega)r$  becomes smaller.  $\log M_0$  is therefore expected to be more stable at short distances.

In order to estimate the magnitude of the distance correction effect, and to determine the optimum distance correction, we examined the attenuation rate of the maximum likelihood moment and  $M_s$  described in the previous section. Figure 23 shows the moment residual  $\log M_0 - \overline{\log M_0}$  at each station for all events with four or more arrivals. The  $\log M_0$  residuals are remarkably distance independent, particularly considering the relatively simple Q models used in the earth structures. This indicates that the attenuation coefficients derived from the Q models are approximately correct. The average attenuation coefficient for the earth models at a period of 20 seconds is  $0.0114 \pm 0.0022/\text{degree}$ .

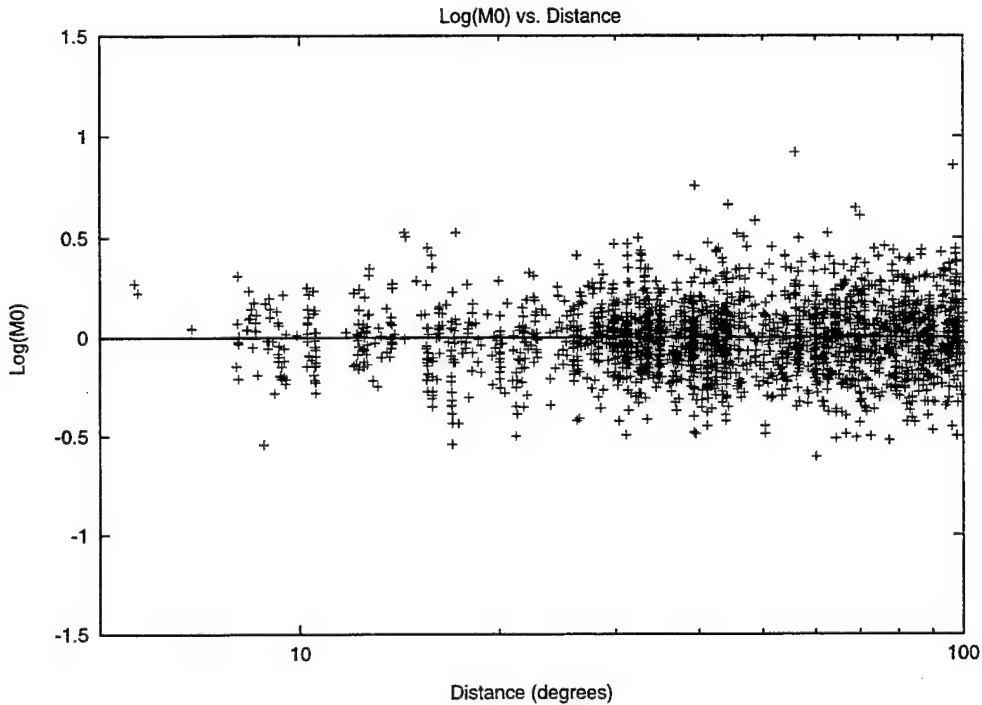


Figure 23. Moment residuals vs. distance derived using regionalized earth models. The residuals exhibit very little distance dependence.

The appropriate distance correction for  $M_s$  has been discussed by a number of authors (von Seggern, 1975a, 1975b; Thomas *et al.*, 1978; Marshall and Basham, 1972; Herak and Herak, 1993; Rezapour and Pearce, 1997). The IASPEI formula for  $M_s$  used here and in most bulletins is:

$$M_s = \log \frac{A}{T} + 1.66 \log \Delta + 0.3 \quad (7.1)$$

where  $A$  is the zero to peak amplitude between 18 and 22 seconds in nanometers,  $T$  is the measured period, and  $\Delta$  is the source to receiver distance in degrees. All of the referenced studies concluded that the distance correction used in the IASPEI formula overcorrects the amplitude at short range. Von Seggern (1975b) recommended replacing the slope of 1.66 with a slope of 1.08, and Herak and Herak (1993) with 1.094. Marshall and Basham (1972) replaced the  $M_s$  formula with a set of tables depending on distance, period, and earth structure type. Thomas *et al.* (1978) found that the attenuation rate changed from  $0.8 \log \Delta$  at regional distances to  $1.5 \log \Delta$  at large distances, with a best fitting average slope of 1.15. Rezapour and Pearce (1997) recommended

using either a slope of 1.155 or replacing the  $M_s$  formula with a form based on the theoretical Rayleigh wave attenuation equation. As several of these studies note, the theoretical Rayleigh wave attenuation does not have the functional form used in the equation for  $M_s$ . Using a saddle point approximation, it can be shown (Sato, 1967) that the time domain Rayleigh wave has the same form as the frequency domain Eq (2.1), except for an additional attenuation factor of  $\Delta^k$  where  $k=1/2$  for a dispersed Rayleigh wave and  $k=1/3$  for an Airy phase. Using this relation,  $M_s$  can be written as:

$$M_s = \log A + k \log \Delta + \frac{1}{2} \log(\sin \Delta) + \gamma \Delta \log e + D \quad (7.2)$$

Rezapour and Pearce (1997) recommended using this form for  $M_s$  using the Airy phase value of  $1/3$  for  $k$  and using a value of .0105 for  $\gamma$ . Eq (7.2) can also be written using  $\log(A/T)$  and increasing  $D$  by  $\log(20)$ .

Figure 24 shows the  $M_s$  residuals with  $M_s$  calculated using the IASPEI formula. The residuals show a pronounced distance dependence, particularly at closer distances. We solved Eq (7.2) for  $\gamma$  and  $D$  minimizing the residual in  $M_s$  for  $k=1/2$  and  $k=1/3$ . With  $k=1/2$ , the best solution is  $\gamma=0.0120$ ,  $D=0.734$ , and for  $k=1/3$ , the best solution is  $\gamma=0.0158$ ,  $D=0.925$ . The dashed lines in Figure 24 shows the calculated residual from the IASPEI  $M_s$  using Eq (7.2) with these values and the recommended values from Rezapour and Pearce (1997) with the arbitrary constant  $D$  adjusted to best fit the data. Although the best fit curves match the data better than the Rezapour and Pearce equation for this data set over this distance range, the difference is small compared to the scatter in the data so it is not possible to select the preferred distance correction based on this information alone. Both the fit with  $k=1/2$  and the Rezapour and Pearce equation have  $\gamma$  values consistent with  $\gamma$  calculated from the regionalized models and used for moment estimation.

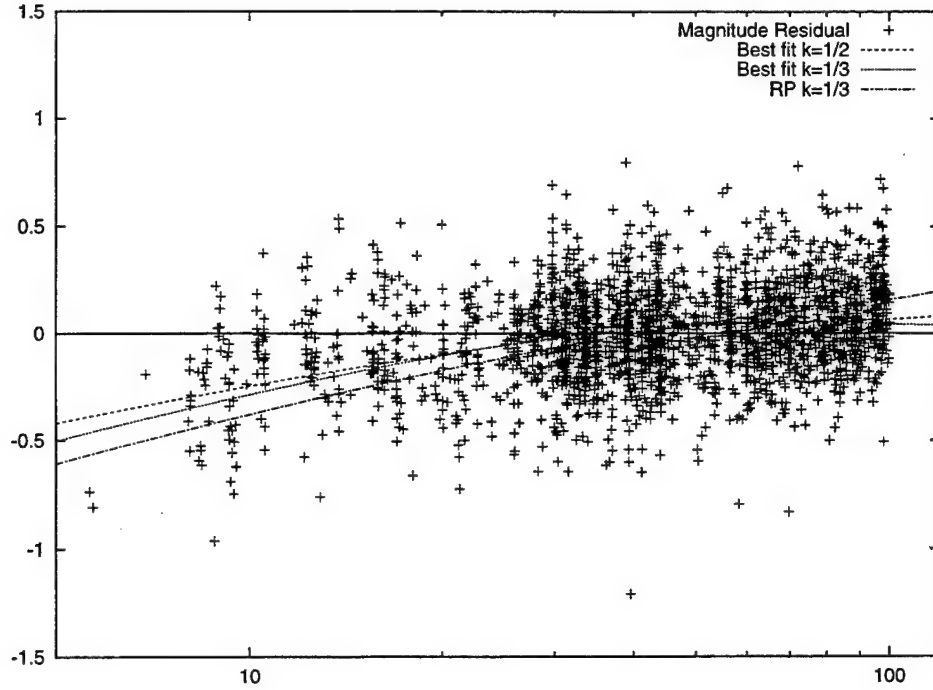


Figure 24.  $M_s$  residuals vs. distance calculated using the IASPEI  $M_s$  formula. The residuals exhibit a strong distance dependence with lower values at shorter distances. The lines labeled "Best fit" are a fit to the data using Eq (7.2) with  $k=1/2$  and  $k=1/3$ , and "RP" refers to the values recommended by Rezapour and Pearce (1997).

Since the constant  $D$  in Eq (7.2) is arbitrary, it can be adjusted to be consistent with other  $M_s$  values.  $M_s$  calculated from Eq (7.2) is equal to IASPEI  $M_s$  at  $100^\circ$  if  $D=0.80$ , slightly higher than the best fit value for the data in the  $20^\circ$ - $100^\circ$  range, and we recommend using this value for better consistency with other  $M_s$  measurements. This leads to the following formula for  $M_s$  based on the best fit curve with  $k=1/2$ :

$$M_s = \log A + \frac{1}{2} \log \Delta + \frac{1}{2} \log(\sin \Delta) + 0.00524\Delta + 0.80 \quad (7.3)$$

Similarly, the Rezapour and Pearce (1997) equation for  $M_s$  is normalized to be equal to IASPEI  $M_s$  at  $83^\circ$  and is given by:

$$M_s = \log A / T + \frac{1}{3} \log \Delta + \frac{1}{2} \log(\sin \Delta) + 0.00456\Delta + 2.484 \quad (7.4)$$

Figure 25 shows a comparison of the distance corrections in Eq (7.3) and (7.4) with the IASPEI and Marshall Basham distance corrections. The new distance corrections are similar to the Marshall Basham corrections at close distances and with IASPEI at intermediate distances. At distances approaching the antipode the distance correction decreases due to the  $\sin \Delta$  term. Von Seggern (1975a) observed increasing amplitudes near the antipode consistent with this equation.

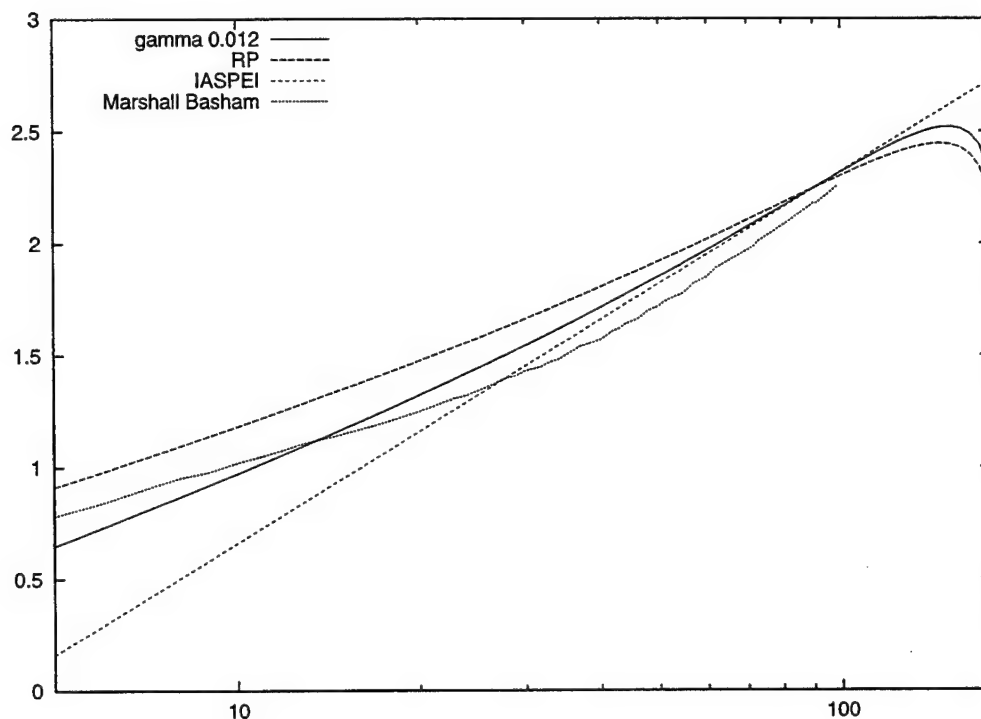


Figure 25. Comparison of distance corrections from the best fit  $\gamma=0.012$  Eq (7.3), the Rezapour and Pearce (1997) Eq (7.4), Marshall and Basham (1972), and the IASPEI formula.

Note that Eq (7.2)-(7.4) could be regionalized, using different values of  $\gamma$  in different regions, and using a different value for  $k$  if that were found to be more appropriate in some regions.  $M_s$  can also be measured at periods other than 20 seconds, however in that case the coefficient  $D$  is frequency dependent and must be calculated or tabulated for each period. It is simpler to calculate the path corrected spectral magnitude using Eq (2.2) because the frequency dependence of the spectrum is automatically removed, there is no ambiguity about the attenuation rate for Airy phase vs. normal dispersion, and it is not necessary to measure the period from the time domain wavetrain.

To evaluate the effect of the revised distance corrections on PIDC magnitudes, we recalculated  $M_s$  for all of the events from the REB and EDR discussed in Section 4.2 with four or more arrivals, and then recalculated the network magnitudes and standard deviations for these events. The results are summarized in the table below.



Table 3. Effect of revised distance corrections on network  $M_s$ .

<i>Data Source</i>	<i>Magnitude Type</i>	<i>Ave <math>\Delta M_s</math></i>	<i>Ave <math>\sigma(M_s)</math></i>
USGS EDR	$M_s$ IASPEI	0.	0.235
	$M_s$ Fit (Eq. 7.3)	0.024	0.227
	$M_s$ RP (Eq. 7.4)	0.052	0.223
PIDC REB	$M_s$ IASPEI	0.	0.250
	$M_s$ Fit (Eq. 7.3)	0.035	0.242
	$M_s$ RP (Eq. 7.4)	0.082	0.239

Both new distance corrections increase the average  $M_s$  and the increase is larger for the REB than for the EDR because of the shorter distance range. Both new distance corrections also reduce the average event standard deviation, however the Rezapour and Pearce equation reduces the standard deviation more than the best fit solution for both the EDR and REB data sets. Eq (7.4) is therefore the recommended equation to replace the IASPEI  $M_s$  formula, although we also recommend additional study be given to data in the 0-20° since there is very little data in this range in the data set studied here, and the best fit solution seems to match the data in that range slightly better than Eq (7.4).

## 8.0 Conclusions and Recommendations

The primary focus of this project has been the development, implementation, and testing of a framework for optimum processing of surface waves under a Comprehensive Test Ban Treaty for the purpose of earthquake/explosion discrimination. Because the number of events increases rapidly at small magnitudes, a decrease in the threshold of reliable surface wave identification and measurement can greatly reduce the number of unidentified events. Improved surface wave analysis methods can reduce the surface wave magnitude threshold, improve identification capability, and reduce the likelihood of unnecessary on-site inspections under a CTBT. Recommended techniques include the use of: regionalized earth models and surface wave parameters, phase-matched filtering to improve signal/noise ratio, path corrected spectral magnitudes (scalar moment) in place of and in addition to  $M_s$ , maximum likelihood magnitudes and maximum likelihood upper bounds on magnitudes, and an improved  $M_s$  distance correction.

The regionalized models developed in this project can be used to calculate surface wave parameters, generate phase-matched filters, and predict dispersive arrival times. In addition, the techniques used here to develop these models can be used on a continuing basis to improve the models. With the large amount of data now coming into the PIDC and the NDC on a continuous basis, it is possible to maintain a rapidly increasing database of dispersion curves, adding to the database used in this study and improving the results by filling in regions with poor coverage and extending the frequency range.

In addition to the improvements discussed here, some changes in operational procedure would improve the reliability of surface wave identification and measurement. The analysis performed in this project used data from the IMS primary stations because data is not collected in the long period arrival time window from auxiliary stations. Since surface wave measurements are best at closer distances, particularly when spectral magnitudes are used, we strongly recommend the use of auxiliary station data and routine analysis of data in the 0-20 degree range in addition to the 20-100 degree range currently being processed. Maxsurf and Maxpmf were designed to be completely automatic, however some operator review would be beneficial, particularly for removal of bad data and for identification of surface waves in cases where the automatic processing results are marginal. In order to do this effectively, analysts will need tools for reviewing beamed array data, data transformed to a common instrument, phase-matched filter cross-correlation functions, and processed group velocity dispersion curves.

Some additional research should be performed using historic explosion data. The data used in this report was a mix of digital and hand digitized data obtained during previous research projects. Most of the previous research concentrated on larger yield explosions. Additional low amplitude, regional explosion data should be acquired and processed in order to better assess the discrimination threshold of the methods described here. Calibration and instrument responses for the data set should also be rechecked. Finally,  $m_b$  from historic explosions needs to be remeasured using current procedures to ensure that discrimination results from current earthquake data and historic explosion data are consistent.

## 9.0 References

- Bache, T. C., W. L. Rodi, and D. G. Harkrider (1978), "Crustal Structures Inferred from Rayleigh-Wave Signatures of NTS Explosions," *Bull. Seism. Soc. Am.*, v. 68, pp. 1399-1413.
- Dziewonski, A. M. and D. L. Anderson (1981), "Preliminary Reference Earth Model," *J Phys. Earth Planet. Inter.*, v. 25, pp. 297-356.
- Ekstrom, G., A. M. Dziewonski, G. P. Smith, and W. Su (1996), "Elastic and Inelastic Structure Beneath Eurasia," in *Proceedings of the 18th Annual Seismic Research Symposium on Monitoring a Comprehensive Test Ban Treaty*, 4-6 September, 1996, Phillips Laboratory Report PL-TR-96-2153, July, pp. 309-318, ADA313692.
- Harkrider, D. G., J. L. Stevens, and C. B. Archambeau (1994), "Theoretical Rayleigh and Love waves from an Explosion in Prestressed Source Regions," *Bull. Seism. Soc. Am.*, v. 84, pp. 1410-1442.
- Herak, M. and Herak, D. (1993), "Distance Dependence of  $M_s$  and Calibrating Function for 20 Second Rayleigh Waves," *Bull. Seism. Soc. Am.*, v. 83, pp. 1881-1892.
- Herrin, E. and T. Goforth (1977), "Phase-Matched Filtering: Application to the Study of Rayleigh Waves," *Bull. Seism. Soc. Am.*, v. 67, pp. 1259-1275.
- Levshin, A. L., M. H. Ritzwoller, and S. S. Smith (1996), "Group Velocity Variations Across Eurasia," in *Proceedings of the 18th Annual Seismic Research Symposium on Monitoring A Comprehensive Test Ban Treaty*, 4-6 September, 1996, Phillips Laboratory Report PL-TR-96-2153, July, pp. 70-79, ADA313692.
- Marshall, P. D. and P. W. Basham (1972), "Discrimination Between Earthquakes and Underground Nuclear Explosions Employing An Improved  $M_s$  scale," *Geophys. J. R. astr. Soc.*, v. 28, pp. 431-458.
- McGarr, A. (1969), "Amplitude Variations of Rayleigh Waves - Propagation Across A Continental Margin," *Bull. Seism. Soc. Am.*, v. 59, pp. 1281-1305.
- McLaughlin, K. L. (1988), "Maximum-Likelihood Event Magnitude Estimation with Bootstrapping for Uncertainty Estimation," *Bull. Seism. Soc. Am.*, v. 78, pp. 855-862.
- Mitchell, B. J., L. Cong and J. Xie, (1996), "Seismic Attenuation Studies in the Middle East and Southern Asia", St. Louis University Scientific Report No. 1, PL-TR-96-2154, ADA317387.
- Mooney, W., G. Laske, and G. Masters (1997), "Crust 5.1: A Global Crustal Model at 5x5 Degrees," *Journal of Geophysical Research*, submitted.
- Murphy, J. R. and B. W. Barker (1996), "A Preliminary Evaluation of Seismic Magnitude Determination at the International Data Center (IDC)," *EOS Transactions of the American Geophysical Union*, November, P. F7.
- Nolet, G. (1987), "Seismic Wave Propagation and Seismic Tomography," in *Seismic Tomography with Applications In Global Seismology and Exploration Geophysics*, G. Nolet, ed., D. Reidel Publishing, Dordrecht, Holland.
- Okal, E. A. and J. Talandier (1987), " $M_m$ : Theory of A Variable-Period Mantle Magnitude," *Geophysical Research Letters*, v. 14, pp. 836-839.
- Rezapour, M. and R. G. Pearce (1997), "Bias and Data Censoring in ISC Surface Wave Magnitudes," *Bull. Seism. Soc. Am.*, submitted.
- Ritzwoller, M. H., A. L. Levshin, L. I. Ratnikova, and D. M. Tremblay (1996), "High Resolution Group Velocity Variations Across Central Asia," in *Proceedings of the 18th Annual Seismic Research*

*Symposium On Monitoring A Comprehensive Test Ban Treaty*, 4-6 September, 1996, Phillips Laboratory Report PL-TR-96-2153, July, pp. 98-107, ADA313692.

Sclater, J. G. and J. Francheteau (1970), "The Implications of Terrestrial Heat Flow Observations On Current Tectonic and Geochemical Models of the Crust and Upper Mantle of the Earth," *Geophys. J. R. astr. Soc.*, v. 20, pp. 509-542.

Stevens, J. L. (1986), "Estimation of Scalar Moments From Explosion-Generated Surface Waves," *Bull. Seism. Soc. Am.*, v. 76, pp. 123-151.

Stevens, J. L. and S. M. Day (1985), "The Physical Basis of the  $m_b$ : $M_s$  and Variable Frequency Magnitude Methods for Earthquake/Explosion Discrimination," *Journal of Geophysical Research*, v. 90, pp. 3009-3020.

Stevens, J. L. and K. L. McLaughlin (1996), "Regionalized Maximum Likelihood Surface Wave Analysis," Maxwell Technologies Technical Report submitted to Phillips Laboratory, PL-TR-96-2273, SSS-DTR-96-15562, September, ADA321813.

Stevens, J. L., and K. L. McLaughlin (1988), "Analysis of Surface Waves from the Novaya Zemlya, Mururoa, and Amchitka Test Sites, and Maximum Likelihood Estimation of Scalar Moments from Earthquakes and Explosions," S-CUBED Technical Report submitted to Air Force Technical Applications Center, SSS-TR-89-9953, September.

Sato, R. (1967), "Attenuation of Seismic Waves," *J. Phys. Earth*, v. 15, p. 32-61.

Thomas, J. H., P. D. Marshall, and A. Douglas (1978), "Rayleigh-Wave Amplitudes from Earthquakes in the Range 0-150 degrees," *Geophys. J. R. astr. Soc.*, v. 53, pp. 191-200.

Von Seggern, D. H. (1975a), "Q for 20-Second Rayleigh Waves from Complete Great-Circle Paths," Teledyne Geotech Report SDAC-TR-75-3 submitted to the Defense Advanced Research Projects Agency, February.

Von Seggern, D. H. (1975b), "Distance-Amplitude Relationships for Long-Period P, S, and LR from Measurements on Recordings of the Long-Period Experimental Stations," Teledyne Geotech Report SDAC-TR-75-15 submitted to the Defense Advanced Research Projects Agency, September.

## 10.0 Acknowledgements

We would like to thank Gabi Laske of the University of California at San Diego for providing the Crust 5.1 earth models, Mike Ritzwoller of the University of Colorado, Brian Mitchell of St. Louis University, Goran Ekstrom of Harvard University, and their coworkers for the use of their data and models in this project, and David Harkrider for many useful discussions.

## Appendix A. Surface Wave Excitation by Arbitrary Sources and Explosions

The vertical component of a Rayleigh wave from a source located at the radial origin and depth  $h$  and measured at distance  $r$  and depth  $z$  in a plane layered medium has the following form<sup>1</sup>

$$u_z(\omega, r, z, \varphi) = A_R \sqrt{2/\pi\omega cr} \exp[i(\pi/4 - \omega r/c)] F_s(\omega, \varphi, h) y_1(\omega, z) \quad (\text{A.1})$$

and the radial component is given by:

$$u_r(\omega, r, z, \varphi) = -iA_R \sqrt{2/\pi\omega cr} \exp[i(\pi/4 - \omega r/c)] F_s(\omega, \varphi, h) y_3(\omega, z) \quad (\text{A.2})$$

where  $A_R$  is the Rayleigh wave amplitude,  $c$  is the phase velocity,  $\omega$  is the angular frequency,  $F_s$  is a function that depends on the source type and source depth,  $y_1$  and  $y_3$  are the vertical and radial Rayleigh wave eigenfunctions as defined by Takeuchi and Saito (1972), respectively, evaluated at receiver depth  $z$ , and  $\varphi$  is the source to receiver azimuth.  $F_s$  can represent any source, and can be expressed as an expansion in cylindrical harmonics which can be derived from a source represented by an expansion in spherical harmonics (Harkrider, *et al.*, 1994). Equations (A.1) and (A.2) are equivalent to Eq (46) of Harkrider *et al.* (1994) except that the following changes were made to make it easier to compare to observations: the Hankel functions have been replaced by their asymptotic expansions, the right hand side of the equation was divided by  $i\omega$  so that a source function with constant moment would have a step rather than delta time function,  $u_z$  is oriented with vertical up, and eigenfunctions at the receiver are included so that the receiver depth may be non-zero.  $A_R$  is related to the kinetic energy in the mode through the relation

$$A_R = \frac{1}{2cUI_1} \quad (\text{A.3})$$

where  $U$  is the group velocity and the kinetic energy  $I_1$  is given by

$$I_1 = \int_0^\infty \rho(z) [y_1(z)^2 + y_3(z)^2] dz \quad (\text{A.4})$$

where  $\rho(z)$  is the density at depth  $z$ .

For the specific case of an explosion source

$$F_s = M_0 \frac{\beta^2}{\alpha^2} \left( y_3 - \frac{y_2}{2\mu k} \right). \quad (\text{A.5})$$

<sup>1</sup> Equations (A.1-4) appear in a variety of forms in the literature with slightly different notations. The definition of  $I_1$  used here follows Takeuchi and Saito (1972) and Harkrider, Stevens, and Archambeau (1994). Kennett (1983) uses the same definition of  $I_1$ . Aki and Richards (1980) define an energy integral  $I_1$  equal to 1/2 the  $I_1$  defined here. McGarr and Alsop (1967) define an integral  $I_7$  which is equivalent to  $I_1$ . The sign of the Fourier transform used by Aki and Richards and Kennett is opposite the sign used in the other references mentioned here, so the equations are the complex conjugate of the equations given here.

where  $\alpha$ ,  $\beta$ , and  $\mu$  are the compressional speed, shear speed, and shear modulus at the source, respectively,  $k$  is the wavenumber  $\omega/c$  and  $y_2$  is the normal stress eigenfunction at the source depth. Since  $y_2$  vanishes at the free surface and is small at typical explosion depths,  $F_s$  is sensitive to Poisson's ratio at the source. As discussed by Stevens (1986), we can define a normalized moment

$$M_0' = 3 \frac{\beta^2}{\alpha^2} M_0$$

so that when  $M_0$  is replaced by  $M_0'$  in Equation A.5,  $F_s$  becomes

$$F_s = \frac{1}{3} M_0' \left( y_3 - \frac{y_2}{2\mu k} \right) \quad (\text{A.7})$$

For a fixed  $M_0'$  at shallow depths,  $F_s$  depends on the eigenfunction  $y_3$  which is a function of the average earth structure and only weakly dependent on material properties at the source.

## Appendix B. Surface Wave Transmission Through Laterally Heterogeneous Media

We are interested in cases where a surface wave is generated in one structure, passes through any number of different structures, and is recorded at a final structure. We can modify Eq (A.1) and (A.2) to be applicable to this case using the approximation that energy is conserved and that there is no mode conversion (McGarr, 1969; Bache *et al*, 1978). The kinetic energy in the mode is defined by

$$K = \frac{1}{2} \omega^2 \int_0^\infty \rho [|u_z|^2 + |u_r|^2] dz \quad (\text{B.1})$$

Energy conservation requires that the energy flux of the surface wave through a cylindrical surface be constant. This condition can be written:

$$K(r_1)U(r_1)r_1 = K(r_2)U(r_2)r_2 \quad (\text{B.2})$$

where  $U$  is the group velocity. The displacement at point  $r_2$  can be written in terms of the displacement at  $r_1$  and a transmission coefficient  $T(r_1, r_2)$ .

$$u_z(r_2) = T(r_1, r_2)u_z(r_1) \quad (\text{B.3})$$

Substituting (A.1) and (A.2) into (B.1),  $K(r) \sim I_1(r)/r$ , so  $I_1(r_1)U(r_1) = T^2 I_1(r_2)U(r_2)$  and

$$T = \sqrt{\frac{I_1(r_1)U(r_1)}{I_1(r_2)U(r_2)}} \quad (\text{B.4})$$

or using (A.3)

$$T = \sqrt{\frac{A_R(r_2)c(r_2)}{A_R(r_1)c(r_1)}} \quad (\text{B.5})$$

We can then rewrite Eq (A.1) in the form

$$u_z(\omega, r, z, \varphi) = \sqrt{2A_{R_1}/\pi\omega c_1^2 r} \sqrt{c_2 A_{R_2}} \exp[i(\pi/4 - \omega r / c_p)] F_s(\omega, \varphi, h) y_1(\omega, z) \quad (\text{B.6})$$

where the 1 and 2 subscripts refer to the source and receiver location, respectively, and the “p” subscript refers to the path averaged value of the phase velocity (the phase slowness is averaged over the path). In an attenuating, spherical earth, Eq (B.6) must also be multiplied by  $\exp(-\gamma_p r) \left( \frac{r}{a_e \sin(r/a_e)} \right)$  where  $a_e$  is the radius of the earth and  $\gamma$  is the frequency dependent attenuation coefficient, so (B.6) becomes

$$u_z(\omega, r, z, \varphi) = \frac{1}{\sqrt{a_e \sin(r/a_e)}} \sqrt{\frac{2A_{R_1}}{\pi\omega c_1^2}} \sqrt{c_2 A_{R_2}} \exp[i(\pi/4 - \omega r / c_p - \gamma_p r)] F_s(\omega, \varphi, h) y_1(\omega, z) \quad (\text{B.7})$$

Each factor in Eq (B.7) depends only on the source location, receiver location, or path. For an explosion source, we can write (B.7) in the simple form:

$$u_z(\omega, h_x, r, z) = M_0' \frac{S_1^x(\omega, h_x) S_2(\omega) \exp[-\gamma_p(\omega) r + i(\varphi_0 - \omega r / c_p(\omega))]}{\sqrt{a_e \sin(r/a_e)}} y_1(\omega, z) \quad (\text{B.8})$$

where  $\varphi_0$  is the initial phase equal to  $-3\pi/4$ ,

$$S_1^x(\omega, h_x) = \sqrt{\frac{2A_{R_1}}{9\pi\omega c_1^2}} \left( \frac{1}{2\mu k} y_2(h_x) - y_3(h_x) \right) \quad (\text{B.9})$$

$$S_2(\omega) = \sqrt{c_2 A_{R_2}} \quad (\text{B.10})$$

$S_1$  and  $S_2$  as defined here correct an extra factor of  $1/\sqrt{c_1}$  in  $S_1$  and  $\sqrt{c_2}$  in  $S_2$  in the corresponding definitions of Stevens (1986).

## Appendix C. Modified Crust 5.1 Models and Group Velocity Contour Plots

The modified Crust 5.1 models used in the tomographic inversion are shown in Figure 26. Five of the Crust 5.1 models, originally labeled A6-AA which had very thick low velocity sediments were removed and replaced because they led to unrealistic (extremely low velocity) dispersion curves. The new model was labeled X2 and was set to model A5 as a starting model. The Crust 5.1 models have little differentiation in oceanic regions, so 16 new oceanic models, labeled X3-XG were added. These models are grouped primarily according to ocean age with the regionalization derived from the current PIDC model (Stevens and McLaughlin, 1996, originally derived from E. Okal and M. Woods, personal communication), with some additional regionalization of the Pacific Ocean following Sclater and Francheteau (1970).

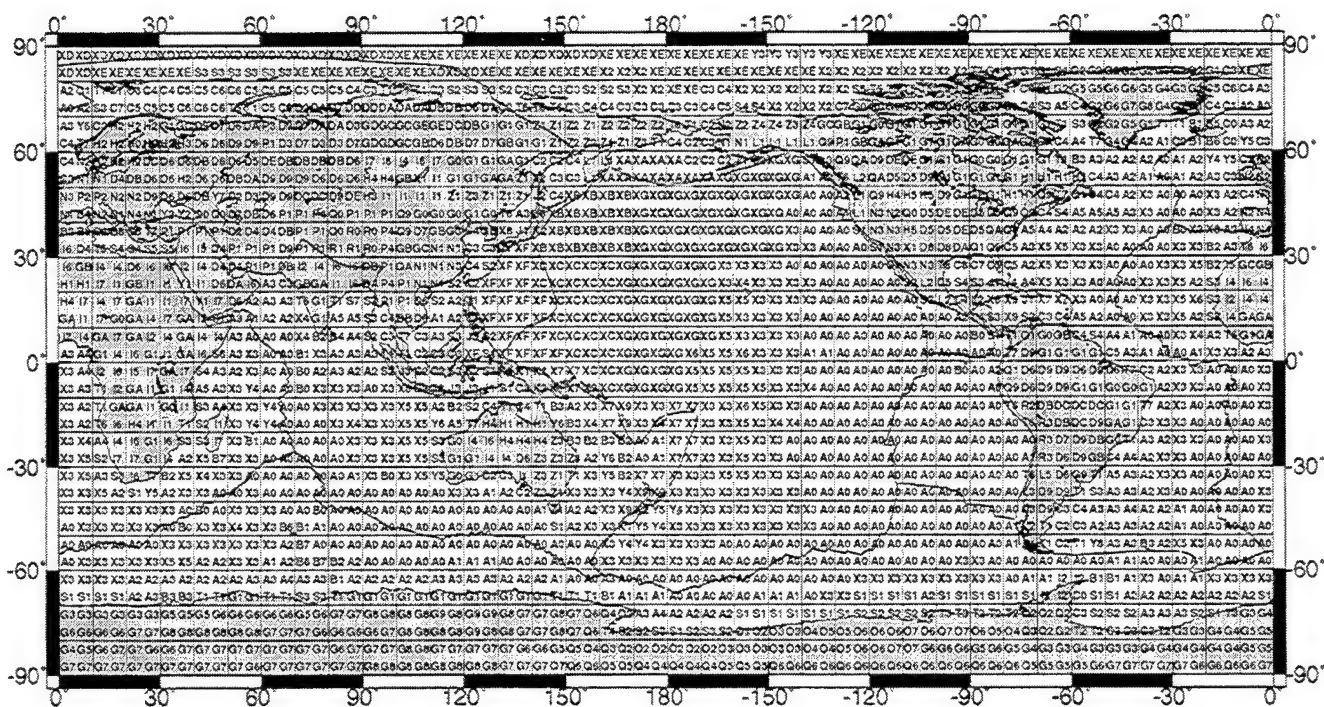


Figure 26. Regionalized inversion models derived from Crust 5.1.

Following are group velocity contour plots calculated using the final inversion models at frequencies of 0.02 through 0.06 Hz.



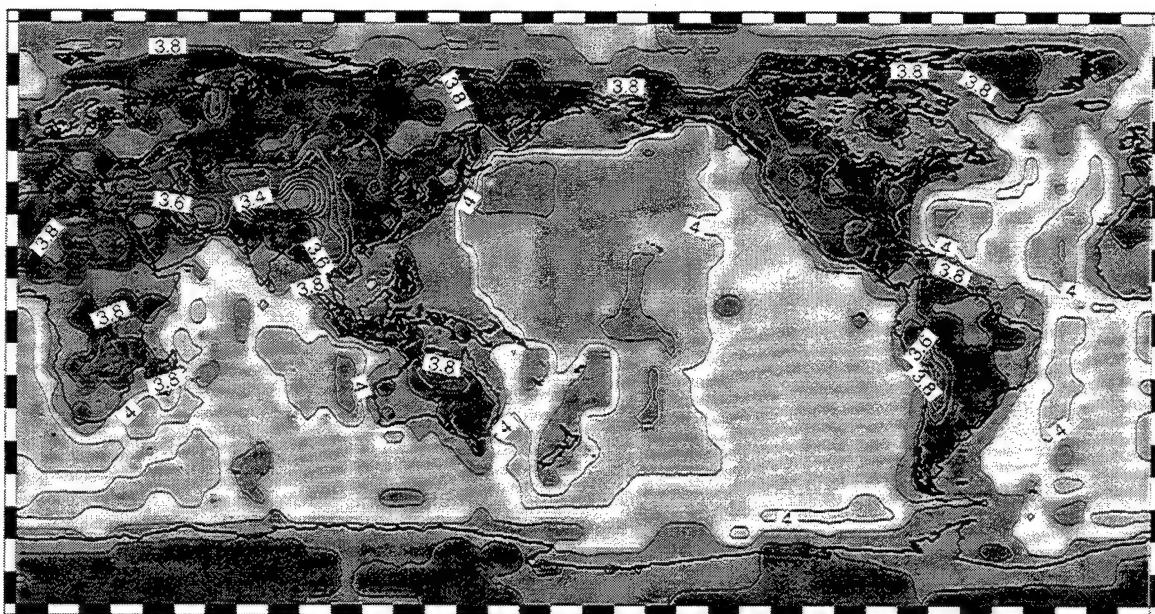


Figure 27. Group velocity contours at 0.02 Hz.

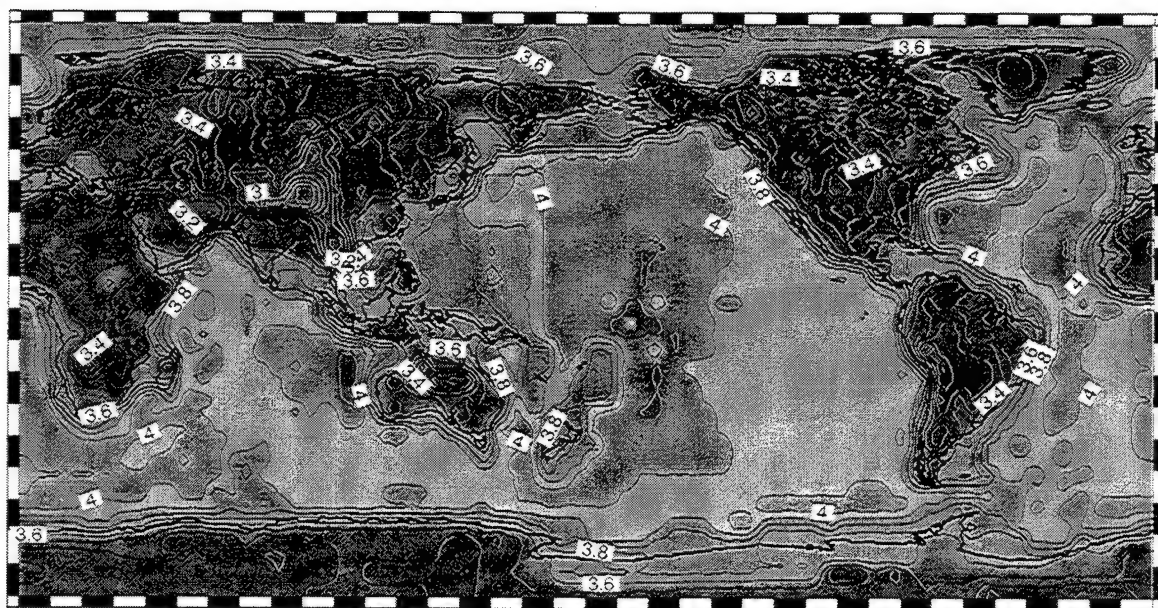


Figure 28. Group Velocity contours at 0.03 Hz.

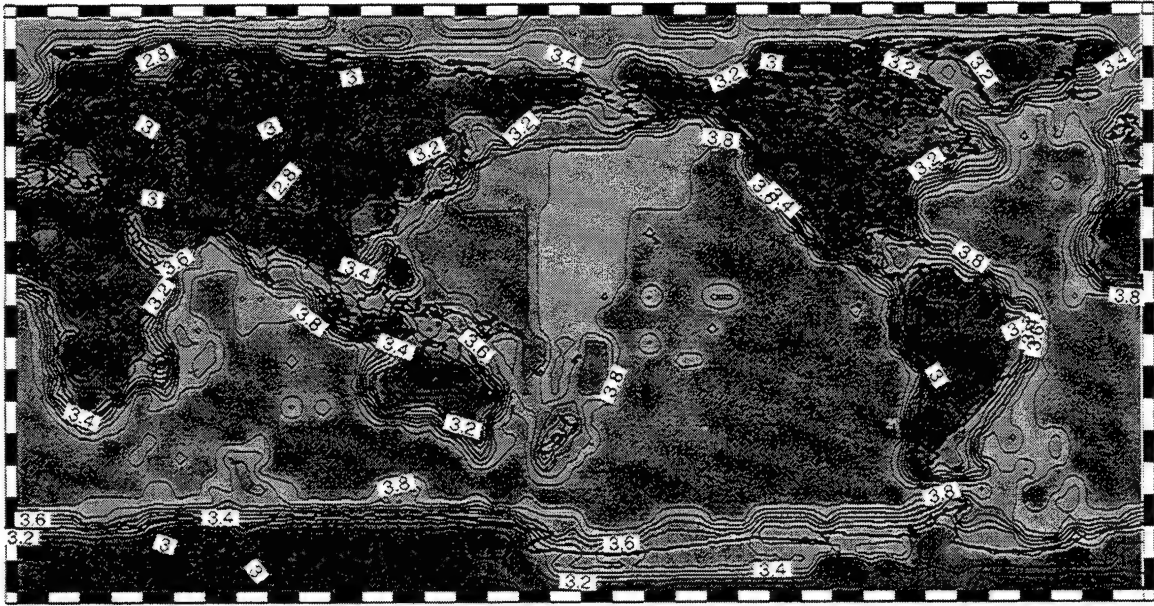


Figure 29. Group velocity contours at 0.04 Hz.

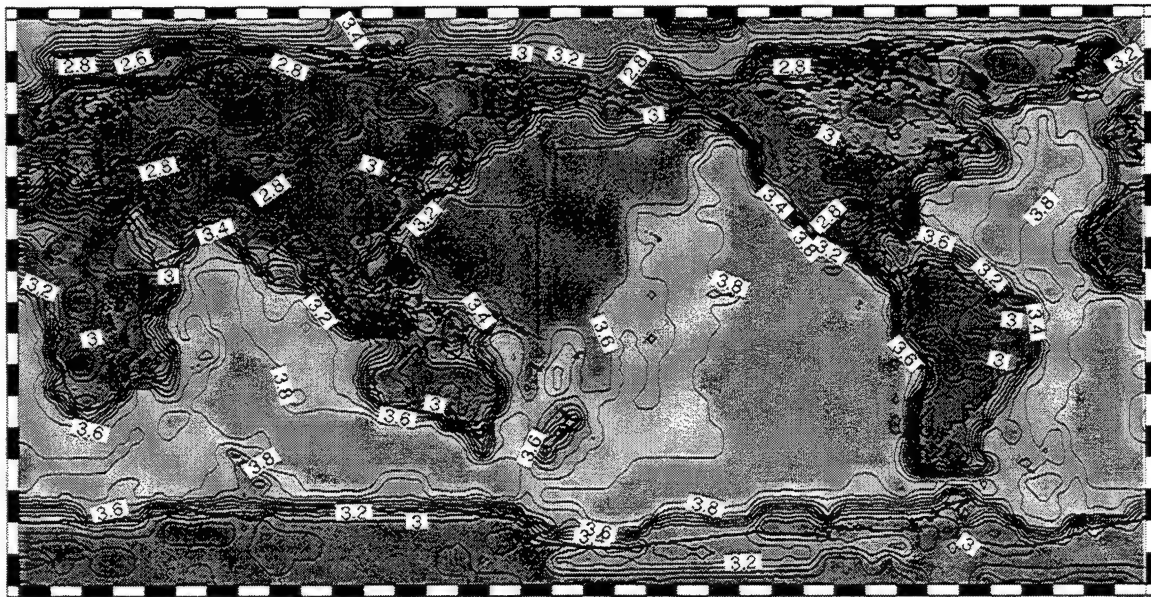


Figure 30. Group velocity contours at 0.05 Hz.

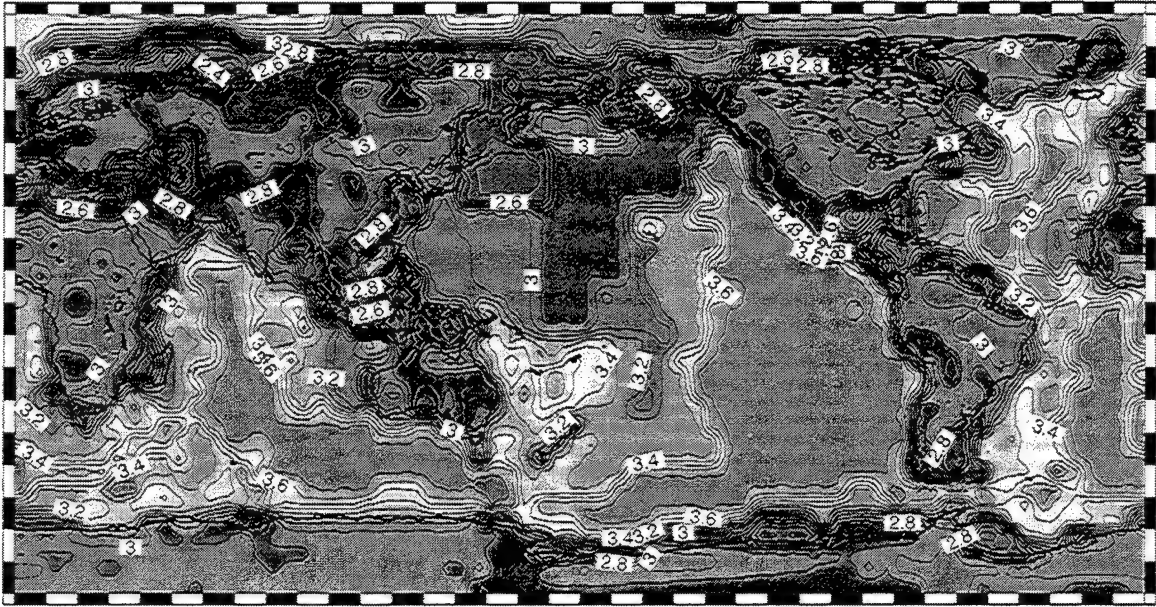


Figure 31. Group velocity contours at 0.06 Hz.

# Appendix D. Maximum Likelihood Station Corrections for $M_s$

Station	Stacor	Sdev	Ndata	Nnoise					
AAE	-0.141	0.053	5	1	KSAR	-0.374	0.014	88	70
AE15	-0.297	0.045	3	2	LEM	-0.014	0.036	7	11
AE16	-0.059	0.078	3	0	LHC	-0.086	0.046	9	8
AE20	0.175	0.028	19	2	LND	0.505	0.065	1	0
AE28	0.396	0.043	1	1	LON	-0.160	0.018	46	41
AE32	0.112	0.024	15	5	LPZ	-0.412	0.021	12	43
AE33	-0.121	0.032	12	1	LZH	-0.057	0.033	13	5
AE34	-0.150	0.039	9	4	MAIO	0.062	0.036	15	0
AE35	0.259	0.053	10	4	MAJO	0.106	0.015	71	35
AFI	-0.222	0.071	2	8	MAT	0.306	0.042	10	5
ALE	0.421	0.054	5	0	MAW	-0.065	0.025	27	85
ALQ	-0.032	0.045	15	3	MBC	0.568	0.035	17	2
ANMO	0.159	0.015	68	44	MDJ	0.363	0.058	2	0
ANTO	-0.235	0.016	41	28	MNT	0.260	0.030	14	4
AQU	0.158	0.050	5	1	MNV	-0.214	0.027	41	89
ARE0	0.172	0.042	6	4	NDI	0.306	0.039	12	2
ASPA	-0.169	0.016	78	84	NIL	-0.030	0.047	10	1
BCAO	-0.305	0.021	7	16	NNA	0.141	0.047	2	1
BDFB	0.076	0.025	27	28	NRE0	0.014	0.016	60	80
BER	-0.192	0.047	4	6	NRI	-0.087	0.020	29	59
BGCA	0.027	0.027	25	35	NUR	0.089	0.048	13	4
BGIO	-0.005	0.079	2	1	NWAO	-0.218	0.016	14	56
BJI	0.289	0.024	16	5	OGD	0.063	0.036	14	5
BLA	0.348	0.023	35	4	OTT	0.132	0.022	32	7
BLC	-0.008	0.041	8	8	PD31	-0.104	0.020	24	77
BOCO	-0.202	0.029	10	16	PDY	-0.125	0.014	51	78
BOSA	0.114	0.029	27	39	PHC	0.526	0.033	22	1
CHG	-0.271	0.050	4	1	PLCA	-0.085	0.027	33	44
CHTO	-0.246	0.017	40	20	PMG	0.164	0.055	3	1
CM16	0.009	0.014	81	81	PNT	-0.302	0.031	19	3
CMB	-0.378	0.068	3	12	POO	-0.042	0.066	7	0
CMC	0.123	0.046	9	0	QUE	0.214	0.054	14	0
COL	0.053	0.014	58	29	RES	0.350	0.030	17	17
COP	0.169	0.053	8	3	RSCP	-0.276	0.036	1	6
COR	-0.194	0.026	27	7	RSNT	-0.185	0.048	3	4
CPUP	-0.084	0.020	28	42	RSNY	-0.115	0.034	1	6
CTA	0.178	0.077	2	0	RSON	0.001	0.026	2	6
CTAO	-0.440	0.019	3	75	RSSD	0.143	0.057	5	4
DAV	0.231	0.043	7	1	SCH	-0.070	0.025	8	8
DBIC	0.015	0.025	28	40	SCHQ	0.019	0.024	17	41
DUG	-0.043	0.048	8	1	SCP	0.305	0.012	54	41
EDM	0.138	0.031	15	7	SES	-0.499	0.048	12	4
EIL	-0.016	0.078	7	0	SFA	0.243	0.044	10	3
ESK	0.015	0.043	5	3	SHI	0.186	0.064	8	3
ESLA	-0.334	0.023	34	72	SHK	0.278	0.049	8	1
FCC	-0.022	0.033	21	1	SHL	-0.087	0.047	8	4
FFC	-0.156	0.035	17	0	SJG	-0.076	0.087	4	1
FRB	-0.158	0.053	4	4	SNZO	-0.055	0.045	7	3
FSJ	-0.488	0.038	10	8	STJ	0.170	0.033	2	4
GAC	0.335	0.020	28	19	STKA	0.011	0.017	80	79
GDH	0.053	0.020	24	19	STU	-0.036	0.055	6	2
GRFO	0.216	0.016	57	19	TATO	-0.278	0.019	40	42
GUMO	-0.064	0.013	51	66	TOL	0.160	0.018	21	26
GWC	-0.292	0.053	5	4	TRI	0.289	0.041	9	1
HIA	0.115	0.026	16	10	TUC	-0.100	0.042	5	2
HNR	0.360	0.049	6	0	TX00	-0.185	0.025	28	77
HON	-0.004	0.024	9	41	ULM	-0.013	0.019	43	64
IL31	-0.584	0.019	56	111	UME	-0.132	0.060	5	1
INK	0.316	0.039	12	8	VIC	-0.221	0.043	9	0
JAS	-0.072	0.029	4	18	VNDA	-0.128	0.024	32	58
JER	0.048	0.062	6	0	WMQ	-0.006	0.033	12	4
KAAO	-0.275	0.027	26	6	YKC	0.815	0.167	1	0
KBL	-0.143	0.082	10	2	YKR8	-0.028	0.016	52	99
KBS	-0.343	0.123	2	8	ZAL	-0.213	0.024	19	70
KBZ	-0.242	0.017	30	84	ZOBO	-0.146	0.023	19	13
KEV	-0.155	0.029	46	11					
KIP	-0.097	0.065	4	0					
KMI	0.289	0.034	13	4					
KON	0.109	0.056	2	2					
KONO	0.118	0.016	70	17					

# Appendix E. Maximum Likelihood Station Corrections for log M<sub>0</sub>

Station	Stacor	Sdev	Ndata	Nnoise					
AAE	-0.041	0.050	5	1	KONO	-0.013	0.012	70	20
AE15	-0.168	0.036	3	2	KSAR	-0.242	0.012	88	79
AE16	0.420	0.048	3	0	LEM	0.010	0.032	7	14
AE20	0.181	0.021	19	3	LHC	-0.135	0.024	9	11
AE28	0.155	0.042	1	1	LND	0.808	0.044	1	0
AE32	0.042	0.025	15	5	LON	-0.053	0.013	46	58
AE33	-0.065	0.021	12	1	LPZ	-0.340	0.020	12	45
AE34	-0.187	0.030	9	5	LZH	-0.214	0.028	13	11
AE35	0.112	0.029	10	4	MAIO	0.187	0.024	15	1
AFI	0.055	0.054	2	12	MAJO	0.013	0.011	71	36
ALE	0.108	0.040	5	0	MAT	0.265	0.038	10	5
ALQ	0.106	0.023	15	11	MAW	-0.013	0.020	27	87
ANMO	0.093	0.014	68	60	MBC	0.346	0.022	17	2
ANTO	-0.243	0.011	41	31	MDJ	0.078	0.061	2	0
AQU	0.225	0.048	5	2	MNT	0.220	0.021	14	5
ARE0	0.004	0.027	6	4	MNV	-0.177	0.017	41	98
ASPA	-0.052	0.013	78	88	NDI	0.305	0.034	12	2
BCAO	-0.263	0.020	7	18	NIL	0.096	0.037	10	1
BDFB	-0.095	0.021	27	29	NNA	0.296	0.051	2	1
BER	0.122	0.031	4	6	NRE0	-0.111	0.010	60	83
BGCA	-0.113	0.018	25	35	NRI	-0.079	0.016	29	122
BGIO	-0.567	0.040	2	3	NUR	0.197	0.031	13	4
BJI	0.071	0.020	16	9	NWAO	-0.376	0.008	14	63
BLA	0.147	0.015	35	6	OGD	0.030	0.021	14	6
BLC	0.034	0.024	8	8	OTT	0.161	0.017	32	8
BOCO	-0.117	0.020	10	21	PD31	-0.112	0.022	24	108
BOSA	-0.044	0.019	27	40	PDY	-0.121	0.012	51	89
CHG	-0.320	0.043	4	1	PHC	0.497	0.031	22	2
CHTO	-0.380	0.012	40	23	PLCA	-0.308	0.020	33	50
CM16	0.072	0.011	81	88	PMG	0.218	0.043	3	1
CMB	-0.146	0.038	3	23	PNT	0.040	0.020	19	4
CMC	0.010	0.033	9	0	POO	0.172	0.051	7	0
COL	0.178	0.012	58	39	QUE	0.086	0.034	14	1
COP	0.061	0.048	8	4	RES	0.082	0.018	17	18
COR	0.118	0.018	27	14	RSCP	-0.364	0.050	1	6
CPUP	-0.252	0.017	28	44	RSNT	-0.292	0.040	3	5
CTA	0.215	0.084	2	0	RSNY	0.015	0.039	1	7
CTAO	-0.852	0.028	3	80	RSON	-0.289	0.028	2	6
DAV	0.250	0.034	7	1	RSSD	-0.082	0.049	5	4
DBIC	-0.133	0.017	28	40	SCH	-0.068	0.023	8	8
DUG	-0.094	0.041	8	1	SCHQ	0.052	0.021	17	45
EDM	0.045	0.020	15	7	SCP	0.097	0.010	54	41
EIL	0.114	0.071	7	0	SES	-0.175	0.023	12	11
ESK	0.117	0.047	5	3	SFA	0.112	0.026	10	6
ESLA	-0.282	0.016	34	78	SHI	0.114	0.050	8	4
FCC	0.102	0.019	21	3	SHK	0.404	0.044	8	1
FFC	-0.016	0.029	17	0	SHL	-0.168	0.044	8	4
FRB	-0.105	0.032	4	5	SJG	0.262	0.065	4	2
FSJ	-0.030	0.027	10	8	SNZO	0.065	0.044	7	3
GAC	0.013	0.014	28	30	STJ	0.064	0.043	2	4
GDH	0.170	0.023	24	26	STKA	0.034	0.012	80	81
GRFO	0.041	0.013	57	26	STU	0.243	0.032	6	3
GUMO	-0.075	0.009	51	71	TATO	-0.330	0.016	40	52
GWC	-0.324	0.045	5	5	TOL	0.109	0.019	21	27
HIA	-0.007	0.023	16	12	TRI	0.069	0.041	9	1
HNR	0.522	0.053	6	0	TUC	-0.268	0.037	5	2
HON	-0.126	0.015	9	50	TX00	-0.465	0.014	28	81
IL31	-0.636	0.013	56	113	ULM	-0.117	0.016	43	70
INK	0.315	0.041	12	13	UME	0.178	0.040	5	1
JAS	-0.010	0.030	4	25	VIC	0.124	0.020	9	8
JER	0.099	0.052	6	0	VNDA	-0.180	0.020	32	61
KA AO	0.041	0.022	26	7	WMQ	-0.024	0.017	12	18
KBL	0.188	0.052	10	7	YKC	0.465	0.103	1	0
KBS	-0.156	0.037	2	12	YKR8	-0.140	0.010	52	99
KBZ	-0.243	0.015	30	90	ZAL	-0.003	0.021	19	118
KEV	0.128	0.016	46	16	ZOBO	-0.204	0.022	19	14
KIP	0.153	0.060	4	0					
KMI	0.031	0.018	13	7					
KON	0.138	0.036	2	3					



## Appendix F. Maximum Likelihood $M_s$ and $\log M_0$ for Explosions

The following table contains maximum the likelihood magnitudes for underground nuclear explosions discussed in Section 5. "Flag" indicates whether  $M_s$  and  $\log M_0$  are a maximum likelihood magnitude/moment (=) or a maximum likelihood upper bound on the magnitude/moment.

Testsite	Date	Event Name	$m_b$	Flag	$M_s$	$\log M_0$
AHAGGAR	1963293	rubis	5.62	=	4.16	16.00
AHAGGAR	1965058	saphir	5.88	=	4.60	16.35
AMCHITKA	1965302	longshot	6.03	=	3.76	15.44
AMCHITKA	1969275	milrow	6.52	=	4.94	16.49
AMCHITKA	1971310	cannikin	6.89	=	5.68	17.26
CLIMAX	1966153	piledriver	5.56	=	3.99	15.86
DEGELEN	1966352	deg18dec66	5.80	<	3.74	15.83
DEGELEN	1967057	deg26feb67	6.00	=	3.64	15.74
DEGELEN	1972345	deg10dec72	5.60	=	4.39	16.07
DEGELEN	1977302	deg29oct77	5.60	=	3.74	15.47
DEGELEN	1978085	deg26mar78	5.61	=	3.61	15.45
DEGELEN	1978112	deg22apr78	5.28	=	3.17	15.06
DEGELEN	1978209	deg28jul78	5.66	=	3.15	15.01
DEGELEN	1978241	deg29aug78	5.20	<	3.12	15.19
DEGELEN	1978304	deg31oct78	5.22	<	2.54	14.81
DEGELEN	1978333	deg29nov78	5.30	<	3.64	15.33
DEGELEN	1979151	deg31may79	5.24	=	3.04	14.83
DEGELEN	1980143	deg22may80	5.49	=	3.12	14.92
DEGELEN	1980213	deg31jul80	5.30	=	3.56	15.35
DEGELEN	1987057	deg26feb87	5.40	<	3.28	15.37
DEGELEN	1987126	deg06may87	5.60	<	4.47	15.54
DEGELEN	1987157	deg06jun87	5.30	=	2.02	14.52
DEGELEN	1987198	deg17jul87	5.80	=	3.33	15.33
DEGELEN	1988292	deg18oct88	4.90	<	2.79	14.62
EKZ	1987261	ekz18sep87	4.10	<	2.46	14.40
KONYSTAN	1988328	koy23nov88	5.10	<	1.53	14.91
KONYSTAN	1989048	koy17feb89	5.00	<	2.61	13.47
LOPNOR	1995135	lop15may95	5.73	<	4.24	15.95
LOPNOR	1995229	lop16sep95	5.54	<	5.20	16.81
LOPNOR	1996160	lop08jun96	5.69	=	4.03	15.75
LOPNOR	1996211	lop29jul96	4.71	<	2.48	13.92
MURUROA	1977078	mur19mar77	5.73	=	4.04	15.88
MURUROA	1977328	mur24nov77	5.80	=	3.95	15.67
MURUROA	1978334	mur30nov78	5.80	=	3.96	15.62
MURUROA	1979206	mur25jul79	6.03	=	3.94	15.65
MURUROA	1980083	mur23mar80	5.70	<	3.55	15.04
MURUROA	1980168	mur16jun80	5.29	<	3.25	14.83
MURUROA	1980201	mur19jul80	5.71	<	3.59	15.20
MURUROA	1980338	mur03dec80	5.58	=	3.52	15.24
MURUROA	1982206	mur25jul82	5.60	=	3.79	15.54
MURUROA	1983109	mur19apr83	5.60	=	3.94	15.75
MURUROA	1983145	mur25may83	5.90	=	3.82	15.64
MURUROA	1984133	mur12may84	5.70	=	3.56	15.37
MURUROA	1984307	mur02nov84	5.70	=	3.71	15.47
MURUROA	1984341	mur06dec84	5.60	=	3.80	15.50
MURUROA	1985128	mur08may85	5.70	<	3.05	15.23
MURUROA	1985330	mur26nov85	5.80	=	3.95	15.65

MURUROA	1986150	mur30may86	5.70	<	3.51	15.26
MURUROA	1987140	mur20may87	5.60	=	3.64	15.34
MURUROA	1995325	mur21nov95	4.63	<	3.40	14.78
MURUROA	1995361	mur27dec95	5.00	<	3.52	14.73
MURUROA	1996027	mur27jan96	5.07	<	3.11	14.86
NN_ZEMLYA	1967294	nnz21oct67	5.99	=	3.69	15.33
NN_ZEMLYA	1968312	nnz07nov68	6.11	=	4.09	15.97
NN_ZEMLYA	1970287	nnz14oct70	6.77	=	4.94	16.49
NN_ZEMLYA	1973255	nnz12sep73	6.96	=	5.29	16.77
NN_ZEMLYA	1974241	nnz29aug74	6.54	=	4.87	16.43
NN_ZEMLYA	1975235	nnz23aug75	6.55	=	4.76	16.14
NN_ZEMLYA	1976273	nnz29sep76	5.77	=	3.41	15.10
NN_ZEMLYA	1976294	nnz20oct76	4.89	=	3.25	14.72
NN_ZEMLYA	1977244	nnz01sep77	5.71	=	4.27	15.33
NN_ZEMLYA	1977282	nnz09oct77	4.51	<	3.78	15.23
NN_ZEMLYA	1978222	nnz10aug78	6.04	=	3.64	15.13
NN_ZEMLYA	1978270	nnz27sep78	5.68	=	4.09	15.74
NN_ZEMLYA	1979267	nnz24sep79	5.80	=	4.14	15.63
NN_ZEMLYA	1979291	nnz18oct79	5.85	=	3.79	15.05
NN_ZEMLYA	1980285	nnz11oct80	5.80	=	3.76	15.36
NN_ZEMLYA	1981274	nnz01oct81	5.91	=	4.10	15.67
NN_ZEMLYA	1982284	nnz11oct82	5.52	=	3.66	15.22
NN_ZEMLYA	1983230	nnz18aug83	5.84	=	3.86	15.54
NN_ZEMLYA	1983268	nnz25sep83	5.71	=	3.52	15.10
NN_ZEMLYA	1984299	nnz25oct84	5.80	=	3.92	15.65
NN_ZEMLYA	1987214	nnz02aug87	5.80	=	3.81	15.42
NN_ZEMLYA	1988128	nnz07may88	5.60	=	3.89	15.45
NN_ZEMLYA	1988339	nnz04dec88	5.90	=	3.93	15.59
NN_ZEMLYA	1990297	nnz24oct90	5.40	=	3.86	15.44
NTS	1987077	middlenote	4.30	<	1.98	14.41
NTS	1987112	presidio	4.20	<	3.37	15.97
NTS	1987171	missionghost	-1.00	<	3.56	14.03
NTS	1987181	panchuela	4.60	<	2.83	14.19
NTS	1987181	panchuelaA	4.20	<	1.76	14.15
PAHUTE	1966181	halfbeak	6.10	=	4.58	16.49
PAHUTE	1967143	scotch	5.70	=	4.50	16.34
PAHUTE	1968082	stinger	5.60	=	4.14	16.04
PAHUTE	1968117	boxcar	6.30	=	5.32	16.94
PAHUTE	1968242	sled	5.90	=	4.23	16.11
PAHUTE	1968354	benham	6.30	=	5.35	16.95
PAHUTE	1969127	purse	5.80	=	4.43	16.24
PAHUTE	1970085	handley	6.50	=	5.22	16.80
PAHUTE	1973157	almendro	6.10	=	4.72	16.49
PAHUTE	1975134	tybo	6.00	=	4.61	16.42
PAHUTE	1975154	stilton	5.90	=	4.18	16.09
PAHUTE	1975170	mast	6.10	=	4.55	16.39
PAHUTE	1976045	cheshire	6.00	=	4.68	16.47
PAHUTE	1976069	estuary	6.00	=	4.67	16.41
PAHUTE	1976077	pool	6.10	=	4.45	16.20
PAHUTE	1978101	backbeach	5.50	=	3.92	15.76
PAHUTE	1978101	fondutta	5.30	<	3.11	15.35
PAHUTE	1978243	panir	5.60	=	3.93	15.74
PAHUTE	1978350	farm	5.50	=	4.07	15.79
PAHUTE	1979162	pepato	5.50	=	4.10	16.03
PAHUTE	1979269	sheepshead	5.60	=	4.01	15.86
PAHUTE	1980117	colwick	5.40	=	3.93	15.79

PAHUTE	1980164	kash	5.60	=	4.11	15.97
PAHUTE	1980207	tafi	5.50	=	4.20	16.01
PAHUTE	1981157	harzer	5.50	=	3.62	15.48
PAHUTE	1987108	delamar	5.50	=	3.97	15.62
PAHUTE	1987120	hardin	5.50	=	3.95	15.76
PAHUTE	1987267	lockney	5.70	=	4.15	15.95
PAHUTE	1988230	kearsarge	5.50	=	3.87	15.61
SHAGAN	1969334	sha30nov69	6.00	=	3.68	15.74
SHAGAN	1972307	sha02nov72	6.14	=	3.80	15.64
SHAGAN	1972345	sha10dec72	6.00	=	4.39	16.07
SHAGAN	1973204	sha23jul73	6.18	=	4.07	15.71
SHAGAN	1973348	sha14dec73	5.82	=	3.76	15.88
SHAGAN	1976186	sha04jul76	5.81	=	3.82	15.65
SHAGAN	1976342	sha07dec76	5.90	=	3.84	15.39
SHAGAN	1977149	sha29may77	5.77	=	3.11	15.16
SHAGAN	1977180	sha29jun77	5.22	=	3.01	14.74
SHAGAN	1977248	sha05sep77	5.74	=	3.81	15.50
SHAGAN	1977302	sha29oct77	5.54	=	3.74	15.47
SHAGAN	1978162	sha11jun78	5.86	=	4.11	15.86
SHAGAN	1978186	sha05jul78	5.83	=	3.39	15.11
SHAGAN	1978241	sha29aug78	5.95	=	3.48	15.44
SHAGAN	1978258	sha15sep78	5.99	=	3.83	15.62
SHAGAN	1978308	sha04nov78	5.56	=	3.65	15.30
SHAGAN	1978333	sha29nov78	6.07	=	3.88	15.64
SHAGAN	1979032	sha01feb79	5.38	=	2.73	14.67
SHAGAN	1979174	sha23jun79	6.22	=	3.82	15.68
SHAGAN	1979188	sha07jul79	5.83	=	3.77	15.67
SHAGAN	1979216	sha04aug79	6.16	=	4.02	15.84
SHAGAN	1979230	sha18aug79	6.12	=	3.74	15.49
SHAGAN	1979301	sha28oct79	5.96	=	4.03	15.82
SHAGAN	1979336	sha02dec79	6.01	=	4.11	15.94
SHAGAN	1979357	sha23dec79	6.18	=	3.77	15.44
SHAGAN	1980116	sha25apr80	5.50	<	2.77	14.55
SHAGAN	1980164	sha12jun80	5.59	=	3.08	14.91
SHAGAN	1980181	sha29jun80	5.74	=	3.35	15.11
SHAGAN	1980258	sha14sep80	6.21	=	3.94	15.71
SHAGAN	1980286	sha12oct80	5.90	=	3.94	15.80
SHAGAN	1980349	sha14dec80	5.95	=	3.85	15.61
SHAGAN	1980362	sha27dec80	5.88	=	3.58	15.35
SHAGAN	1981088	sha29mar81	5.61	=	3.37	15.12
SHAGAN	1981112	sha22apr81	6.05	=	4.03	15.87
SHAGAN	1981147	sha27may81	5.46	=	2.79	14.70
SHAGAN	1981256	sha13sep81	6.18	=	4.01	15.90
SHAGAN	1981291	sha18oct81	6.11	=	4.10	15.87
SHAGAN	1981361	sha27dec81	6.31	=	4.17	15.86
SHAGAN	1982115	sha25apr82	6.10	=	3.96	15.68
SHAGAN	1982185	sha04jul82	6.10	<	4.45	16.55
SHAGAN	1982339	sha05dec82	6.10	=	4.00	15.76
SHAGAN	1983163	sha12jun83	6.10	=	4.27	16.04
SHAGAN	1983279	sha06oct83	6.00	=	4.15	15.95
SHAGAN	1983299	sha26oct83	6.10	=	4.11	15.80
SHAGAN	1984050	sha19feb84	5.80	=	4.08	15.79
SHAGAN	1984089	sha29mar84	5.90	=	3.88	15.71
SHAGAN	1984116	sha25apr84	5.90	=	4.11	15.93
SHAGAN	1984147	sha26may84	6.00	<	3.76	15.47
SHAGAN	1984196	sha14jul84	6.20	=	4.28	16.06



SHAGAN	1984301	sha27oct84	6.20	=	4.14	15.84
SHAGAN	1984337	sha02dec84	5.80	=	3.92	15.64
SHAGAN	1984351	sha16dec84	6.10	=	4.17	16.01
SHAGAN	1984363	sha28dec84	6.00	=	4.06	15.76
SHAGAN	1985041	sha10feb85	5.90	=	4.15	15.94
SHAGAN	1985115	sha25apr85	5.90	=	3.75	15.55
SHAGAN	1985166	sha15jun85	6.00	=	3.90	15.65
SHAGAN	1985181	sha30jun85	6.00	=	3.92	15.68
SHAGAN	1985201	sha20jul85	5.90	=	3.90	15.64
SHAGAN	1987071	sha12mar87	5.40	=	3.67	15.49
SHAGAN	1987093	sha03apr87	6.20	=	4.39	16.15
SHAGAN	1987107	sha17apr87	6.00	=	3.68	15.56
SHAGAN	1987171	sha20jun87	6.10	=	3.95	15.72
SHAGAN	1987214	sha02aug87	5.90	=	3.78	15.52
SHAGAN	1987259	sha16sep87	4.50	<	2.67	13.58
SHAGAN	1987319	sha15nov87	6.00	=	4.39	16.17
SHAGAN	1987347	sha13dec87	6.10	=	4.11	15.84
SHAGAN	1987361	sha27dec87	6.10	=	3.99	15.72
SHAGAN	1988044	sha13feb88	6.10	=	4.10	15.89
SHAGAN	1988094	sha03apr88	6.00	=	4.20	15.87
SHAGAN	1988125	sha04may88	6.10	=	3.94	15.81
SHAGAN	1988166	sha14jun88	4.90	<	1.95	14.84
SHAGAN	1988258	shaganjve	6.10	=	4.21	16.03
SHAGAN	1988317	sha12nov88	5.26	=	2.70	14.91
SHAGAN	1988352	sha17dec88	5.67	=	4.01	15.87
SHAGAN	1988363	sha28dec88	3.90	<	2.92	14.46
SHAGAN	1989022	sha22jan89	5.95	=	4.17	15.94
SHAGAN	1989043	sha12feb89	5.71	=	4.19	15.87
SHAGAN	1989189	sha08jul89	5.48	=	3.78	15.51
SHAGAN	1989245	sha02sep89	4.98	=	3.31	15.17
SHAGAN	1989292	sha19oct89	5.74	=	4.17	16.00
SN_ZEMLYA	1973270	snz27sep73	5.83	=	3.69	15.44
SN_ZEMLYA	1973300	snz27oct73	6.90	=	5.49	16.98
SN_ZEMLYA	1973300	snz27oct73A	4.20	<	3.87	14.52
SN_ZEMLYA	1973300	snz27oct73B	4.40	<	3.66	15.28
SN_ZEMLYA	1974306	snz02nov74	6.75	=	5.25	16.73
SN_ZEMLYA	1975291	snz18oct75	6.70	=	4.87	16.42
USA	1964296	salmon	-1.00	<	2.13	14.68
USA	1967344	gasbuggy	5.10	=	3.61	15.55
USA	1968019	faultless	6.30	=	4.99	16.97
USA	1969253	rulison	5.30	=	3.42	15.36
USA	1973137	rioblanco	5.40	=	3.51	15.60
USSR	1968183	sov01jul68	5.70	<	3.15	14.89
USSR	1970346	sov12dec70	6.60	=	4.07	15.88
USSR	1970357	sov23dec70	6.60	=	4.23	15.95
USSR	1971082	sov23mar71	5.90	=	3.79	15.53
USSR	1976211	sov29jul76	5.90	=	3.85	15.33
YUCCA	1965337	corduroy	5.60	=	4.07	15.96
YUCCA	1966139	dumont	5.80	=	4.05	15.98
YUCCA	1967054	agile	5.80	=	4.05	15.77
YUCCA	1967140	commodore	5.90	=	4.47	16.19
YUCCA	1967270	zaza	5.70	=	4.40	16.19
YUCCA	1967291	lanpher	5.70	=	3.90	15.79
YUCCA	1968250	noggin	5.60	=	4.02	15.90
YUCCA	1969302	calabash	5.70	=	3.78	15.75
YUCCA	1970146	flask	5.60	=	3.59	15.58

YUCCA	1970287	tijeras	5.50	=	4.11	15.97
YUCCA	1970351	carpetbag	5.70	=	4.13	15.93
YUCCA	1972265	oscuro	5.70	=	4.11	16.03
YUCCA	1973116	starwort	5.60	=	3.78	15.65
YUCCA	1974191	escabosa	5.70	=	4.33	16.11
YUCCA	1974242	portmanteau	5.80	=	3.78	15.75
YUCCA	1975059	topgallant	5.70	=	3.65	15.71
YUCCA	1975154	mizzen	5.70	=	3.97	15.96
YUCCA	1975354	chiberta	5.70	=	4.09	16.03
YUCCA	1976035	esrom	5.70	=	3.72	15.70
YUCCA	1976035	keelson	5.80	=	4.01	16.02
YUCCA	1976077	strait	5.80	=	4.30	16.11
YUCCA	1976363	rudder	5.50	<	3.91	15.59
YUCCA	1977095	marsilly	5.60	=	3.59	15.55
YUCCA	1977117	bulkhead	5.40	<	3.70	15.53
YUCCA	1977145	crewline	5.30	=	3.50	15.96
YUCCA	1977231	scantling	5.60	=	4.04	15.96
YUCCA	1977231	yuc19aug77A	-1.00	<	4.18	16.18
YUCCA	1977313	sandreef	5.70	=	4.28	16.16
YUCCA	1977348	farallones	5.70	=	4.04	15.81
YUCCA	1977348	yuc14dec77A	-1.00	<	3.90	15.21
YUCCA	1978054	reblochon	5.60	=	3.88	15.73
YUCCA	1978082	iceberg	5.60	=	3.98	15.98
YUCCA	1978193	lowball	5.50	=	3.95	15.74
YUCCA	1978270	draughts	5.00	<	3.45	14.71
YUCCA	1978270	rummy	5.70	=	4.20	16.07
YUCCA	1978322	quargel	5.10	=	3.74	15.20
YUCCA	1979039	quinella	5.50	=	3.92	15.71
YUCCA	1979249	hearts	5.80	=	4.19	16.02
YUCCA	1980107	pyramid	5.30	=	3.80	15.63
YUCCA	1987034	hazebrook	-1.00	<	1.77	14.57
YUCCA	1987169	brie	-1.00	=	2.88	15.33
YUCCA	1987197	midland	4.80	=	3.27	15.04
YUCCA	1987197	midlandA	-1.00	=	2.08	14.34
YUCCA	1987225	tahoka	5.90	=	4.18	15.84

## Appendix G. Maximum Likelihood $M_s$ and $\log M_0$ for Earthquakes

The following table contains maximum the likelihood magnitudes for earthquakes discussed in Section 5. "Flag" indicates whether  $M_s$  and  $\log M_0$  are a maximum likelihood magnitude/moment (=) or a maximum likelihood upper bound on the magnitude/moment.

Date	Orid	Lat	Lon	Depth	$m_b$	Flag	$M_s$	$\log M_0$
1997159	1059384	-53.71	140.42	0.00	3.83	=	3.30	15.15
1997159	1059398	51.14	-178.78	0.00	3.52	<	2.75	14.53
1997159	1059445	38.94	89.30	0.00	3.96	=	3.16	15.06
1997159	1059766	13.00	127.19	0.00	3.48	<	2.83	14.37
1997159	1059787	-15.02	-175.24	0.00	3.82	<	3.06	14.72
1997159	1059791	-47.76	32.09	0.00	4.36	=	4.38	16.36
1997159	1059810	-13.00	166.15	51.94	3.43	=	3.34	14.87
1997159	1059817	-3.90	-104.02	0.00	4.09	=	4.48	16.39
1997159	1059829	-22.08	163.23	0.00	3.41	<	2.99	14.77
1997159	1059843	50.74	179.90	0.00	3.55	=	2.85	14.46
1997159	1059867	26.83	-111.73	0.00	3.85	=	3.07	14.88
1997159	1059889	38.21	89.92	64.33	3.61	=	2.90	14.77
1997159	1059891	28.29	130.26	38.91	4.15	=	4.22	15.61
1997159	1059900	30.62	67.62	0.00	3.76	=	3.42	15.20
1997159	1059902	-22.25	-169.76	0.00	3.90	<	3.37	15.07
1997159	1059921	-5.36	154.63	0.00	3.63	<	2.80	14.55
1997159	1059934	-24.91	-69.05	0.00	3.18	<	2.29	14.66
1997159	1059935	35.70	22.53	0.00	4.67	=	3.83	15.52
1997159	1059936	-55.28	-128.67	25.02	4.26	=	4.89	16.75
1997159	1059951	-16.97	-173.58	0.00	3.44	<	3.30	14.83
1997159	1059961	28.07	51.80	0.00	4.08	<	2.69	14.55
1997159	1059984	-3.07	142.34	0.00	3.27	<	2.80	14.76
1997159	1060423	31.08	137.96	0.00	3.28	<	2.82	14.44
1997159	1060475	20.95	-45.99	0.00	4.03	=	3.68	15.57
1997159	1060550	35.39	138.99	0.00	3.42	<	2.94	14.61
1997159	1060575	-14.93	-174.33	0.00	4.03	=	3.54	15.08
1997159	1060578	11.92	144.77	40.75	3.38	<	3.20	14.53
1997159	1060580	-17.35	-174.81	0.00	3.97	<	3.32	14.82
1997159	1060583	51.82	-174.92	0.00	3.79	=	2.66	14.48
1997159	1060802	4.84	-80.53	0.00	3.47	<	3.19	15.07
1997159	1060804	38.27	76.94	0.00	3.98	=	2.41	14.65
1997160	1059797	-3.26	134.96	0.00	4.15	=	3.28	14.94
1997160	1059808	-6.45	39.31	0.00	4.10	=	3.25	14.93
1997160	1059811	-0.07	136.20	0.00	3.72	<	2.93	14.64
1997160	1059828	41.33	142.20	67.28	3.30	=	2.46	14.40
1997160	1059840	62.27	-124.18	0.00	3.07	<	2.21	14.45
1997160	1059845	2.87	128.31	0.00	3.50	<	2.78	14.39
1997160	1059857	9.20	125.88	0.00	3.64	<	3.41	15.15
1997160	1059881	-21.16	171.50	0.00	4.75	=	5.65	17.67
1997160	1059896	-43.49	-75.80	0.00	4.43	<	3.73	16.00
1997160	1059914	38.56	16.26	0.00	3.87	=	2.97	14.82
1997160	1059940	-21.24	171.52	0.00	4.11	=	4.19	16.26
1997160	1060030	-19.76	171.11	0.00	4.17	=	4.06	16.09
1997160	1060040	-35.16	-179.64	0.00	3.78	<	3.22	15.38
1997160	1060046	-5.67	149.92	0.00	4.04	<	3.31	15.22
1997160	1060068	-21.20	171.59	0.00	4.30	<	3.71	14.51
1997160	1060080	-21.99	-177.57	0.00	3.97	<	3.86	15.26
1997160	1060090	-0.21	131.38	0.00	3.85	<	3.50	15.60

1997160	1060528	25.32	128.82	0.00	3.66	<	2.88	14.53
1997160	1060557	-31.92	-71.43	51.58	4.34	=	4.32	16.42
1997160	1060640	-2.64	142.10	0.00	3.65	<	2.85	14.65
1997160	1061190	0.20	125.33	0.00	3.98	=	3.01	14.68
1997160	1061246	32.82	-109.27	0.00	3.43	=	2.30	14.58
1997160	1061260	43.30	35.89	22.17	3.76	=	2.78	14.79
1997166	1064311	22.23	146.98	0.00	3.59	<	2.93	14.42
1997166	1064323	-0.82	149.29	0.00	4.05	<	2.95	14.48
1997166	1064368	-12.64	-73.88	0.00	3.75	=	2.43	14.62
1997166	1064370	-13.19	165.80	0.00	4.05	=	3.51	14.95
1997166	1064371	-1.18	131.42	0.00	3.90	<	2.71	14.49
1997166	1064376	-11.70	66.27	0.00	3.87	=	3.81	15.57
1997166	1064733	15.05	-99.83	0.00	3.53	<	2.96	15.02
1997166	1064745	-3.19	134.79	0.00	3.94	<	3.21	14.73
1997166	1064757	-12.43	168.77	0.00	3.72	<	3.49	14.73
1997166	1064770	-6.37	151.67	66.37	3.72	<	3.01	14.47
1997166	1064772	-32.64	-178.42	0.00	3.89	=	3.91	15.64
1997166	1064780	-56.14	-129.67	0.00	3.88	=	4.24	16.10
1997166	1064825	-4.43	159.20	0.00	3.79	<	2.80	14.39
1997166	1064830	-3.85	150.61	0.00	3.95	<	3.02	14.49
1997166	1064869	-25.47	-176.59	0.00	4.27	=	4.12	15.27
1997166	1064873	-7.42	156.44	0.00	3.77	=	3.02	14.62
1997166	1065007	-5.08	149.17	30.71	3.64	<	2.86	14.62
1997166	1065011	-19.74	-176.07	0.00	3.36	<	3.46	14.66
1997166	1065013	37.40	22.29	0.00	3.46	<	2.75	14.89
1997166	1065015	-22.49	-177.87	0.00	3.97	<	3.23	14.49
1997166	1065020	-2.59	130.10	0.00	3.98	<	2.85	14.59
1997166	1065029	-7.26	130.68	0.00	3.78	<	2.54	14.23
1997166	1065032	-16.03	-174.01	0.00	4.18	<	3.06	14.56
1997166	1065084	-31.64	-178.73	0.00	3.53	<	3.25	15.04
1997166	1065486	-22.40	169.54	0.00	3.88	<	3.07	14.60
1997166	1065513	-2.16	136.37	0.00	3.75	<	2.63	14.61
1997166	1065527	51.93	-177.37	0.00	3.31	<	2.52	14.23
1997166	1065534	-10.07	121.14	0.00	4.10	<	2.69	14.36
1997166	1065547	-2.43	127.80	0.00	3.27	<	2.55	14.27
1997166	1065626	-1.75	135.42	0.00	3.95	<	2.75	14.49
1997166	1065636	-7.59	151.55	0.00	3.29	<	2.63	14.35
1997166	1065677	-56.91	-25.08	0.00	4.79	=	4.85	16.83
1997166	1065698	-11.50	66.32	0.00	4.39	=	4.27	16.15
1997166	1065701	-21.19	179.87	0.00	3.54	<	3.35	15.16
1997166	1065709	-15.91	168.85	23.95	3.74	=	3.49	15.01
1997166	1065710	-6.25	154.92	54.80	4.46	=	4.46	16.17
1997166	1065719	-7.17	155.75	39.51	4.75	=	5.09	16.58
1997166	1065802	-2.85	129.79	0.00	3.72	<	2.68	14.16
1997166	1065813	-15.57	-177.12	0.00	4.05	<	3.22	14.46
1997166	1065872	-7.29	155.61	59.92	4.30	=	4.62	16.22
1997166	1065889	34.26	96.66	0.00	3.75	<	2.40	14.80
1997166	1066406	44.82	-110.65	0.00	3.71	=	2.98	14.85
1997166	1066418	-7.06	155.62	0.00	4.06	<	4.25	15.66
1997166	1066522	-13.94	-177.39	0.00	4.32	<	3.11	14.48
1997166	1066528	-5.36	152.26	35.33	3.80	<	2.93	14.53
1997166	1066534	-15.61	167.38	0.00	4.18	<	3.44	14.88
1997167	1064420	-7.28	155.81	74.99	4.07	=	3.95	15.50
1997167	1064425	0.45	98.64	0.00	4.22	<	2.79	14.64
1997167	1064436	-57.30	-25.36	0.00	4.77	=	3.76	15.75
1997167	1064451	40.99	20.55	0.00	3.79	<	2.42	14.43

1997167	1064756	-3.34	134.64	0.00	4.77	=	4.14	15.67
1997167	1064779	30.08	130.91	63.35	3.69	=	4.21	15.50
1997167	1064807	15.00	-91.16	0.00	3.59	<	2.92	14.50
1997167	1064810	-3.24	134.94	0.00	4.13	<	2.86	14.60
1997167	1064817	-17.09	-177.73	0.00	3.98	<	3.16	14.53
1997167	1064819	-22.65	170.99	0.00	3.98	=	3.32	14.98
1997167	1064842	35.37	78.46	0.00	3.85	=	2.78	14.55
1997167	1064870	62.18	-151.70	0.00	3.66	<	1.75	14.21
1997167	1064880	24.14	122.59	0.00	3.76	<	2.15	14.32
1997167	1064885	-20.49	168.90	0.00	3.81	=	3.15	14.70
1997167	1064897	44.91	-110.43	0.00	3.48	=	2.85	14.76
1997167	1064898	-5.84	153.64	0.00	4.05	<	2.91	14.38
1997167	1064972	7.02	120.43	0.00	3.89	<	2.74	14.51
1997167	1065006	43.58	146.69	37.24	3.71	=	3.09	14.58
1997167	1065010	37.64	29.26	0.00	3.82	=	2.49	14.55
1997167	1065023	-33.02	-178.63	0.00	4.52	=	4.75	16.24
1997167	1065044	8.13	-82.86	0.00	4.18	=	4.11	15.80
1997167	1065063	-33.16	-177.96	0.00	4.36	<	4.37	15.63
1997167	1065070	-32.81	-178.48	0.00	4.47	=	3.96	15.53
1997167	1065074	33.14	60.09	45.46	4.51	=	4.38	15.99
1997167	1065080	-48.11	125.31	0.00	4.51	=	3.88	15.89
1997167	1065096	-1.06	-24.47	0.00	4.22	=	3.97	15.96
1997167	1065119	-31.49	-178.27	0.00	3.93	<	3.35	14.89
1997167	1065133	2.37	31.30	0.00	4.30	=	3.81	15.67
1997167	1065139	40.69	-134.60	29.27	4.41	=	4.30	16.37
1997167	1065664	38.88	146.58	0.00	3.96	<	2.13	14.09
1997168	1064946	-56.88	-24.91	0.00	4.36	=	3.53	15.31
1997168	1064971	19.19	143.49	0.00	4.08	<	2.71	14.35
1997168	1065043	12.35	143.64	26.45	3.95	=	4.59	16.03
1997168	1065661	-15.60	-174.80	18.88	4.32	=	4.85	16.32
1997168	1065679	17.77	-65.32	47.49	3.49	<	2.91	14.32
1997168	1065680	-4.56	140.14	0.00	3.68	<	2.99	14.74
1997168	1065690	-33.03	-178.50	41.00	4.36	=	4.78	16.32
1997168	1065702	12.46	124.85	0.00	4.03	=	3.43	15.09
1997168	1065703	12.39	143.29	0.00	4.17	=	4.09	15.50
1997168	1065706	-3.07	148.11	0.00	3.90	=	3.33	14.74
1997168	1065707	11.81	145.44	23.93	3.79	<	3.44	14.85
1997168	1065727	-32.95	-178.59	0.00	4.10	<	3.42	15.19
1997168	1065732	-32.89	-178.31	0.00	4.21	=	3.59	15.22
1997168	1065771	11.73	125.58	0.00	3.86	=	2.79	14.45
1997168	1065799	30.06	68.03	36.47	4.15	=	4.87	16.38
1997168	1065814	-33.05	-178.35	0.00	4.65	=	3.66	15.35
1997168	1065825	-6.81	102.91	0.00	3.72	<	3.09	14.02
1997168	1065827	-17.84	177.02	0.00	4.00	<	3.34	15.04
1997168	1065861	1.84	97.68	13.89	3.83	<	2.67	14.38
1997168	1065863	-23.23	171.13	0.00	4.18	<	3.40	15.15
1997168	1065866	-23.35	170.86	31.60	4.02	<	3.37	15.26
1997168	1065867	31.37	132.78	22.63	4.16	=	3.20	15.00
1997168	1065880	33.29	89.85	15.54	3.61	=	3.16	14.84
1997168	1065949	-34.31	75.43	0.00	3.62	=	3.93	15.93
1997168	1065977	10.76	-86.56	0.00	3.93	<	3.04	14.67
1997168	1066377	26.98	-112.43	0.00	3.30	=	3.31	15.07
1997168	1066401	12.42	143.64	18.14	3.63	<	2.99	14.56
1997168	1066451	-19.52	174.02	0.00	3.80	<	3.11	14.98
1997168	1066491	-14.65	167.95	0.00	3.97	=	3.40	14.98
1997168	1066547	5.83	127.06	0.00	3.67	<	2.42	14.34

1997168	1066576	3.22	128.29	62.61	4.05	=	3.56	15.04
1997168	1066613	-27.75	-64.88	25.16	5.23	=	5.03	16.90
1997168	1066624	-5.12	102.62	0.00	3.88	<	2.78	14.43
1997168	1066653	-6.65	155.28	0.00	3.89	<	4.47	15.97
1997168	1066680	51.27	-179.21	0.00	6.07	=	6.33	17.93
1997168	1066695	17.11	-96.39	0.00	3.60	<	2.83	14.73
1997168	1066721	-6.74	103.32	0.00	3.49	<	3.00	14.55
1997168	1066722	-26.06	28.96	0.00	3.97	<	1.98	14.74
1997168	1066987	-6.82	155.69	29.93	3.88	<	4.03	15.77
1997168	1066996	-12.74	166.33	0.00	4.08	<	4.13	15.79
1997168	1067165	-5.16	108.22	0.00	4.04	<	3.27	14.40
1997168	1067180	42.39	140.60	0.00	3.54	=	2.68	14.57
1997169	1066342	51.82	-173.67	29.00	3.49	<	2.80	14.69
1997169	1066373	44.11	147.81	42.09	3.97	<	2.80	14.48
1997169	1066391	51.25	-179.29	0.00	4.20	=	3.80	15.26
1997169	1066400	11.33	139.13	0.00	4.31	=	3.91	15.20
1997169	1066404	23.49	127.79	0.00	3.73	<	2.38	14.15
1997169	1066410	30.47	143.03	0.00	3.78	<	2.53	14.50
1997169	1066412	0.27	138.45	0.00	3.49	<	2.95	14.47
1997169	1066420	-6.04	131.59	45.66	4.04	<	2.57	14.31
1997169	1066421	-32.91	-178.50	0.00	4.02	=	3.35	15.08
1997169	1066428	12.06	123.77	0.00	3.52	=	2.81	14.60
1997169	1066436	18.05	-106.97	0.00	3.41	=	3.46	15.50
1997169	1066444	18.83	-108.80	0.00	3.90	<	3.31	15.52
1997169	1066445	18.93	-108.80	0.00	3.70	=	3.48	15.66
1997169	1066450	-7.59	158.22	58.61	3.47	<	2.97	14.63
1997169	1066469	64.89	137.11	18.41	3.94	=	3.03	14.97
1997169	1066472	1.17	99.27	0.00	3.79	<	1.48	14.53
1997169	1066473	-8.29	128.78	0.00	3.82	<	2.62	14.51
1997169	1066479	34.36	-36.73	0.00	3.95	=	3.60	15.57
1997169	1066480	11.72	145.61	0.00	3.56	<	2.84	14.07
1997169	1066489	9.31	122.19	0.00	4.17	=	3.31	14.83
1997169	1066490	-2.35	128.28	0.00	3.83	<	2.94	14.39
1997169	1066492	4.42	-76.22	0.00	3.95	=	3.35	15.02
1997169	1066512	-32.98	-178.32	0.00	4.35	<	4.05	15.96
1997169	1066539	-38.22	177.38	0.00	4.44	<	3.12	14.84
1997169	1066554	30.70	142.78	39.93	3.71	<	3.29	14.46
1997169	1066560	12.38	143.43	19.21	4.36	=	4.76	16.19
1997169	1066561	12.34	145.16	0.00	4.07	<	4.36	15.81
1997169	1066569	10.27	126.36	37.17	3.92	<	3.05	14.48
1997169	1066583	50.92	173.39	0.00	3.62	=	2.62	14.51
1997169	1066595	51.22	98.36	24.26	3.92	=	3.84	15.62
1997169	1066603	47.40	153.12	59.17	4.14	=	3.65	15.14
1997169	1066612	-15.54	-175.23	0.00	4.08	<	3.33	14.55
1997169	1066955	-13.39	-178.93	0.00	3.57	<	3.21	14.53
1997169	1066993	-22.55	173.99	0.00	3.74	<	3.24	14.88
1997169	1067015	-19.00	-175.26	0.00	3.64	<	3.17	14.68
1997169	1067018	-6.60	150.30	0.00	3.41	<	2.76	14.50
1997169	1067019	-2.46	130.21	0.00	3.61	<	2.76	14.52
1997169	1067024	12.41	143.57	23.46	3.55	=	3.38	14.72
1997169	1067031	13.84	143.16	0.00	3.81	<	3.51	14.75
1997169	1067032	-32.98	-178.29	0.00	4.63	=	4.92	16.57
1997169	1067036	-18.31	-171.51	0.00	3.94	<	3.76	14.78
1997169	1067041	-8.09	105.61	0.00	3.87	<	2.93	14.51
1997169	1067050	-5.76	153.82	60.49	3.06	<	2.90	14.50
1997169	1067084	-7.78	129.82	0.00	3.83	<	2.91	14.42

1997169	1068962	-32.85	-178.49	0.00	4.21	<	3.38	15.09
1997170	1066566	-32.14	-179.20	56.02	4.27	<	3.32	15.24
1997170	1067007	-7.44	155.69	0.00	3.77	=	3.17	14.70
1997170	1067023	-32.10	-179.00	0.00	3.64	<	3.20	14.97
1997170	1067029	3.39	95.03	31.90	4.00	=	3.69	15.23
1997170	1067157	31.31	-115.71	0.00	3.91	=	3.10	14.62
1997170	1067178	11.88	143.84	24.41	3.76	<	3.53	14.74
1997170	1067190	-40.73	174.72	17.59	4.77	=	4.12	16.02
1997170	1067192	12.40	143.59	26.51	4.30	=	3.94	15.45
1997170	1067194	-8.97	119.56	0.00	3.73	<	2.91	14.68
1997170	1067202	34.47	-36.59	0.00	3.73	=	3.35	15.27
1997170	1067226	-29.90	-178.22	0.00	3.86	<	3.30	14.59
1997170	1067257	7.40	-74.96	44.84	3.61	<	2.93	14.52
1997170	1067265	-46.40	-11.05	0.00	4.01	=	3.72	15.77
1997170	1067320	24.31	126.35	0.00	4.12	<	3.23	14.18
1997170	1067334	-21.80	170.18	0.00	3.96	<	3.07	13.71
1997170	1067382	-7.08	128.93	0.00	3.91	<	2.63	14.45
1997170	1067392	40.16	21.96	0.00	3.67	<	2.53	14.36
1997170	1067398	13.46	-88.75	60.48	3.59	=	3.17	14.94
1997170	1068817	-32.78	-178.49	0.00	4.51	=	4.85	16.41
1997170	1068829	51.51	159.35	30.77	4.27	=	4.62	16.03
1997170	1068862	-19.49	-177.27	0.00	3.81	<	3.32	14.60
1997170	1068863	35.49	21.71	0.00	3.72	<	2.44	14.55
1997170	1068877	2.81	126.00	0.00	3.88	<	2.90	14.40
1997170	1068903	-8.85	122.34	46.54	4.81	=	4.03	15.90
1997170	1068933	-29.65	-177.72	0.00	4.26	<	3.47	14.81
1997170	1068965	-5.00	129.37	0.00	3.97	<	3.31	14.82
1997170	1068985	14.08	-92.39	0.00	3.68	=	3.06	14.80
1997170	1069085	-21.10	-177.76	0.00	3.81	<	4.20	14.91
1997170	1069095	-5.09	142.06	0.00	4.11	<	3.36	14.73
1997170	1069164	24.86	125.40	52.01	4.71	=	4.32	15.89
1997170	1069520	4.32	143.49	0.00	3.85	<	3.18	14.62
1997170	1069584	-15.77	-173.46	0.00	4.10	<	3.37	14.63
1997170	1069588	-9.33	113.28	0.00	3.92	<	3.02	14.35
1997171	1067158	51.48	-173.78	21.59	4.49	=	4.80	16.08
1997171	1067161	51.56	159.28	40.43	3.63	<	3.18	14.73
1997171	1067162	34.76	23.04	0.00	4.04	<	2.77	14.75
1997171	1067163	-5.51	68.70	0.00	4.13	=	4.28	16.37
1997171	1067208	51.59	159.34	35.47	3.55	=	2.94	14.81
1997171	1068798	32.72	-117.96	0.00	3.86	=	3.80	15.39
1997171	1068803	-21.47	161.71	0.00	3.43	<	2.88	14.59
1997171	1068809	20.00	120.78	26.37	3.37	<	2.67	14.49
1997171	1068820	76.11	-117.81	0.00	3.88	<	2.11	14.31
1997171	1068849	-40.81	174.60	23.40	4.99	=	4.47	16.36
1997171	1068861	32.78	-117.98	0.00	4.36	=	4.28	15.87
1997171	1068890	64.79	147.00	0.00	3.67	<	2.83	14.84
1997171	1068914	-13.12	166.34	0.00	4.15	=	3.61	15.15
1997171	1068924	32.11	59.92	0.00	4.70	=	5.35	17.06
1997171	1068926	51.52	159.43	36.14	3.95	=	3.88	15.36
1997171	1068934	-33.14	-178.38	0.00	4.34	=	3.44	15.24
1997171	1068940	-7.41	156.23	0.00	3.34	<	3.04	14.60
1997171	1068943	-30.21	-174.89	0.00	3.89	<	3.50	15.04
1997171	1068947	31.96	60.02	0.00	4.01	<	3.69	15.40
1997171	1068948	32.99	-117.66	0.00	3.97	=	3.71	15.13
1997171	1068949	32.17	60.01	0.00	3.92	<	3.63	15.18
1997171	1068950	12.38	143.60	17.77	3.78	<	2.95	14.49

1997171	1068951	-32.61	-178.40	0.00	3.60	<	3.97	15.37
1997171	1068952	-14.95	-171.55	0.00	3.95	<	3.30	14.55
1997171	1068953	43.24	146.75	0.00	3.98	<	3.06	14.50
1997171	1068954	38.32	142.93	0.00	3.64	<	2.47	14.75
1997171	1068970	-19.23	-171.25	0.00	3.49	<	3.43	14.72
1997171	1068994	21.41	145.72	17.03	4.73	=	4.50	15.73
1997171	1069019	33.95	141.69	33.02	3.86	=	3.36	14.82
1997171	1069108	-32.53	-178.44	0.00	4.09	=	4.00	15.59
1997171	1069154	4.53	126.95	0.00	4.01	<	2.95	14.42
1997171	1069163	-32.65	-178.47	0.00	3.89	<	3.01	14.92
1997171	1069175	-28.75	-177.54	0.00	3.49	<	3.33	14.58
1997171	1069525	60.96	167.05	0.00	3.67	<	2.81	14.78
1997171	1069543	16.85	124.57	0.00	3.70	<	2.46	14.42
1997171	1069545	29.57	65.67	0.00	3.77	=	3.03	14.80
1997172	1068872	34.74	26.62	55.76	3.86	=	3.14	14.92
1997172	1068896	16.98	147.42	16.69	4.61	=	4.95	16.19
1997172	1068902	13.55	148.80	0.00	3.43	<	2.87	14.46
1997172	1068918	-13.11	165.26	0.00	3.96	<	3.17	14.57
1997172	1068937	38.10	16.30	0.00	3.71	=	3.19	14.76
1997172	1068963	16.98	147.24	0.00	3.95	<	3.12	14.53
1997172	1068969	-6.78	147.74	0.00	3.64	<	2.75	14.55
1997172	1068972	65.33	-134.15	0.00	3.43	<	1.54	14.10
1997172	1068984	51.48	-174.89	42.39	3.46	<	2.55	14.35
1997172	1068987	-6.90	150.57	0.00	3.71	<	3.05	14.42
1997172	1068990	32.04	142.08	34.02	3.88	=	3.49	14.74
1997172	1069002	12.21	126.37	0.00	3.66	<	2.86	14.15
1997172	1069006	-4.71	150.40	0.00	3.68	<	2.97	14.41
1997172	1069011	-6.11	103.82	0.00	4.30	=	3.65	15.13
1997172	1069012	-19.37	-178.71	0.00	3.64	<	3.30	14.65
1997172	1069018	27.22	143.65	0.00	3.80	=	2.90	14.42
1997172	1069021	-16.14	67.28	0.00	4.21	=	3.89	15.78
1997172	1069049	14.63	-91.52	0.00	3.96	=	3.39	14.91
1997172	1069086	-33.15	-178.66	49.37	3.58	<	3.34	14.97
1997172	1069503	-23.21	170.22	30.31	4.01	=	3.42	15.20
1997172	1069540	-7.45	149.81	0.00	3.70	<	2.89	14.57
1997172	1069549	-32.17	-71.21	44.34	4.30	=	3.07	15.04
1997172	1069587	16.46	-98.94	20.24	4.01	=	3.28	14.88
1997172	1069596	-5.70	148.37	0.00	3.74	<	2.90	14.65
1997172	1069609	-5.97	149.17	0.00	3.58	=	3.09	14.70
1997172	1069726	-7.22	129.29	73.32	3.47	<	2.88	14.52
1997172	1069746	-7.75	148.99	0.00	3.52	<	3.02	14.51
1997172	1070531	-16.02	-174.52	0.00	4.02	<	3.41	14.72
1997172	1070548	12.29	143.78	0.00	3.54	<	2.96	14.40
1997172	1070552	-2.34	128.76	0.00	3.83	<	3.02	14.36
1997172	1070573	39.47	68.42	0.00	3.72	<	2.69	14.56
1997172	1070591	-10.52	166.35	0.00	3.62	<	3.13	14.62
1997172	1070599	34.65	71.29	0.00	3.94	<	2.62	14.41
1997172	1070672	33.14	60.16	0.00	4.21	=	3.31	15.00
1997173	1068956	71.73	-1.76	0.00	3.10	=	2.90	14.92
1997173	1068983	-6.10	106.84	0.00	3.97	<	3.20	14.66
1997173	1069010	-24.37	-177.95	0.00	4.59	<	3.28	14.66
1997173	1069015	-4.48	152.24	0.00	3.46	<	2.97	14.40
1997173	1069050	33.62	131.45	0.00	3.91	=	3.03	14.84
1997173	1069073	51.49	-178.24	49.44	4.18	=	4.13	15.78
1997173	1069507	19.62	-71.39	0.00	3.71	<	2.97	14.83
1997173	1069542	30.57	96.83	0.00	3.90	<	2.46	14.48



1997173	1069593	-3.37	147.29	0.00	3.40	<	3.09	14.46
1997173	1069595	39.84	143.19	31.06	3.81	=	3.78	15.45
1997173	1069621	-1.51	129.76	0.00	4.10	<	2.65	14.53
1997173	1069624	-3.31	101.69	0.00	4.18	=	3.32	14.75
1997173	1069645	2.11	121.87	0.00	4.12	=	3.47	14.88
1997173	1069648	33.97	82.64	0.00	3.91	=	3.82	15.45
1997173	1069650	56.87	123.56	0.00	3.65	=	2.91	14.82
1997173	1069651	40.08	77.83	74.11	3.44	<	2.78	14.17
1997173	1069653	31.07	141.95	0.00	4.47	=	4.73	15.89
1997173	1069666	33.18	60.11	11.81	4.20	=	3.26	15.15
1997173	1069679	-6.60	130.22	0.00	4.00	<	2.56	14.40
1997173	1069682	-9.97	124.24	0.00	3.87	<	2.96	14.56
1997173	1069695	31.09	141.75	19.54	4.11	=	4.00	15.14
1997173	1069717	21.93	121.53	35.61	4.39	=	4.58	16.45
1997173	1069736	-1.44	119.16	0.00	3.59	<	2.95	14.49
1997173	1069747	-30.38	-177.96	0.00	3.56	<	3.38	14.88
1997173	1069762	26.99	129.40	69.87	3.57	=	3.15	14.76
1997173	1069788	-20.54	-178.24	0.00	3.84	<	3.34	14.65
1997173	1069790	-19.52	-177.36	0.00	3.85	<	3.28	14.57
1997173	1069813	52.91	-174.72	0.00	3.65	=	2.92	14.51
1997173	1069850	-2.15	137.60	0.00	4.05	=	3.10	14.71
1997173	1070400	-0.94	126.77	0.00	3.12	<	3.07	14.38
1997173	1070460	-17.05	-179.21	0.00	3.39	<	3.46	14.61
1997173	1070468	2.97	95.70	72.12	3.78	<	3.05	14.61
1997173	1070472	-2.86	139.94	0.00	3.74	<	2.73	14.60
1997173	1070747	33.50	28.16	0.00	3.51	<	2.64	14.39
1997173	1070778	36.19	76.36	0.00	3.57	<	2.85	14.49
1997173	1070809	29.89	96.05	20.54	3.51	<	1.95	14.58
1997173	1071113	-23.40	-177.36	0.00	3.67	=	3.38	14.88
1997173	1071145	-10.70	154.11	0.00	3.54	<	2.86	14.42
1997173	1071206	-8.03	129.19	0.00	3.75	<	2.81	14.47
1997173	1071233	-5.73	148.24	0.00	3.27	<	3.02	14.66
1997173	1071236	-6.23	130.86	0.00	4.19	<	3.18	14.39
1997173	1071865	39.53	49.26	30.15	3.72	<	2.15	14.38
1997174	1069564	36.67	73.03	0.00	4.24	<	2.45	14.43
1997174	1069577	14.04	121.08	0.00	3.93	=	3.03	14.76
1997174	1069623	-5.92	152.51	28.32	3.83	<	2.85	14.37
1997174	1069637	10.66	125.03	0.00	3.72	<	2.47	14.27
1997174	1069644	29.41	69.61	0.00	3.69	<	2.93	14.68
1997174	1069646	14.83	121.52	0.00	3.81	<	2.87	14.34
1997174	1069808	-1.58	130.80	0.00	3.70	<	2.91	14.48
1997174	1069856	-2.87	129.82	0.00	3.88	<	3.08	14.50
1997174	1069864	5.22	119.67	0.00	4.05	<	3.05	14.47
1997174	1070311	10.59	-83.35	0.00	4.90	=	4.51	16.32
1997174	1070317	57.61	-156.01	71.62	3.39	<	2.63	14.78
1997174	1070328	-48.73	124.34	0.00	3.69	=	3.78	15.48
1997174	1070339	28.55	140.03	0.00	3.32	<	2.57	14.33
1997174	1070351	52.72	161.30	0.00	3.59	<	2.64	14.35
1997174	1070365	-29.81	-178.38	33.79	3.48	<	3.33	14.62
1997174	1070381	52.89	-35.52	0.00	3.32	<	2.85	14.89
1997174	1070398	32.03	141.01	52.98	4.45	=	4.27	15.93
1997174	1070403	12.28	143.60	25.96	4.11	=	4.18	15.63
1997174	1070411	35.71	52.44	64.06	3.53	<	2.89	14.44
1997174	1070413	47.90	-122.18	13.50	4.31	=	3.74	15.51
1997174	1070438	14.30	-92.13	28.58	4.12	=	3.63	15.11
1997174	1070461	61.97	-148.85	0.00	3.26	=	2.53	14.61

1997174	1070473	27.96	51.85	33.59	4.08	<	2.92	14.54
1997174	1070475	46.17	153.00	35.80	3.94	=	4.31	15.57
1997174	1070479	-15.03	-173.79	0.00	4.30	=	3.78	15.10
1997174	1070482	31.84	49.21	0.00	3.59	<	2.14	14.43
1997174	1070485	25.72	97.77	0.00	3.61	<	2.01	14.06
1997174	1070515	11.63	145.50	0.00	3.54	=	3.16	14.61
1997174	1070518	-5.80	150.63	0.00	4.03	<	3.13	14.52
1997174	1070553	34.64	26.74	64.15	3.33	<	2.47	14.33
1997174	1070583	68.39	-127.21	0.00	3.54	<	1.57	14.34
1997174	1070630	13.32	-88.46	56.57	3.68	=	2.87	14.95
1997174	1070644	-1.54	135.46	0.00	3.91	=	3.06	14.75
1997174	1071398	-31.23	-176.94	0.00	3.66	<	3.24	14.94
1997174	1071403	-2.16	128.80	0.00	3.84	<	2.85	14.39
1997174	1071408	31.94	141.11	59.27	3.69	=	2.68	14.37
1997174	1071428	1.82	125.24	0.00	4.24	<	2.89	14.46
1997174	1071478	5.21	127.67	0.00	4.26	<	3.04	14.60
1997174	1071518	-2.30	142.55	0.00	3.70	<	3.12	14.65
1997174	1071527	52.37	159.45	0.00	3.74	<	2.77	14.54
1997174	1071896	3.91	130.74	0.00	3.82	<	3.02	14.32
1997174	1071976	11.65	-83.31	34.93	3.39	=	3.13	14.74
1997175	1070486	-15.28	-173.71	0.00	3.96	<	3.35	14.62
1997175	1070525	13.25	-88.07	0.00	3.84	<	2.97	14.63
1997175	1070529	-7.17	148.71	0.00	3.83	<	2.97	14.57
1997175	1070536	49.53	-123.53	0.00	4.12	=	3.07	15.02
1997175	1070558	10.45	126.35	0.00	3.83	=	3.15	14.51
1997175	1070600	30.20	96.85	71.09	3.68	=	2.66	14.68
1997175	1070619	-40.94	174.42	0.00	4.32	=	3.35	15.15
1997175	1070636	25.09	92.15	39.60	3.64	<	2.11	14.37
1997175	1070645	-22.65	-10.68	0.00	4.52	=	4.10	16.15
1997175	1070667	26.08	65.68	0.00	3.80	<	2.85	14.76
1997175	1070683	52.32	159.64	0.00	3.90	=	3.13	14.82
1997175	1070689	-19.12	172.89	0.00	3.44	=	3.71	15.62
1997175	1070690	21.93	143.33	0.00	3.36	<	2.59	14.21
1997175	1070698	11.82	-86.80	54.88	3.90	=	3.39	15.04
1997175	1070699	-22.54	-171.16	0.00	4.01	<	4.10	15.29
1997175	1070719	79.59	6.24	0.00	3.71	<	2.88	14.95
1997175	1070723	51.62	16.10	0.00	3.75	<	2.59	14.34
1997175	1070766	30.43	96.99	48.16	3.88	=	2.61	14.80
1997175	1070772	30.22	97.23	59.25	3.60	<	2.57	14.75
1997175	1070776	-3.29	136.47	0.00	3.73	<	2.86	14.59
1997175	1070783	14.54	-92.91	54.81	3.70	=	3.52	15.02
1997175	1070792	12.34	143.58	0.00	4.19	=	4.59	15.94
1997175	1070808	37.63	-25.39	0.00	3.49	=	3.13	15.13
1997175	1070820	33.43	142.48	36.63	3.89	<	2.84	14.43
1997175	1071223	-32.51	-178.26	25.48	3.92	=	3.46	15.01
1997175	1071261	25.76	89.83	0.00	3.74	<	2.17	14.36
1997175	1071277	-4.35	101.99	0.00	4.20	=	3.24	14.74
1997175	1071284	2.68	127.36	0.00	3.78	<	2.67	14.36
1997175	1071306	32.01	59.83	0.00	4.02	=	3.06	14.81
1997175	1071340	-1.92	128.00	26.79	5.63	=	6.15	17.87
1997175	1071354	39.45	76.89	70.83	4.21	=	4.68	16.34
1997175	1071370	36.33	71.18	0.00	4.01	<	2.98	15.03
1997175	1071371	-5.33	145.49	0.00	3.59	<	3.07	14.92
1997175	1071376	-23.33	-176.11	0.00	4.35	<	3.66	14.95
1997175	1071387	-57.56	-141.50	0.00	4.21	=	3.58	15.37
1997175	1071422	36.20	140.03	47.85	3.58	=	4.59	16.36

1997175	1071471	-0.82	136.40	0.00	4.46	=	3.94	15.47
1997175	1071491	13.56	121.18	0.00	3.83	<	3.40	14.94
1997175	1071990	-15.46	-176.56	0.00	4.23	<	3.63	15.03
1997175	1072002	26.53	96.12	28.25	3.88	<	3.27	15.07
1997175	1072009	14.23	-92.58	0.00	3.94	<	3.54	14.99
1997175	1072021	-14.70	-173.34	0.00	3.68	<	3.49	14.65

THOMAS AHRENS  
SEISMOLOGICAL LABORATORY 252-21  
CALIFORNIA INSTITUTE OF TECHNOLOGY  
PASADENA, CA 91125

AIR FORCE RESEARCH LABORATORY  
ATTN: VSOE  
29 RANDOLPH ROAD  
HANSCOM AFB, MA 01731-3010 (2 COPIES)

AIR FORCE RESEARCH LABORATORY  
ATTN: RESEARCH LIBRARY/TL  
5 WRIGHT STREET  
HANSCOM AFB, MA 01731-3004

AIR FORCE RESEARCH LABORATORY  
ATTN: AFRL/SUL  
3550 ABERDEEN AVE SE  
KIRTLAND, NM 87117-5776 (2 COPIES)

RALPH ALEWINE  
NTPO  
1901 N. MOORE STREET, SUITE 609  
ARLINGTON, VA 22209

MUAWIA BARAZANGI  
INSTITUTE FOR THE STUDY OF THE CONTINENTS  
3126 SNEE HALL  
CORNELL UNIVERSITY  
ITHACA, NY 14853

T.G. BARKER  
MAXWELL TECHNOLOGIES  
8888 BALBOA AVE.  
SAN DIEGO, CA 92123-1506

DOUGLAS BAUMGARDT  
ENSCO INC.  
5400 PORT ROYAL ROAD  
SPRINGFIELD, VA 22151

THERON J. BENNETT  
MAXWELL TECHNOLOGIES  
11800 SUNRISE VALLEY DRIVE SUITE 1212  
RESTON, VA 22091

WILLIAM BENSON  
NAS/COS  
ROOM HA372  
2001 WISCONSIN AVE. NW  
WASHINGTON, DC 20007

JONATHAN BERGER  
UNIVERSITY OF CA, SAN DIEGO  
SCRIPPS INSTITUTION OF OCEANOGRAPHY IGPP, 0225  
9500 GILMAN DRIVE  
LA JOLLA, CA 92093-0225

ROBERT BLANDFORD  
AFTAC  
1300 N. 17TH STREET  
SUITE 1450  
ARLINGTON, VA 22209-2308

LESLIE A. CASEY  
DEPT. OF ENERGY/NN-20  
1000 INDEPENDENCE AVE. SW  
WASHINGTON, DC 20585-0420

CENTER FOR MONITORING RESEARCH  
ATTN: LIBRARIAN  
1300 N. 17th STREET, SUITE 1450  
ARLINGTON, VA 22209

ANTON DAINTY  
HQ DSWA/PMP  
6801 TELEGRAPH ROAD  
ALEXANDRIA, VA 22310-3398

CATHERINE DE GROOT-HEDLIN  
UNIVERSITY OF CALIFORNIA, SAN DIEGO  
INSTITUTE OF GEOPHYSICS AND PLANETARY PHYSICS  
8604 LA JOLLA SHORES DRIVE  
SAN DIEGO, CA 92093

DEFENSE TECHNICAL INFORMATION CENTER  
8725 JOHN J. KINGMAN ROAD  
FT BELVOIR, VA 22060-6218 (2 COPIES)

DIANE DOSER  
DEPARTMENT OF GEOLOGICAL SCIENCES  
THE UNIVERSITY OF TEXAS AT EL PASO  
EL PASO, TX 79968

MARK D. FISK  
MISSION RESEARCH CORPORATION  
735 STATE STREET  
P.O. DRAWER 719  
SANTA BARBARA, CA 93102-0719

LORI GRANT  
MULTIMAX, INC.  
311C FOREST AVE. SUITE 3  
PACIFIC GROVE, CA 93950

HENRY GRAY  
SMU STATISTICS DEPARTMENT  
P.O. BOX 750302  
DALLAS, TX 75275-0302

DAVID HARKRIDER  
BOSTON COLLEGE  
INSTITUTE FOR SPACE RESEARCH  
140 COMMONWEALTH AVENUE  
CHESTNUT HILL, MA 02167

MICHAEL HEDLIN  
UNIVERSITY OF CALIFORNIA, SAN DIEGO  
SCRIPPS INSTITUTION OF OCEANOGRAPHY IGPP, 0225  
9500 GILMAN DRIVE  
LA JOLLA, CA 92093-0225

EUGENE HERRIN  
SOUTHERN METHODIST UNIVERSITY  
DEPARTMENT OF GEOLOGICAL SCIENCES  
DALLAS, TX 75275-0395

VINDELL HSU  
HQ/AFTAC/TTR  
1030 S. HIGHWAY A1A  
PATRICK AFB, FL 32925-3002

THOMAS JORDAN  
MASSACHUSETTS INSTITUTE OF TECHNOLOGY  
EARTH, ATMOSPHERIC & PLANETARY SCIENCES  
77 MASSACHUSETTS AVENUE, 54-918  
CAMBRIDGE, MA 02139

LAWRENCE LIVERMORE NAT'L LABORATORY  
ATTN: TECHNICAL STAFF (PLS ROUTE)  
PO BOX 808, MS L-221  
LIVERMORE, CA 94551

LAWRENCE LIVERMORE NATIONAL LABORATORY  
ATTN: TECHNICAL STAFF (PLS ROUTE)  
PO BOX 808, MS L-208  
LIVERMORE, CA 94551

LAWRENCE LIVERMORE NATIONAL LABORATORY  
ATTN: TECHNICAL STAFF (PLS ROUTE)  
PO BOX 808, MS L-195  
LIVERMORE, CA 94551

THORNE LAY  
UNIVERSITY OF CALIFORNIA, SANTA CRUZ  
EARTH SCIENCES DEPARTMENT  
EARTH & MARINE SCIENCE BUILDING  
SANTA CRUZ, CA 95064

I. N. GUPTA  
MULTIMAX, INC.  
1441 MCCORMICK DRIVE  
LARGO, MD 20774

THOMAS HEARN  
NEW MEXICO STATE UNIVERSITY  
DEPARTMENT OF PHYSICS  
LAS CRUCES, NM 88003

DONALD HELMBERGER  
CALIFORNIA INSTITUTE OF TECHNOLOGY  
DIVISION OF GEOLOGICAL & PLANETARY SCIENCES  
SEISMOLOGICAL LABORATORY  
PASADENA, CA 91125

ROBERT HERRMANN  
ST. LOUIS UNIVERSITY  
DEPARTMENT OF EARTH & ATMOSPHERIC SCIENCES  
3507 LACLEDE AVENUE  
ST. LOUIS, MO 63103

RONG-SONG JIH  
HQ DSWA/PMP/CTBT  
6801 TELEGRAPH ROAD  
ALEXANDRIA, VA 22310-3398

LAWRENCE LIVERMORE NAT'L LABORATORY  
ATTN: TECHNICAL STAFF (PLS ROUTE)  
PO BOX 808, MS L-200  
LIVERMORE, CA 94551

LAWRENCE LIVERMORE NATIONAL LABORATORY  
ATTN: TECHNICAL STAFF (PLS ROUTE)  
PO BOX 808, MS L-175  
LIVERMORE, CA 94551

LAWRENCE LIVERMORE NATIONAL LABORATORY  
ATTN: TECHNICAL STAFF (PLS ROUTE)  
PO BOX 808, MS L-202  
LIVERMORE, CA 94551

LAWRENCE LIVERMORE NATIONAL LABORATORY  
ATTN: TECHNICAL STAFF (PLS ROUTE)  
PO BOX 808, MS L-205  
LIVERMORE, CA 94551

ANATOLI L. LEVSHIN  
DEPARTMENT OF PHYSICS  
UNIVERSITY OF COLORADO  
CAMPUS BOX 390  
BOULDER, CO 80309-0309

JAMES LEWKOWICZ  
WESTON GEOPHYSICAL CORP.  
325 WEST MAIN STREET  
NORTHBORO, MA 01532

LOS ALAMOS NATIONAL LABORATORY  
ATTN: TECHNICAL STAFF (PLS ROUTE)  
PO BOX 1663, MS F659  
LOS ALAMOS, NM 87545

LOS ALAMOS NATIONAL LABORATORY  
ATTN: TECHNICAL STAFF (PLS ROUTE)  
PO BOX 1663, MS F665  
LOS ALAMOS, NM 87545

LOS ALAMOS NATIONAL LABORATORY  
ATTN: TECHNICAL STAFF (PLS ROUTE)  
PO BOX 1663, MS D460  
LOS ALAMOS, NM 87545

LOS ALAMOS NATIONAL LABORATORY  
ATTN: TECHNICAL STAFF (PLS ROUTE)  
PO BOX 1663, MS C335  
LOS ALAMOS, NM 87545

GARY MCCARTOR  
SOUTHERN METHODIST UNIVERSITY  
DEPARTMENT OF PHYSICS  
DALLAS, TX 75275-0395

KEITH MCLAUGHLIN  
MAXWELL TECHNOLOGIES  
8888 BALBOA AVE.  
SAN DIEGO, CA 92123-1506

BRIAN MITCHELL  
DEPARTMENT OF EARTH & ATMOSPHERIC SCIENCES  
ST. LOUIS UNIVERSITY  
3507 LACLEDE AVENUE  
ST. LOUIS, MO 63103

RICHARD MORROW  
USACDA/IVI  
320 21ST STREET, N.W.  
WASHINGTON, DC 20451

JOHN MURPHY  
MAXWELL TECHNOLOGIES  
11800 SUNRISE VALLEY DRIVE SUITE 1212  
RESTON, VA 22091

JAMES NI  
NEW MEXICO STATE UNIVERSITY  
DEPARTMENT OF PHYSICS  
LAS CRUCES, NM 88003

ROBERT NORTH  
CENTER FOR MONITORING RESEARCH  
1300 N. 17th STREET, SUITE 1450  
ARLINGTON, VA 22209

OFFICE OF THE SECRETARY OF DEFENSE  
DDR&E  
WASHINGTON, DC 20330

JOHN ORCUTT  
INSTITUTE OF GEOPHYSICS AND PLANETARY PHYSICS  
UNIVERSITY OF CALIFORNIA, SAN DIEGO  
LA JOLLA, CA 92093

PACIFIC NORTHWEST NATIONAL LABORATORY  
ATTN: TECHNICAL STAFF (PLS ROUTE)  
PO BOX 999, MS K6-48  
RICHLAND, WA 99352

PACIFIC NORTHWEST NATIONAL LABORATORY  
ATTN: TECHNICAL STAFF (PLS ROUTE)  
PO BOX 999, MS K6-40  
RICHLAND, WA 99352

PACIFIC NORTHWEST NATIONAL LABORATORY  
ATTN: TECHNICAL STAFF (PLS ROUTE)  
PO BOX 999, MS K6-84  
RICHLAND, WA 99352

PACIFIC NORTHWEST NATIONAL LABORATORY  
ATTN: TECHNICAL STAFF (PLS ROUTE)  
PO BOX 999, MS K5-12  
RICHLAND, WA 99352

FRANK PILOTTE  
HQ AFTAC/TT  
1030 S. HIGHWAY A1A  
PATRICK AFB, FL 32925-3002

KEITH PRIESTLEY  
DEPARTMENT OF EARTH SCIENCES  
UNIVERSITY OF CAMBRIDGE  
MADINGLEY RISE, MADINGLEY ROAD  
CAMBRIDGE, CB3 0EZ UK

JAY PULLI  
BBN  
1300 NORTH 17TH STREET  
ROSSLYN, VA 22209

PAUL RICHARDS  
COLUMBIA UNIVERSITY  
LAMONT-DOHERTY EARTH OBSERVATORY  
PALISADES, NY 10964

DAVID RUSSELL  
HQ AFTAC/TTR  
1030 SOUTH HIGHWAY A1A  
PATRICK AFB, FL 32925-3002

SANDIA NATIONAL LABORATORY  
ATTN: TECHNICAL STAFF (PLS ROUTE)  
DEPT. 5704  
MS 0979, PO BOX 5800  
ALBUQUERQUE, NM 87185-0979

SANDIA NATIONAL LABORATORY  
ATTN: TECHNICAL STAFF (PLS ROUTE)  
DEPT. 5704  
MS 0655, PO BOX 5800  
ALBUQUERQUE, NM 87185-0655

THOMAS SERENO JR.  
SCIENCE APPLICATIONS INTERNATIONAL CORPORATION  
10260 CAMPUS POINT DRIVE  
SAN DIEGO, CA 92121

ROBERT SHUMWAY  
410 MRAK HALL  
DIVISION OF STATISTICS  
UNIVERSITY OF CALIFORNIA  
DAVIS, CA 95616-8671

JEFFRY STEVENS  
MAXWELL TECHNOLOGIES  
8888 BALBOA AVE.  
SAN DIEGO, CA 92123-1506

TACTEC  
BATTELLE MEMORIAL INSTITUTE  
505 KING AVENUE  
COLUMBUS, OH 43201 (FINAL REPORT)

LAWRENCE TURNBULL  
ACIS  
DCI/ACIS  
WASHINGTON, DC 20505

DELAINE REITER  
SENCOM CORP.  
73 STANDISH ROAD  
WATERTOWN, MA 02172

MICHAEL RITZWOLLER  
DEPARTMENT OF PHYSICS  
UNIVERSITY OF COLORADO  
CAMPUS BOX 390  
BOULDER, CO 80309-0309

CHANDAN SAIKIA  
WOODWARD-CLYDE FEDERAL SERVICES  
566 EL DORADO ST., SUITE 100  
PASADENA, CA 91101-2560

SANDIA NATIONAL LABORATORY  
ATTN: TECHNICAL STAFF (PLS ROUTE)  
DEPT. 9311  
MS 1159, PO BOX 5800  
ALBUQUERQUE, NM 87185-1159

SANDIA NATIONAL LABORATORY  
ATTN: TECHNICAL STAFF (PLS ROUTE)  
DEPT. 5736  
MS 0655, PO BOX 5800  
ALBUQUERQUE, NM 87185-0655

AVI SHAPIRA  
SEISMOLOGY DIVISION  
THE INSTITUTE FOR PETROLEUM RESEARCH AND  
GEOPHYSICS  
P.O.B. 2286, NOLON 58122 ISRAEL

DAVID SIMPSON  
IRIS  
1200 NEW YORK AVE., NW  
SUITE 800  
WASHINGTON, DC 20005

BRIAN SULLIVAN  
BOSTON COLLEGE  
INSITUTE FOR SPACE RESEARCH  
140 COMMONWEALTH AVENUE  
CHESTNUT HILL, MA 02167

NAFI TOKSOZ  
EARTH RESOURCES LABORATORY, M.I.T.  
42 CARLTON STREET, E34-440  
CAMBRIDGE, MA 02142

GREG VAN DER VINK  
IRIS  
1200 NEW YORK AVE., NW  
SUITE 800  
WASHINGTON, DC 20005

FRANK VERNON  
UNIVERSITY OF CALIFORNIA, SAN DIEGO  
SCRIPPS INSTITUTION OF OCEANOGRAPHY IGPP, 0225  
9500 GILMAN DRIVE  
LA JOLLA, CA 92093-0225

JILL WARREN  
LOS ALAMOS NATIONAL LABORATORY  
GROUP NIS-8  
P.O. BOX 1663  
LOS ALAMOS, NM 87545 (5 COPIES)

RU SHAN WU  
UNIVERSITY OF CALIFORNIA SANTA CRUZ  
EARTH SCIENCES DEPT.  
1156 HIGH STREET  
SANTA CRUZ, CA 95064

JAMES E. ZOLLWEG  
BOISE STATE UNIVERSITY  
GEOSCIENCES DEPT.  
1910 UNIVERSITY DRIVE  
BOISE, ID 83725

TERRY WALLACE  
UNIVERSITY OF ARIZONA  
DEPARTMENT OF GEOSCIENCES  
BUILDING #77  
TUCSON, AZ 85721

DANIEL WEILL  
NSF  
EAR-785  
4201 WILSON BLVD., ROOM 785  
ARLINGTON, VA 22230

JIAKANG XIE  
COLUMBIA UNIVERSITY  
LAMONT DOHERTY EARTH OBSERVATORY  
ROUTE 9W  
PALISADES, NY 10964